Effect of Pile-Driving Induced Vibrations on Nearby Structures and Other Assets

Final report

Submitted to

Michigan Department of Transportation
ORBP Number OR10-046

by

Adda Athanasopoulos Zekkos (PI)
Richard D. Woods (Co-PI)
Athena Grizi (Graduate Research Assistant)

Department of Civil & Environmental Engineering
University of Michigan
2350 Hayward
Ann Arbor, MI 48109-2125

November 2013

Technical Report Documentation Page

1. Report No.	2. Government Accession No.	3. MDOT Project Manager
RC-1600		Richard Endres

4. Title and Subtitle	5. Report Date
Effect of Pile-Driving Induced Vibrations on Nearby Structures and Other Assets	November 30, 2013
	6. Performing Organization Code

7. Author(s)	8. Performing Organization Report No.
Adda Athanasopoulos-Zekkos, Richard D. Woods and Athena Grizi	None

9. Performing Organization Name and Address	10. Work Unit No. (TRAIS)
The Regents of the University of Michigan 3003 South State St. Ann Arbor, MI 48109	
	11. Contract or Grant No. 2010-0296

12. Sponsoring Agency Name and Address	13. Type of Report and Period Covered
Michigan Department of Transportation Office of Research and Best Practices 8885 Ricks Road Lansing, MI 48917	Final Report 10/01/2011 to 09/30/2013
	14. Sponsoring Agency Code

15. Supplementary Notes

16. Abstract

The work described here represents an attempt to understand the mechanisms of energy transfer from steel H-piles driven with diesel hammers to the surrounding soil and the energy attenuation through the soil by measuring ground motion vibrations in the near vicinity of the pile. Attenuation rates of vibration decay with radial distance from the driven pile were calculated. A spreadsheet tool was developed to estimate distances from the pile at which the threshold settlement vibrations may be exceeded.

17. Key Word	18. Distribution Statement
H-Piles, Vibration, Attenuation Rate, Ground Settlement Thresholds.	No restrictions. This document is available to the public through the Michigan Department of Transportation.

19. Security Classify. (of this report)	20. Security Classify. (of this page)	21. No. of Pages	22. Price
Unclassified	Unclassified	146	

Table of Contents

List of Figures

List of Tables

Symbols

A_c contact area between pile and soil (ft^2)

Dr relative density of cohesionless soils

E_o 0.5 times rated energy of hammer (ft-lb)

k dimensionless ratio = $[2(1-v)/(1-2v)]^{0.5}$

N field standard penetration number (blows/ft)

N_1 corrected standard penetration number for overburden stress (blows/ft)

$N_{1,60}$ corrected standard penetration number for field procedures and overburden stress (blows/ft)

P_a atmospheric pressure (2116 psf)

Q_p impedance of pile at tip = $A_c\rho_p V_p$ (lb-sec/ft)

Q_s impedance of soil at tip of pile = $A_c\rho_s Vs_p$* (lb-sec/ft)

R dimensionless reduction factor

R_R dimensionless correction factor accounting for soil compaction in cohesionless soils and remolding in cohesive soils

R_s dynamic factor to account for fines content

r radial distance from source to point (ft)

Su undrained strength of cohesive soils (psf)

V_p compression wave velocity in pile (ft/sec)

V_s shear wave velocity (ft/sec)

V_s* reduced shear wave velocity of soil at the contact with the pile =RV_s (ft/sec)

V_{sp} primary wave velocity of the second kind in soil (Biot wave) (ft/sec)

V_{sp}* reduced primary wave velocity in the soil at the contact with the tip of pile = RV_{ps} (ft/sec)

$\dot{z}$ peak particle velocity (ft/sec)

$\dot{z}_s$ peak particle velocity in the soil at the pile-soil interface (ft/sec)

$\dot{z}_t$ vertical component of particle velocity in the soil at pile tip (ft/sec)

α	coefficient of attenuation for vibrations (Bornitz formula) (1/ft)
γ_d	dry unit weight of soil (pcf)
γ_s	saturated unit weight of soil (pcf)
γ_f	shearing strain threshold
γ_{shaft}	shearing strain in shaft of pile
γ_{tip}	shearing strain in tip of pile
θ	angle between any ray of spherical wave and vertical (radians)
ν	Poisson's ratio
ρ	mass density (lb-sec^2/ft^4)
ρ_s	mass density of the soil (lb-sec^2/ft^4)
ρ_p	mass density of the pile (lb-sec^2/ft^4)
σ_v'	effective overburden stress (psf)
τ	shearing strength (psf)
ϕ	friction angle (degrees)
Я	coefficient of attenuation for soil (1/ft)

Acknowledgements

The authors would like to thank the Michigan Department of Transportation (MDOT) for funding this project. They wish to thank especially Tony Pietrangelo, Geotechnical Construction Support Engineer, for the coordination with the contractors of the tested sites, his help during the days that the sites were tested, and his immediate response to the research team's inquiries. The authors would also like to thank Bob Fischer and Rick Burch, Lab Technicians of the University of Michigan (UofM), who helped with the preparation of the special sensor casings that were used in this project. Finally, the research team wishes to thank Mohammad Kabalan, Adam Lobbestael, Jane Gregg and Zaher Hamzeh, current and alumni UofM students who helped in different tasks of this research project.

Executive Summary

The construction and retrofit of bridges and retaining walls often includes driving piles for foundation support. Pile-driving is performed typically by use of impact or vibratory hammers. This process induces vibrations into the ground which can be transmitted to nearby structures and underground utilities and threaten their integrity and serviceability. More specifically, these vibrations can cause ground settlements and deformations that may lead to differential settlements of foundations, and deformations or cracking of underground utilities. This report presents results of a research project focused on developing a simplified procedure for the evaluation of pile-driving induced vibrations and induced shear strain thresholds and providing guidance to MDOT on identifying potentially troublesome sites.

Pile driving-induced vibrations in the vicinity of driven H-piles were measured. The measurements were conducted by installing vibration sensors (accelerometers and geophones) at different horizontal distances from the driven pile and at various depths into the ground. The sensor packages (sensor cones) were designed and manufactured to be “sacrificial” so they did not have to be recovered after the piles were installed. Ground vibration data was collected at 5 sites (M-25 over Harbor Beach Creek, M-66 over Wanadoga Creek, M-139 over Dowagiac River and US-131 over St. Joseph River at both bridge abutments). The collected data was analyzed to help refine our understanding of the energy coupling from pile to ground during impact pile driving and to develop attenuation rates for pile driving induced vibrations propagating away from the driven pile.

The Bornitz form of equation was determined to be the best way to most accurately represent attenuation. However, the conventional way of including material damping through the coefficient of attenuation, α, was determined to be too simple for driven piles as a source of energy, so a different symbol for coefficient of attenuation, $я$, has been chosen. Based on: (1) the limited pile type, (2) pile driver type and (3) site conditions encountered in this research, refined characterization of $я$ could not be made but a simplified range was chosen: $0.1<я<0.15$. Coefficient of attenuation, α, for typical ground material should not be used for attenuation of pile driving vibrations. Based on these mechanisms of energy coupling and vibration attenuation, a spreadsheet based template was developed for estimating the distance from the pile to which threshold shear strain vibrations would propagate. This spreadsheet has been calibrated based on measurements in each sandy stratum of the simplified soil profiles. This template can be used to estimate recommended standoff distances from sensitive structures or facilities to prevent likelihood of settlement due to impact pile driving of H-piles through cohesionless, loose to medium dense sandy soils.

1 INTRODUCTION

1.1 Organization of report

Section 1 presents the objectives of this research report and an extensive literature review. Section 2 provides details on the equipment that was used to measure ground motion vibrations and information about the sites that were tested. Sections 3 and 4 present the ground motions measured at the selected sites and analysis of these results. Section 5 discusses how these results were used to formulate a spreadsheet tool for the evaluation of the potential for a soil to undergo shakedown settlement from pile driving. Section 6 compares predicted and measured values from the sites that were tested. Section 7 lists research conclusions and recommendations for future research. Finally, Section 8 provides a reccomended implementation plan as a product of this research.

1.2 Objectives

The main research objective was the development of a simplified procedure for estimating pile-driving induced ground settlement. The three objectives as listed in the original research proposal are itemized below.

a) *Improvement and calibration of existing analytical models for estimating shear wave attenuation and man-made ground vibration induced settlements.*
An extensive literature review of the available methods, guidelines and regulations at the national and international level was performed in order to accumulate information on the transfer of energy from pile to soil, the dissipation of energy through soil and vibration levels causing ground settlement.

b) *Characterization of typical vibration sources for MDOT projects.*
A database with the vibration characteristics and hammer-pile combinations commonly used by MDOT contractors was developed. This database is important because it was included as an input parameter in the software tool.

c) *Development of screening criteria for identifying potentially troublesome sites.*
After testing different sites with pile-driving operations selected by available MDOT projects, the research team was able to evaluate the results and propose a settlement software tool for identifying potentially troublesome sites.

It is also anticipated that the mechanisms of energy transfer to the ground from driven piles, postulated in the FHWA Synthesis # 253 by Woods (1997) as shown in Figure 1-1, would be confirmed or modified. This idealized schematic assumes a half-space consisting of a homogeneous, isotropic, elastic material with a Poisson's ratio, μ. Primary waves (P-waves) radiate from the pile tip and cylindrical waves (S-waves) radiate from the pile shaft and form the developing Rayleigh waves on the surface. However, this hypothesis has not been proven with physical ground motion measurements. Likewise, vibration attenuation in three general soil behavior zones, plastic, non-linear, and nearly elastic, shown in Figure 1-2, is unsubstantiated. Shearing strain, γ, is suggested for defining boundaries of these zones. To verify these assumed soil behaviors, measurements of ground motion in the vicinity of a driven pile are required and such measurements were not documented in available literature. The work described here represents a first attempt to make ground motion measurements in close proximity to driven H-piles.

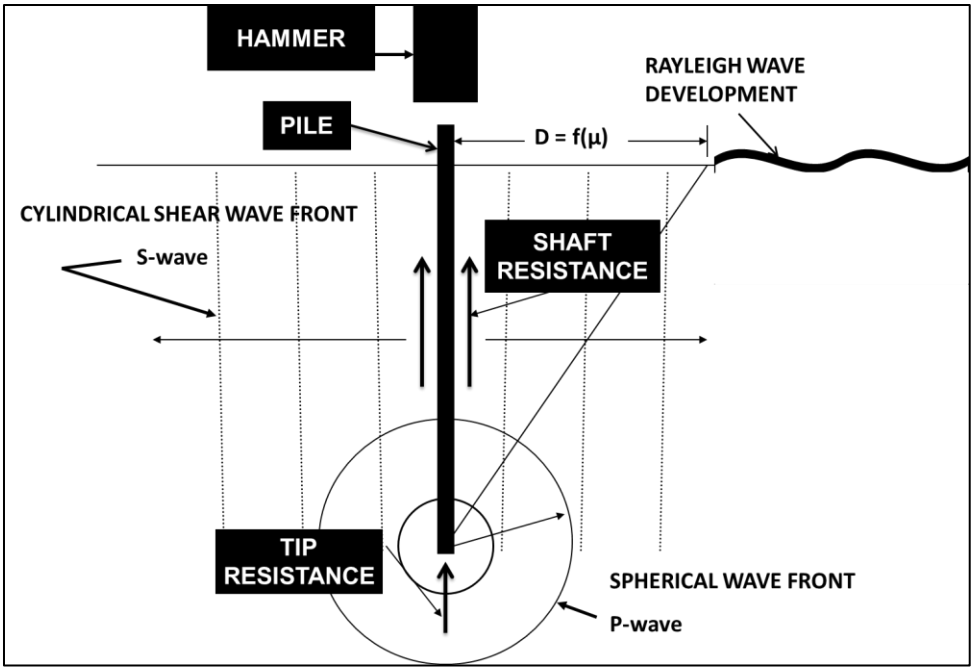

Figure 1-1 Basic mechanisms of energy transfer from pile to soil (after Woods, 1997)

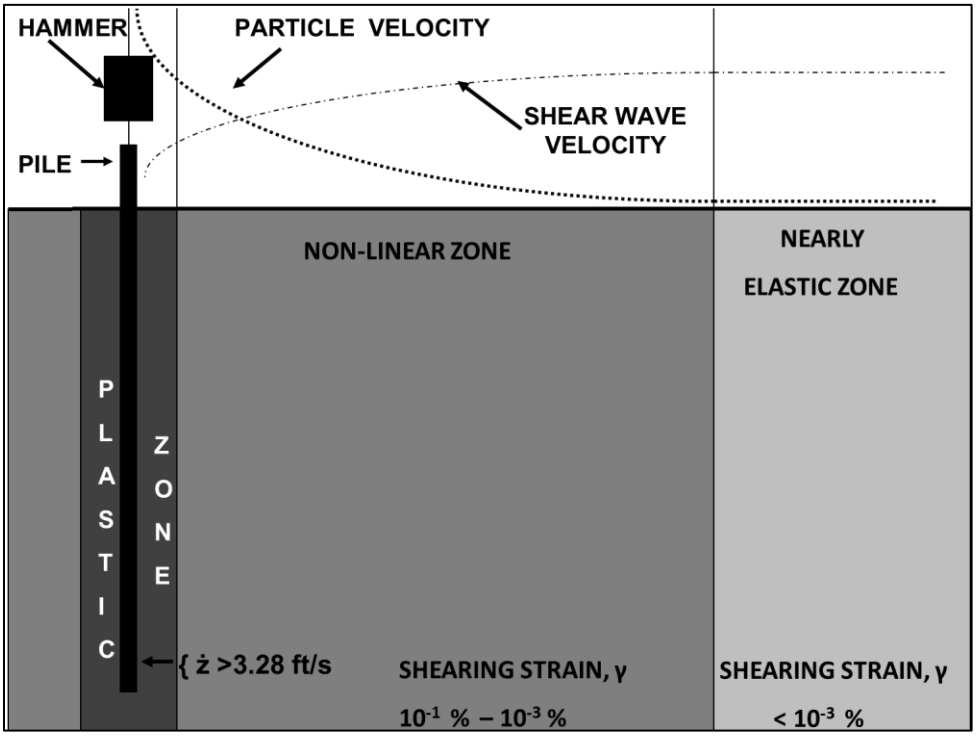

Figure 1-2 Assumed soil behavior zones near driven pile (after Massarsch, 2002)

1.3 Literature review

Research in soil dynamics has followed two principle paths, one directed at earthquake problems and the other directed at design of machine and sensitive instrument foundations and vibration damage from construction operations like blasting and pile driving. With respect to the second path, much of the published research has dealt with the potential for surface waves to cause direct damage to structures. A smaller number of studies dealt with damage caused by settlement due to pile driving vibrations. One characteristic of pile driving vibrations that separates them from earthquake events is the number of cycles of vibrations. Earthquake events seldom produce more that 10 to 12 cycles of high amplitude vibrations while driving piles for a large foundation can require thousands of pile hammer blows and even more cycles of vibration.

Pile installation is a complicated, energy intensive process where codes and regulatory standards provide some guidance, but little is understood about coupling and transmission of pile driving energy into and through the ground in the form of vibrations.

The mechanism of the energy transfer process includes the following steps:

- energy is generated by the pile hammer
- energy is transmitted through the pile
- interaction between the pile and the soil
- propagation of the waves in the surrounding soil
- soil to structure interaction

The capability of the pile to transmit the longitudinal force caused by the hammer is measured by the impedance of the pile, which varies significantly with pile type. The energy transmitted from pile to soil depends on the type of hammer and the impedance of the pile.

There is an increased need for a better understanding of several aspects that are involved in the pile installation process because reconstruction of parts of the aging infrastructure must take place while infrastructure elements are functioning. This may require pile driving in close proximity to functioning components of a facility under reconstruction. Some of the aspects that need to be studied are the attenuation rate with distance from vibrating source, the effect of the number of cycles of vibration, the strain threshold to cause settlement, and the presence of fines in the soil through which the vibrations travel from the pile.

Technical literature contains some guidance to the components of the pile driving/neighboring structure damage as described in the following.

1.3.1 Vibration Criteria

Sources of Construction Vibration include:

- Transient or Impact Vibration (e.g. blasting, impact pile driving, demolition).
- Steady-state or Continuous (e.g. vibratory pile drivers, compressors, large pumps).
- Pseudo-steady-state vibrations (e.g. jackhammers, trucks, cranes, scrapers).

Vibration intensities reported from the operation of construction equipment are usually recorded on the surface of the earth. Peak particle velocity is most often used as the measure of vibration intensity and in the United States, 4 in/sec for commercial buildings and 2 in/sec for residential structures, were for many years considered to be thresholds of possible damage (Wiss, 1981). These criteria ignored the influence of frequency and have been supplanted with more correct criteria that include frequency described later.

A simple relationship has been proposed by Massarsch and Broms (1991) for determining the critical peak vertical particle velocity that would cause damage by ground vibration. This relationship takes into account the rate of loading, the number of vibration cycles, building type and type of damage.

Woods (1997) related the amount of energy coupled into the ground to the vibration induced from pile driving. Approaches for estimating the input energy as a percentage of the hammer rated energy were recently seen as too crude for reliable analysis of ground vibrations as it omits the importance of soil properties and soil resistance.

Massarsch and Fellenius (2008) devised a transmission efficacy approach between different components of the pile driving system using their relative impedances. It also includes effects of strain-softening on wave velocities in soil which allows for determining attenuation characteristics of waves generated during soil-pile interaction. This approach is promising and allows for proper estimation of energy transmission from the hammer to the soil, and thus allows for more accurate estimation of vibrations induced and their attenuation characteristics.

A prediction model of vibration induced settlement for small to intermediate vibration levels (0.1 to 0.7 in/sec) was presented by Kim et al. (1994). They included other factors apart from peak particle velocity, namely vibration amplitude, stress, confining pressure, grain size distribution, duration of vibration, moisture content and relative density.

Jackson (2007) indicated that 2 in/sec is the vibration limit criteria used for construction projects by Florida Department of Transportation. This limit is based on criteria proposed by federal, state and foreign agencies to mitigate direct damage to structures.

The U.S Bureau of Mines, which developed criteria for blasting activities, recommended a "safe blasting limit" of 2 in/sec peak particle velocity. This value seems to be adopted nationwide with some additional criteria for special historical and ancient ruins and for recognition of influence of frequency (Siskind and Stagg, 2000).

Hendriks (2002) indicated that Caltrans set an architectural damage risk level of 0.2 in/sec for continuous vibrations and a much lower level for ancient monuments and historical buildings (0.08 in/sec). Internationally, the British standard 7385 reported a similar limit 2 in/sec while Australian standard 2187.2 was more conservative adopting a limit of (0.39 in/sec to 1 in/sec) depending on the type of building in vicinity of the source of vibration. For pile driving in confined areas with sustained pile driving activities, damage was seen with a lower level of vibrations (0.3 in/sec) in areas within 25 ft. of the source. Caltrans technical advisory for vibrations indicated that the 2 in/sec criterion is still being used and could be seen as a safe criterion for well-engineered and reinforced structures; however for normal dwellings, vibrations must be limited to 0.3 in/sec.

1.3.2 Vibration induced settlement

Vibration induced settlements can occur in loose soils subject to ground borne vibrations from any contiguous source like construction operations, forging operations, or other dynamic event like blasting. The soil may be saturated in which case liquefaction may occur or non-saturated in which case shakedown settlement may occur. Damage may occur to structures supported on soils due to settlement by vibrations. Factors that increase the total vibration energy input will increase settlements. Such factors are: depth of overburden, intensity of final driving resistance, number of piles and size of the site.

Silver and Seed (1971) performed laboratory tests that showed a decrease can occur in a soil volume at low cyclic strain amplitude after many repetitions, as in pile driving, as well as under a few cycles at large strain, as in seismic disturbance.

Vibration-induced settlements and soil shakedown is known to occur due to densification of loose saturated sands subjected to vibrations. Therefore, understanding vibrations resulting from pile driving is essential to alleviate risk of damage to buildings and structures in the vicinity of pile driving activities. Massarsch (2000) devised an analytical approach that allows estimation of settlements due to ground vibrations close to the pile. This method, however, estimates vertical vibration velocity at depth based on measured ground surface vibrations.

It has been indicated in many cases that settlements can occur even at low vibration levels in loose granular soils. As the vibration amplitude is largest close to the ground surface,

settlements will be larger in the upper soil layers, where the confining stress is low. Peak particle velocities of 0.1 to 0.2 in/sec measured on the ground surface at some sites gave significant settlements in case histories measured by Lacy and Gould (1985). Installation of piles to support a foundation system for a railroad bridge, led to significant settlements of a pipeline that was adjacent to the construction work (Linehan, Longinow and Dowding, 1992). In this case the estimated construction vibrations were considered acceptable. Leznicki et al. (1994) reported unacceptable settlements in a case of driving pipe piles with impact hammer when peak particle velocities were not more than 0.2 in/sec (far less than the vibration limit to cause damage).

Ground settlements are more significant near the piles and in loose fill deposits. Only minimal settlements were observed until acceleration levels exceeded 0.05g in a case history reported by Clough and Chameau, (1980). Szechy and Varga (1978) also stated that settlement can be expected if accelerations exceed 0.10g.

Clean sands with relative densities less than 50 to 55% are considered susceptible to densification as implicated by Lacy and Gould (1985). They also stated that prediction of settlement in sands requires knowledge of gradation, relative density, site geometry, groundwater levels, hammer energy and the scale of the project. In addition, soil properties that may influence settlement include: grain shape, permeability, anisotropy and magnitude of effective stress.

Foundation support was needed in a project encountered by Picornell and Monte (1985), in which steel H-piles were driven in an area with loose to medium-dense silty sand layers. Consolidation and load tests indicated that the settlements should be attributed to the dynamic compaction induced by the pile driving.

Time-delayed settlement appears to occur after piling has been completed and can be a significant contributor to total settlement as indicated by Leznicki et al. (1994).

Drabkin et al. (1996) proposed a polynomial model to estimate settlement taking into consideration several factors including soil properties and number of cycles of load. This method allows for good estimation of settlement, however, it is based on a laboratory approach modeling vibration data obtained from field ground surface measurements. The calculated settlements from the prediction equation by Kim et al. (1994) were compared with two case histories after extrapolation to the in-situ condition (Clough and Chameau (1980), Lacy and Gould (1985)) and were found to match closely.

Parametric assessment of settlement demonstrated that settlement increases significantly with increasing stress anisotropy (Kim and Drabkin, 1995).

1.3.3 Attenuation with distance and material damping

The ground vibration attenuation relative to distance is frequently calculated with the Bornitz's formula (Bornitz, 1931):

$$\dot{z}_2 = \dot{z}_1(r_1/r_2)^{0.5} \exp[-\alpha(r_2-r_1)] \quad (1.1)$$

where:

r_1 = distance from source to point of known amplitude, (ft.)
r_2 = distance from source to point of unknown amplitude, (ft.)
$\dot{z}_1$ = amplitude of motion at distance r_1 from source, (ft./sec)
$\dot{z}_2$ = amplitude of motion at distance r_2 from source, and (ft./sec)
α = coefficient of attenuation for vibrations. (1/ft.)

Since this is a surface wave attenuation formula, no information is provided about ground vibration close to a source due to body waves (Yang, 1995). A modified Bornitz equation was introduced containing empirical factors in order to account for different wave types, the effect of frequency of vibration and the effect of geometry of the vibration source and the dependence of attenuation coefficient on soil type. However, Massarsch et al. (1995) commented that the Bornitz equation could be readily modified to apply to body waves instead of introducing new empirical factors.

The attenuation of accelerations with distance from the piles depends upon soil conditions as indicated by Clough and Chameau (1980). Dense natural soils showed less attenuation relative to areas underlain by soft bay mud which is due to their greater damping capacity. Structures more than 80 ft. from pile driving operations should not suffer structural damage even in the loosest fills.

The ground movements induced by pile driving drop from a maximum near the affected footing to zero in the closest unaffected footing located 39 ft. apart as measured in a project by Picornell and Monte (1985). Observed attenuation rates by Dalmatov et al. (1968) indicated that the ground movements were zero at distances beyond 26 ft. from the pile center, which is in agreement with the previous case.

Densification of loose clean sands can extend as far horizontally as the piling is long as reported by Dowding (1994) who examined case histories presented by Clough and Chameau

(1980) and Linehan et al. (1992). Thus-the small distances at which densification is expected can be described in terms of pile length for piling.

The volume of the sand stratum contributing to the settlements was assumed to extend an average 10 ft. beyond the perimeter of the pile driving area in a project encountered by Leathers (1994). This assumption was based on the observation that driving piles about 10 ft. from an inclinometer caused ground movements.

Settlement induced by pile driving activities can extend to as far as 1300 ft. from pile driving activities (Woods 1997). Thus the attenuation characteristics of vibrations are an important factor in determining how far vibration induced-settlement might extend and under what levels of vibrations this settlement might occur.

Jedele (2005) concluded that actual vibrations were not necessarily equal to the predicted vibrations and site specific attenuation monitoring must be used in the scaled distance approach. Athansopoulos and Pelekis (2000) indicated that non-uniform soil is the greatest challenge for the scaled energy approach.

1.3.4 Effect of number of cycles

Vibrations due to pile driving operations resemble in some ways the effect of seismic vibrations but they differ greatly in intensity and number of loading cycles. Strains causing settlement tend to accumulate with the increasing number of loading cycles. Laboratory tests by Seed and Silver (1972) on a shaking table on clean sand showed a first indication of increasing settlements with increasing number of cycles. According to Drabkin and Kim (1996), pile driving operations can generate up to 500,000 cycles which is orders of magnitude greater that earthquake cycles. Increase of number of vibration cycles can cause substantial settlement especially for large vibration amplitudes. If low-level vibrations are analyzed for long-term impact, the accumulation of vibrations may be sufficient for considerable densification of sandy soils.

1.3.5 Effect of fines

Most research studying liquefaction and vibration induced settlements were limited to fine clean saturated sands. Not much research has been done to better understand the effect of the presence of fines on the energy coupling mechanism. Massarsch (2000) suggested models for settlement estimation in clean sands only. Kim and Drabkin (1995) indicated that coarse sand specimens with small content of fines are more susceptible to vibration induced settlement.

Borden et al (1994) and Borden and Shao (1995) reported on experiments and field observations to evaluate the importance of fines content on potential for settlement of granular materials. These tests showed that for fines contents greater than about 10%, the threshold for vibration settlement increased.

1.3.6 Numerical Analysis

Several researchers are currently using numerical approaches to model pile driving. Selby (2002) assumed ground waves during pile driving are fully harmonic. This approach is promising based on the case studies analyzed, but the researcher concluded that the peak particle velocities are very sensitive to the input energy which was determined not to be closely linked to the rating of the hammer. This implies the need for deeper understanding of the energy input during pile driving.

Masoumi (2007) used a dynamic-soil interaction finite element formulation to predict free field vibrations due to pile driving. The results were consistent with the theoretical understanding of the generation of the three different waves during driving. However, layer thicknesses might significantly influence ground vibrations during pile penetration due to reflection and refraction phenomena. Thus, greater understanding of the effect of superposition of the different waves on vibration velocities must be achieved.

1.3.7 Case Histories

When an obstruction is encountered in pile driving, the ground vibrations and the noise increase as stress waves passing through the pile are reflected from the obstructions (Clough and Chameau, 1980).

Amplification of waves can occur as a result of soil resonance when the dominating frequency of propagating wave coincides with the natural frequency of a soil layer. This phenomenon is connected with vibratory hammers as it occurs during starting-up and switching-off the vibrator. In order to avoid excessive vibrations, the frequency and amplitude of vibrator can be adjusted (Massarsch, 1992). Thus, for efficient pile installation the vibrator should operate at a high frequency, while soil settlement is worst at a low frequency (resonance frequency of soil).

Recommendation for reaching maximum operating frequency as quickly as possible when using a vibratory hammer is made by Linehan et al. (1992), in order to avoid amplification of ground vibrations.

2 METHODOLOGY

2.1 Ground Motion Transducer Design and Fabrication

2.1.1 Background

Construction operations are not compatible with installation and recovery of buried transducers. Conductor cables are also vulnerable to breakage in the pile driving construction environment so it was decided to develop sacrificial transducer packages that could be pushed into the ground and not recovered.

2.1.2 Selection of Transducers

Two types of motion sensor (motion transducer) cones were designed and fabricated to be pushed into the ground with a common drill rig and not recovered after pile driving measurements had been made. These sacrificial transducers consisted of single component (vertical) geophones and triaxial accelerometers. The least expensive approach was to use single axis, 4.5 Hz geophones (Figure 2-1). The geophone cores, model RGI-20DX, were supplied by Racotech Geophysical Instruments. Since the range of ground motion was not known in advance, more expensive triaxial, MEMS based accelerometers were also prepared. Based on preliminary tests, it was estimated that ground acceleration could be as high as 5 g so accelerometers with this capability were procured. Triaxial accelerometer units to meet this criterion were custom designed and fabricated by Civionics, LLC, Colorado Springs, Colorado. Model MMA7361LCT triaxial, MEMS type accelerometers, supplied by Freescale, with an acceleration range of ± 6 g were the basis of Civionics' design. A 3.3 V voltage regulator that allowed any voltage source from 4V to 14 V was used to provide a zero level, 1.65V (0 – 3.3 volt range) output with a sensitivity of 206 mV/g. These components were mounted on a 1in.x1in. printed circuit board, as shown in Figure 2-2.

2.1.3 Sensor cones

Sensor cones were machined from steel so they could be pushed vertically into the ground to their planned elevations. These cones had 60 degrees tapered tips and a hollowed-out cylindrical center to house the sensors. A special adaptor was designed that allowed downward pushing of the cone with rods from the drill rig but would not allow a withdrawing force to the sensor cone, see drawing, Figure 2-3 and photos, Figure 2-4 and Figure 2-5. The cone has a larger diameter than the push rod and the shoulder created by the difference in diameter was intended to engage soil to hold the cone body in place as the drill rod was withdrawn. Figure

2-6 shows a geophone potted into push cone and Figure 2-6 shows an accelerometer chip being fitted into a cone cavity.

2.1.4 Data acquisition system

The conducting cable from the sensors was fed upward through the adapter and hollow of the drill rods to the ground surface to the recording instruments, Figure 2-8. The National Instruments, Model NI CDAQ-9178 battery powered Data Acquisition, chassis was chosen. This unit consisted of a 3.3V voltage regulator that supplied a 1.65V (0-3.3 volt range) output. Plug-in modules consisted of 5- NI 9232, 1- NI 9205, and 2- NI 9221. Simple voltage was recorded for the accelerometers and geophones and calibration factors applied after data collection. Voltage output was displayed on and stored in a laptop computer.

2.2 Ground Motion Transducer Installation

2.2.1 Background

Based on prior experience, it was anticipated that the push cone sensor packages (herein after called sensor cones) could be pushed into soil for which Standard Penetration Blow count (N) was less than 40. Experience on this project was that for several reasons, the full downward capacity of the drill rig could not be applied and pushing worked for blow counts up to about 30. Also, if a thin gravel rich layer was encountered (as judged by drillers) in sand even with low blow counts, N less than 10, the sensor cone could not push through. Figure 2-9 shows installation of sacrificial sensors with the drill rig.

2.2.2 Problem soil conditions

During installation of the sensor cones, two extreme conditions were problematical: sand too loose and sand too dense. Sand too loose resulted in a condition where the sensor cone would not stick or stay in place where planned. Sometimes pushing the cone deeper caused the cone to stick. Other attempts to make the sensor cone stick included: 1) filling the drill rod core with water to put hydraulic pressure on cone to drive it out of push rods, and 2) making the rod to cone adapter very loose so the sensor cone would fall out of the drill string. Each of these methods worked once or twice but neither could not be relied on to accomplish the goal every time. A loose adapter connection with weak tape, masking or scotch tape holding sensor cone in adapter, was the most successful.

The other extreme, sand too dense, called for different solutions. First tried was installing the sensor cone through the hollow of a hollow stem flight auger. With this method it was difficult to push the sensor cone past the end of hollow stem auger. Sand at the exit point pinched the cone and contact was lost between cone and push rod causing the cable to be cut. Another approach that worked in some instances involved pre-drilling a hole with a solid stem flight auger and backing the auger out leaving loose soil in the hole and then pushing the sensor cone into the loosened sand.

2.2.3 Post installation problems

Successful installation of a sensor cone did not ensure successful operation. Situations were experienced where the driven pile destroyed the sensor because the evident surface position of the sensor was not necessarily the at depth position of the sensor. Also, because of the construction operations around the ground surface locations of the sensor conducting cables, these cables were accidentally broken.

2.2.4 Specific installation experience

While it was intended to install two sets of sensor cones at two depths of embedment and at three distances from the face of the pile, actual experience was different. No single reason explained all cases so each site will be described separately, and Table 2-1 is a summary of installation attempts and results.

M-25 (MDOT Project 100622A, C19 of 32092, M-25 over Harbor Beach Creek) - Two sensor cones were installed at a planned depth of 6 ft. but the third in the row at this depth would not stay in place until a depth of 10 ft. was reached. In addition, the 6 ft. depth was too shallow as was observed when the pile was driven because the pile penetrated about 12 ft. with only about 3 blows. For the deeper set intended to be set at about 20 ft., blow counts of 34 stopped the penetration and two sensor cones were lost; the third was not attempted because of this problem. The water table was at a depth of about 14 ft. and did not seem to affect installations.

M-66 (MDOT Project 89916A, B02 of 13032, M-66 over Wanadoga Creek) - All three of the deep sensor cones were installed with the available push limiting depth to 35 ft. The shallow sensor cones would not stay in place in very loose material and after losing one, second and third were not tried. Only one depth achieved at this site. Water table was at a depth of about 15 ft.

M-139 (MDOT Project 86785A, B01 of 11052, M-139 over Dowagiac River) – At this site difficulty of positioning the close-in sensor cone at a planned depth of 10 ft. was experienced, so another try at 10 ft. depth was not attempted at greater ranges. All three deep sensor cones were pushed successfully to 25.5 ft. The water table was at a depth of about 15 ft.

US 131 (MDOT Project 46269A, B01 of 78015, M-139 over St. Joseph River, near Constantine) - At abutment A, South abutment, trial installation methods were performed. Pre-augering with a small diameter, solid stem, flight auger was used to bore to the planned depth. Flights were backed out leaving loose sand in hole and then the sensor cone was pushed to planned depth. This worked very well at this site allowing installation of sensors at two depths and three distances from the pile. Water table depth was at about 10 ft.

At abutment B, North abutment, the same installation method used at abutment A, did not work for unknown reasons. Planned shallow depths were not achieved because sensor cones would not stick and planned deep sensors did not reach depth because of insufficient push capacity. At abutment B an attempt was made to determine if there was a difference in vibration transmission based on the orientation of the H-pile. Sensor cones were set at 6 in. from the open side of the H and at the flange side of the H. Unfortunately the open side close-in sensor cones were destroyed during pile driving. Conductor circuits were checked before driving and found to be good. During and after pile installation circuits were open. Furthermore, one of the conductor cables was also cut or broken during operations around the pile either during initial driving or during driving operations. These circumstances prevented the planned comparison between open side and flat side wave propagation from the H-pile. Water table was at about 10 ft.

2.2.5 Installation summary

As shown in Table 2-1, 20 out of 23 accelerometer sensor cones and 8 of the 9 geophone sensor cones were successfully installed. These statistics do not reflect the situations where installation was abandoned because of experience at that site. Successful sensor cone installation did not, however, assure successful data recovery.

Because of the uncertain construction schedule, best use could not be made of the learning curve associated with sensor cone installation. For example, most sensor cones were fabricated at the same time, i.e. potted to be ready to go to the field on short notice. If only a few cones required for a given site had been potted, a larger shoulder cone or other remedy could have

been fabricated and tried in the attempt to stick the cones. The expensive accelerometers were already in potting compound and could not be removed without destroying them when it became evident that some other approach to sticking the cones was needed.

Table 2-1 Installation of sensor cones-Success Rate

Site	Attempted Installation		Successful Installation					
	# Geophones	# Accelerometers	Geophones			Accelerometers		
			Number	Range	Depth	Number	Range	Depth
M-25	N/A	5	N/A	N/A	N/A	A2	6 in.	6 ft.
						A3	24 in.	6.2 ft.
						A4	72 in.	10.5 ft.
M-66	1	4	SG	69 in.	5.4 ft.	A1	9 in.	34 ft.
			N/A	N/A	N/A	A2	38 in.	35 ft.
						A3	64 in.	34.3 ft.
M-139	N/A	5	N/A	N/A	N/A	A1	6 in.	10.5 ft.
						A2	6 in.	11.5 ft.
						A3	6 in.	25.5 ft.
						A4	30 in.	25.5 ft.
						A5	77 in.	25.5 ft.
US 131A	2	5	SG1	26 in.	15 ft.	A1	6 in.	17 ft.
			SG2	77 in.	35.3 ft.	A2	6 in.	35.3 ft.
			N/A	N/A	N/A	A3	30 in.	15 ft.
						A4	30 in.	35.3 ft.
						A5	79 in.	15 ft.
US 131B	6	4	SG1	7.5 in.	34 ft.	A1	5 in.	25.5 ft.
			SG2	7.5 in.	16.3 ft.	A2	5 in.	30.3 ft.
			SG3	30 in.	31.5 ft.	A3	1.94 ft.	14.3 ft.
			SG4	2.1 in.	16.3 ft.	A4	1.94 ft.	30.2 ft.
			SG5	77 in.	18.5 ft.	N/A	N/A	N/A
Total	9	23	8			20		

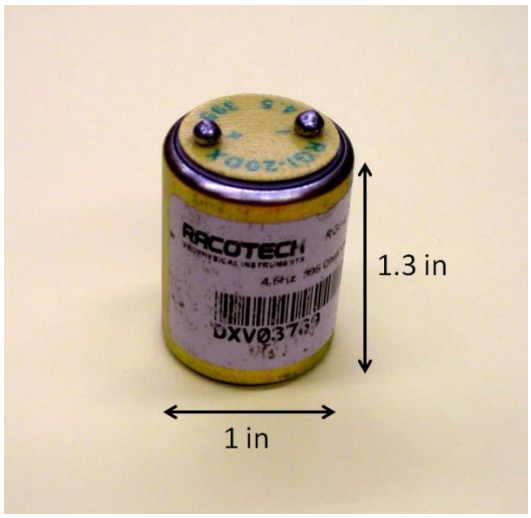

Figure 2-1 4.5 Hz geophone can

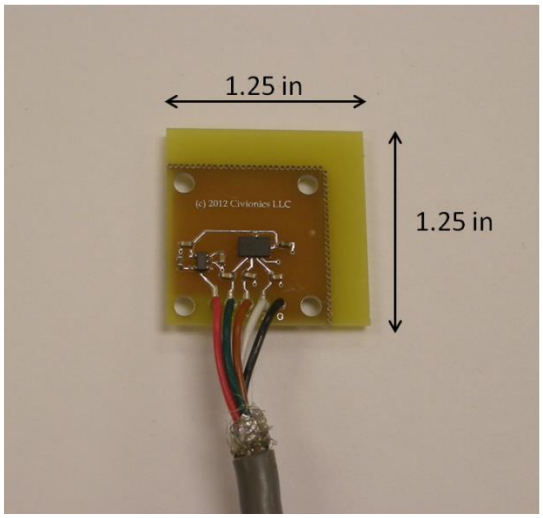

Figure 2-2 Civionics triaxial MEMS

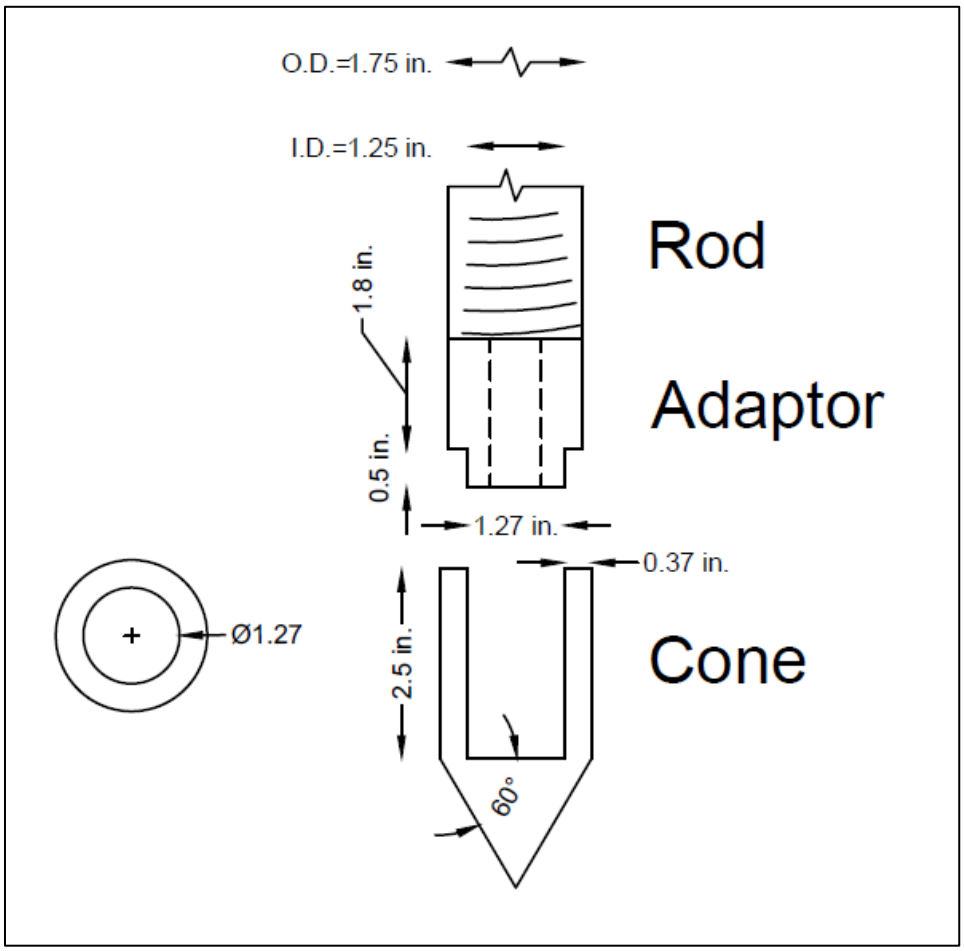

Figure 2-3 Cross section of cone casing, adaptor and rod

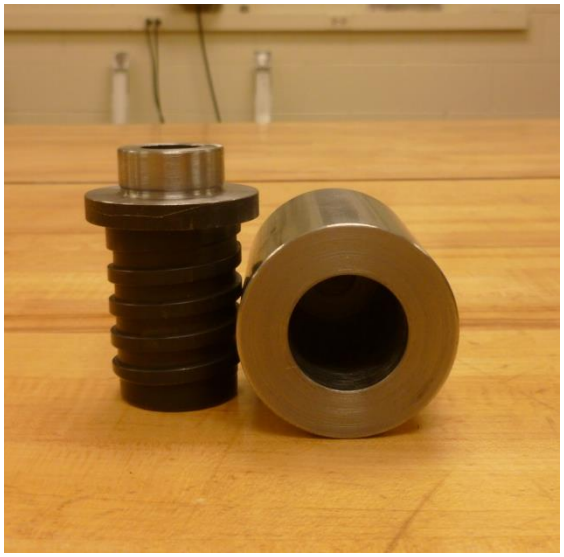

Figure 2-4 Cone and push adaptor

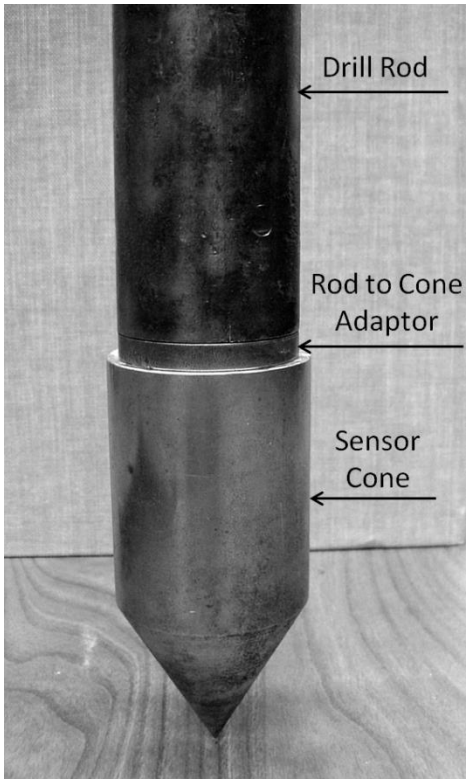

Figure 2-5 Rod, adaptor and push cone

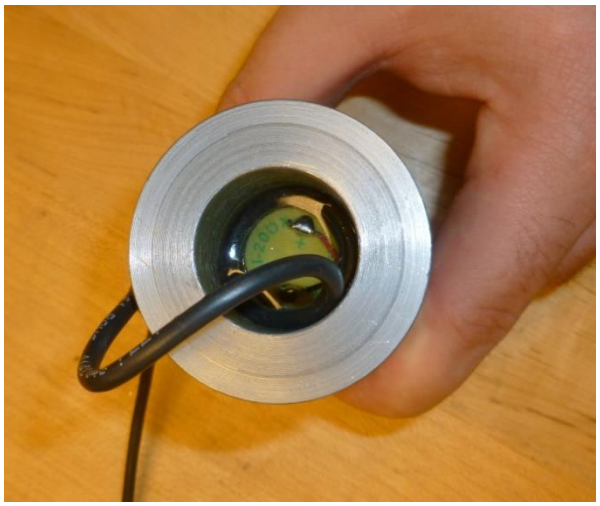

Figure 2-6 Geophone potted in push cone

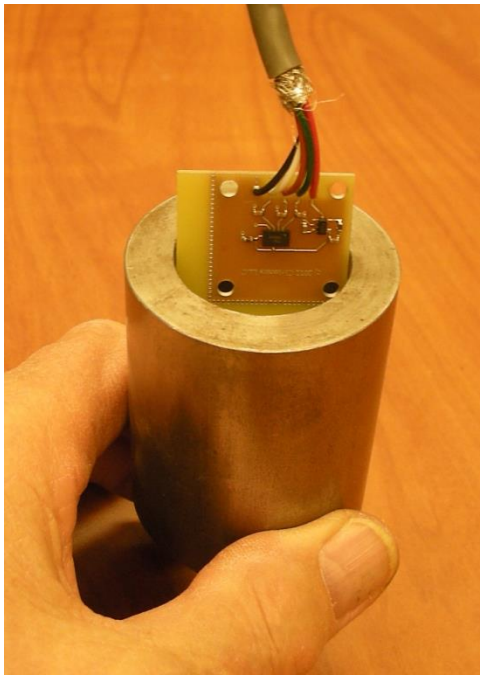

Figure 2-7 Accelerometer chip being fitted into push cone cavity

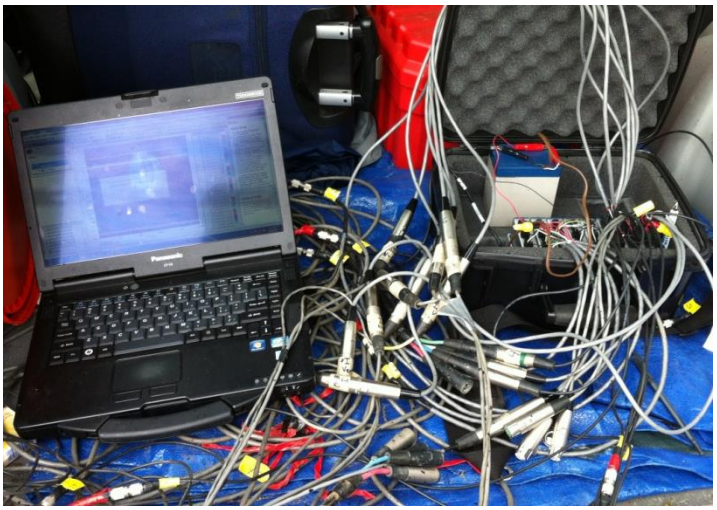

Figure 2-8 Data acquisition system and laptop

Figure 2-9 Installation of embedded sensors

2.3 Monitored Sites

The original proposal to MDOT suggested seven sites to be monitored for the developement of the simplified procedure to be more robust and to reduce uncertainty in measurements and data analysis. However, due to changes in the progress schedule the research team was able to visit and monitor 5 sites in total. The 112th Ave. over I-96 project was the first to visit and was used as a dry-run for the testing procedure as it consisted mostly by dense clayey soils (CL). Based on results from this first testing, buried geophone sensors were replaced with accelerometers to better capture the high level of vibrations very near the pile. The new system was used in all the other sites which consisted generally of loose to medium dense sands (SP & SW). Pile driving vibration data was collected at the following sites: (a) M-25 over Harbor Beach Creek, (b) M-66 over Wanadoga Creek, (c) M-139 over Dowagiac River and (d) US-131 over St. Joseph River.

MDOT provided soil profile and groundwater measurement information based on borings and laboratory testing that were performed for all the sites. From these soil profiles, N values were obtained for each of the sites. The research team measured the shear wave velocity (V_s) in-situ using the Multichannel Analyses of Surface Waves (MASW) method to have a better understanding of the characterization of the soil stratigraphy and also provide data for correlating V_s values with N blowcount values. The MASW shear wave velocities were used along with the blow count profile to develop the following V_s versus N equation:

$$V_s = 300.8\ N^{0.368} \qquad (2.1)$$

where:
V_s = shear wave velocity (ft./sec)
N = SPT Blow count

The fit of equation 2.1 with measured shear wave velocity is shown in Figure 2-10a. This MDOT site specific equation is compared in Figure 2-10b with a widely accepted similar equation by Imai and Tonouchi (1982). In the low blow count region (most important region for this research) in Figure 2-10b, the coincidence of the two curves is good. Equation 2.1 was then used along with the N profile to generate V_s profiles.

In the following figures the soil boring locations along with the proposed structure of the project and the location of the tested pile are presented. The soil condition based on the N values and V_s measurements and pictures for every site are also shown. The V_s profiles show more detail than the N profiles because the N profiles were simplified to minimize number of

significant strata for analyses. Table 2-2 presents piles and hammers that were used for every site tested.

Table 2-2 Piles and Hammers used in tested sites

Site	Pile Size	Pile length/Weld Section (ft)	Penetration (ft)	Hammer
M-25	HP 12x53	40	32.5	Pileco D30-32
M-66	HP 12x53	40/49.5	47.5	Delmag D16x32
M-139	HP 14x73	55	53	Pileco D30-32
US-131 A	HP 14x73	55	43	Delmag D30-32
US-131 B	HP 14x73	64.5	53.25	Delmag D30-32

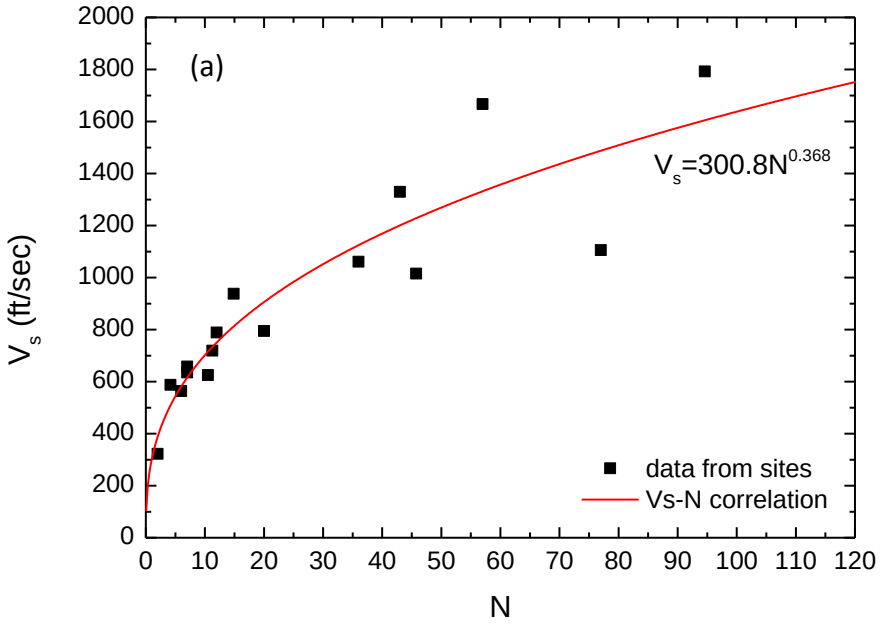

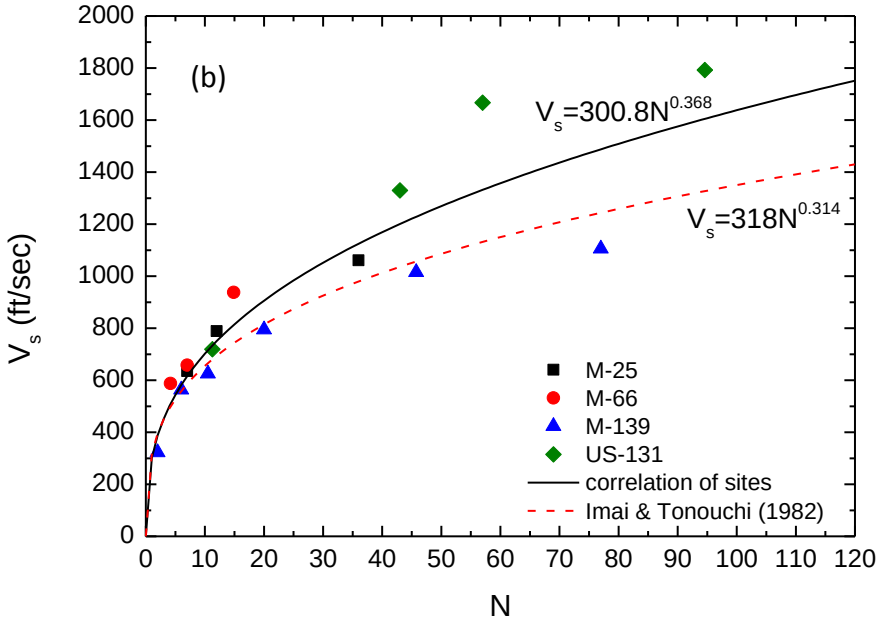

Figure 2-10 Shear wave velocity, V_s versus blow count, N, (a) Data from these sites and (b) comparison with accepted equation

a) **M-25 Site**

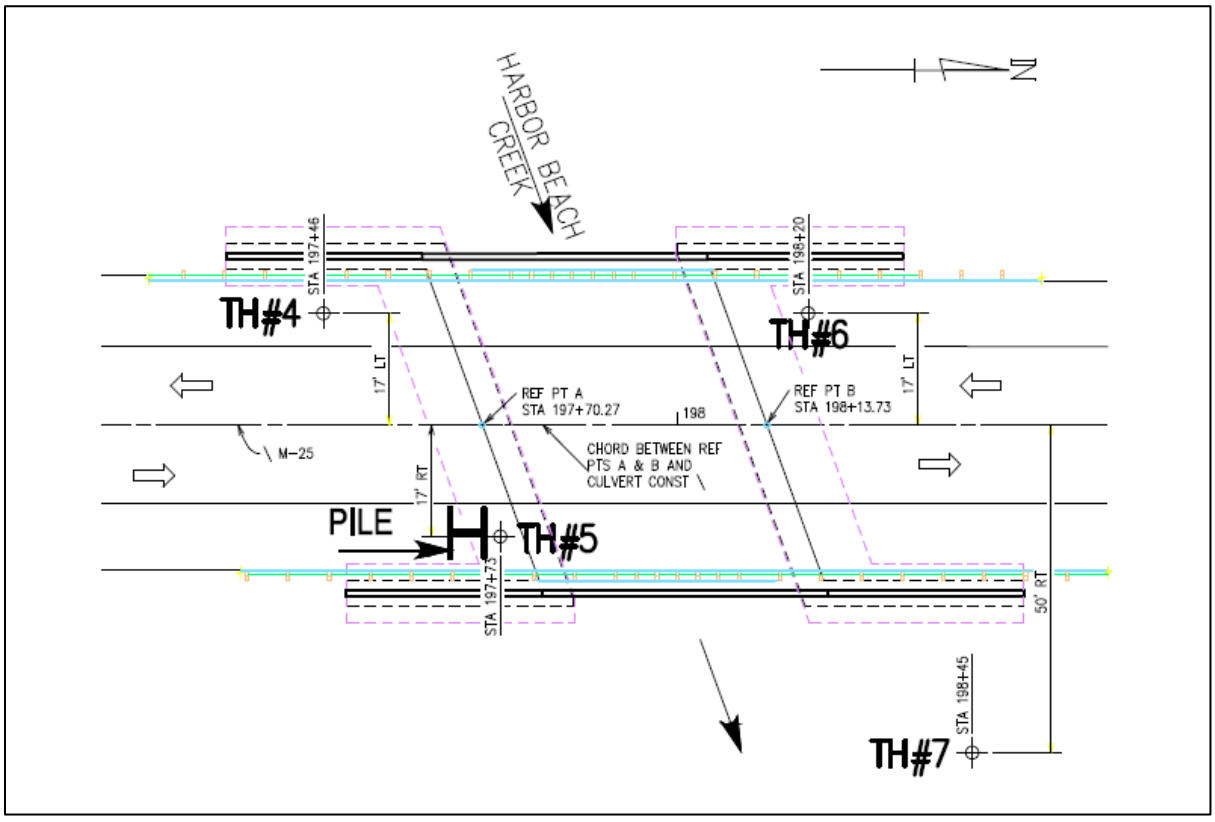

Figure 2-11 Locations of tested pile and test holes at M- 25 Site

Figure 2-12 Pile driving at M-25 site

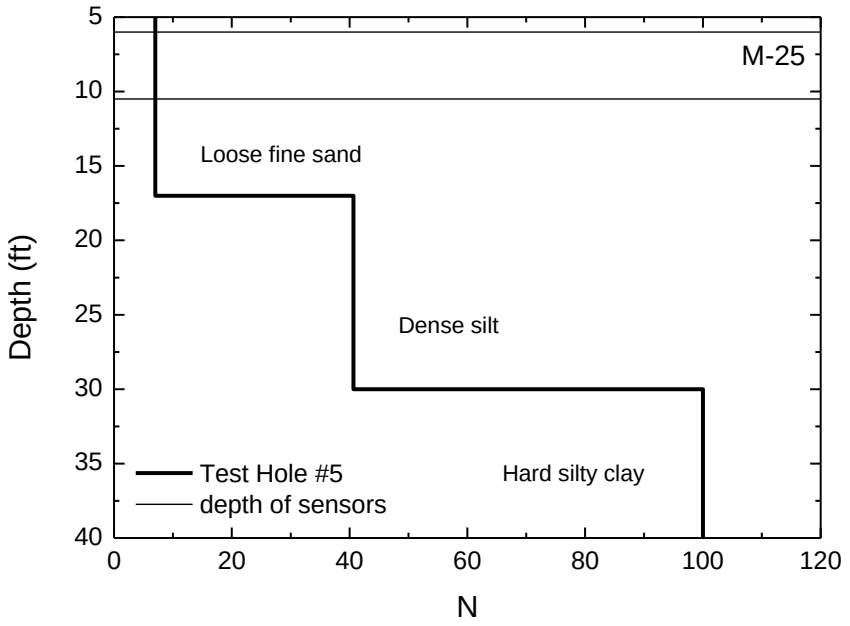

Figure 2-13 Blow count (N) profile for M-25 site

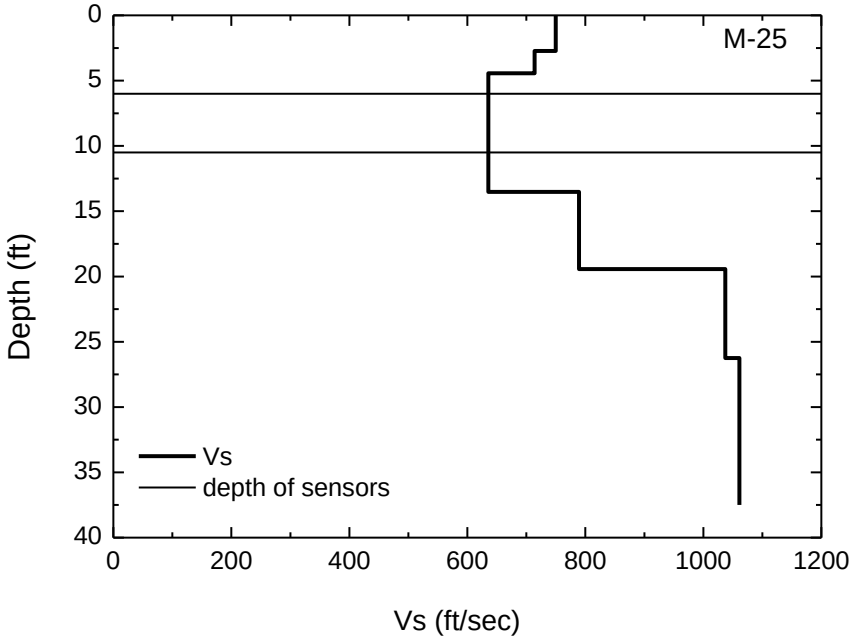

Figure 2-14 Shear wave velocity (Vs) profile for M-25 site

b) M-66 Site

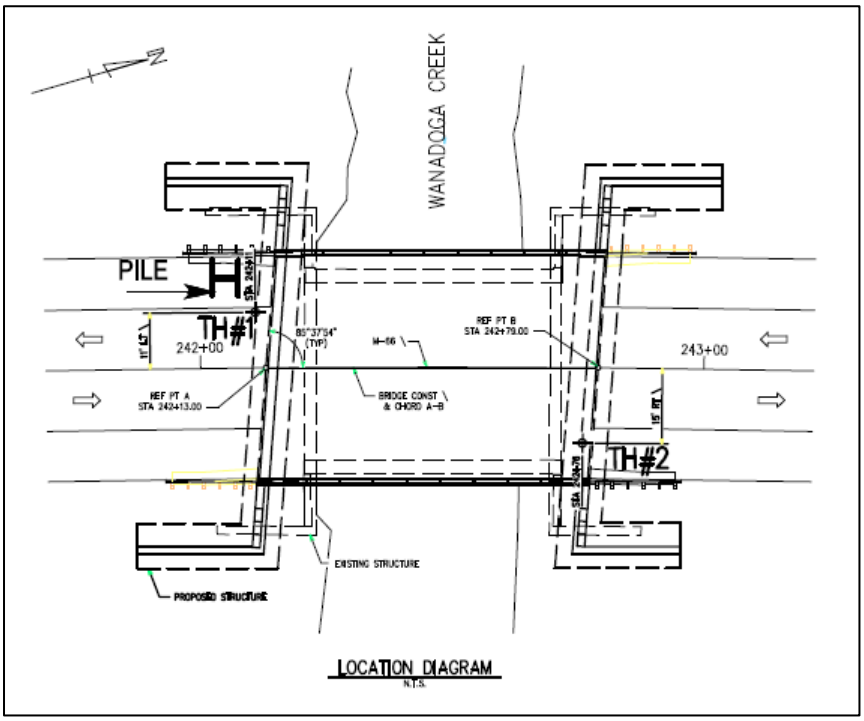

Figure 2-15 Locations of tested pile and test holes at M-66 Site

Figure 2-16 Welding second section of pile

Figure 2-17 Pile driving at M-66 site

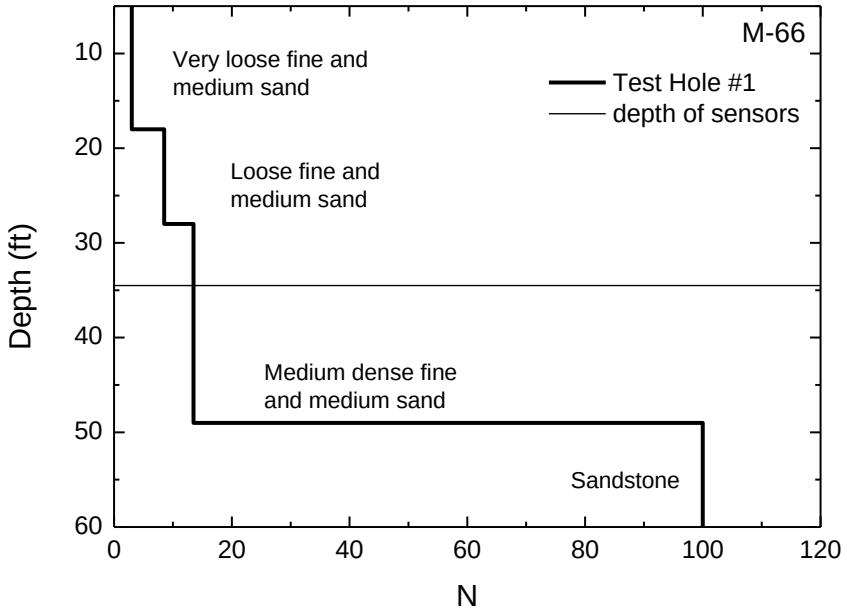

Figure 2-18 Blow count (N) profile for M-66 site

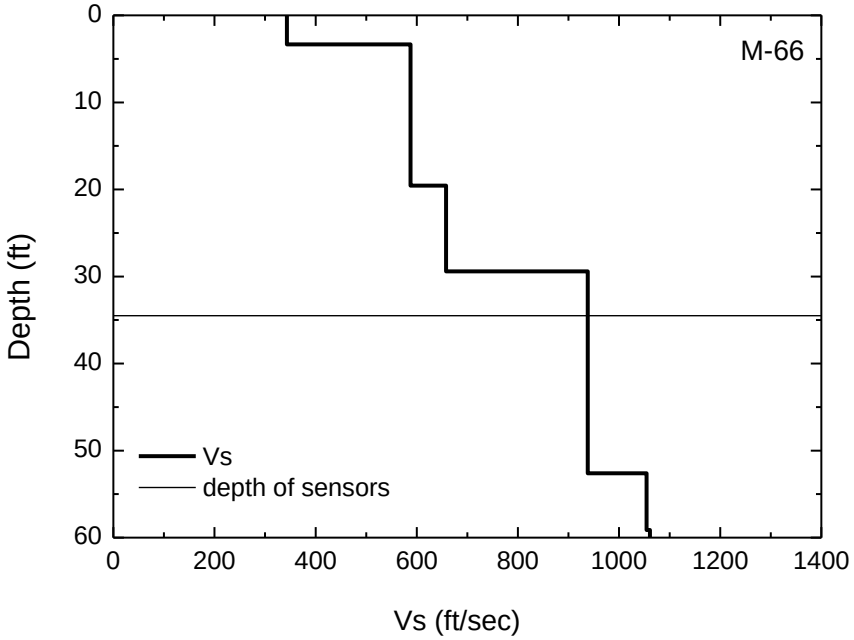

Figure 2-19 Shear wave velocity (Vs) profile for M-66 site

c) M-139 Site

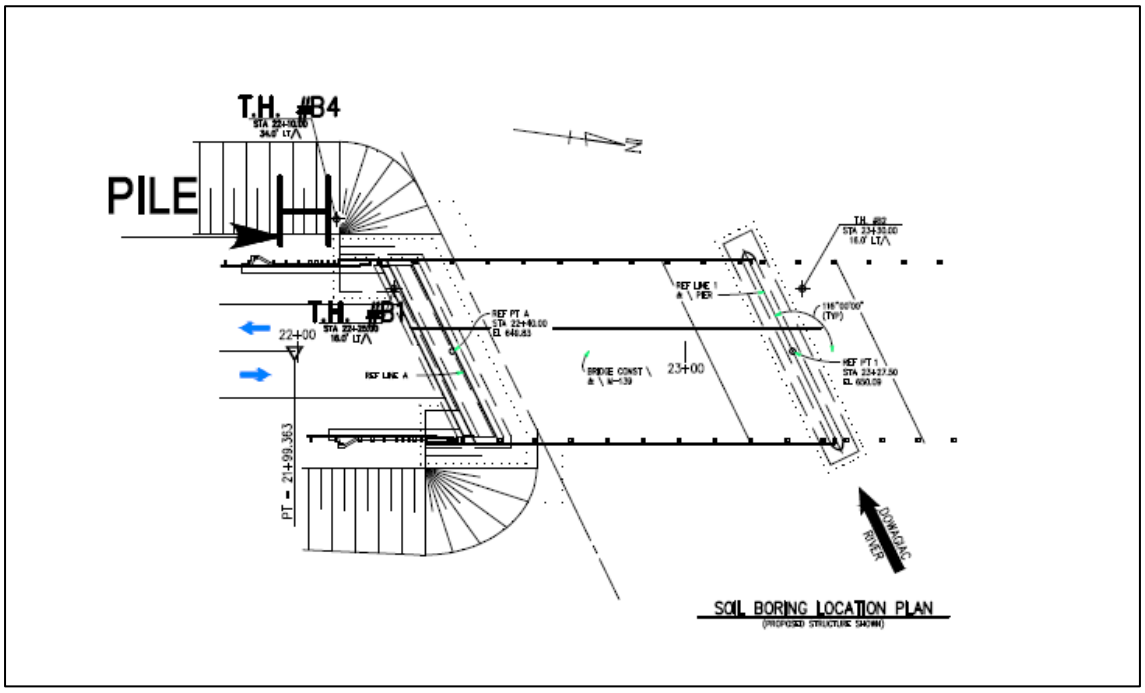

Figure 2-20 Locations of tested pile and test holes at M-139 site

Figure 2-21 Test pile after end of pile driving at M-139 site

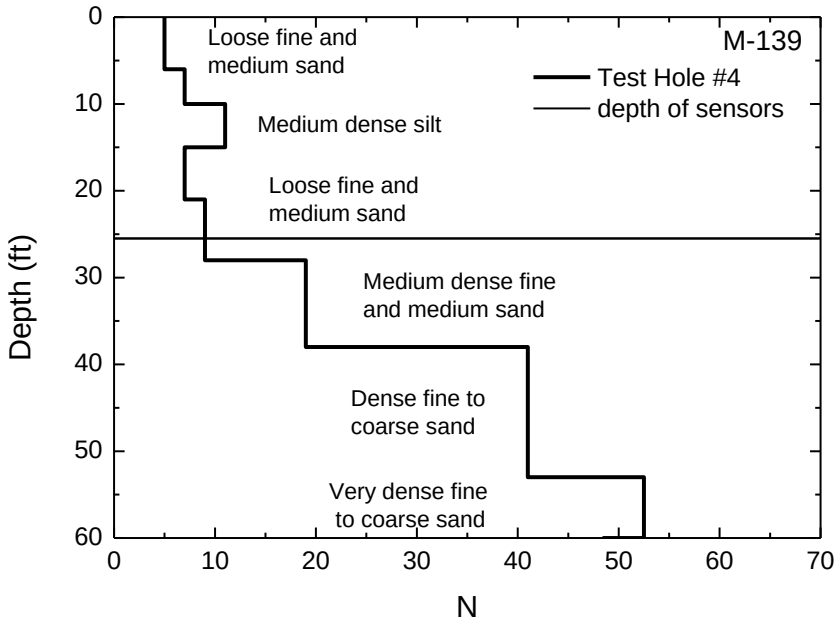

Figure 2-22 Blow count (N) profile for M-139 site

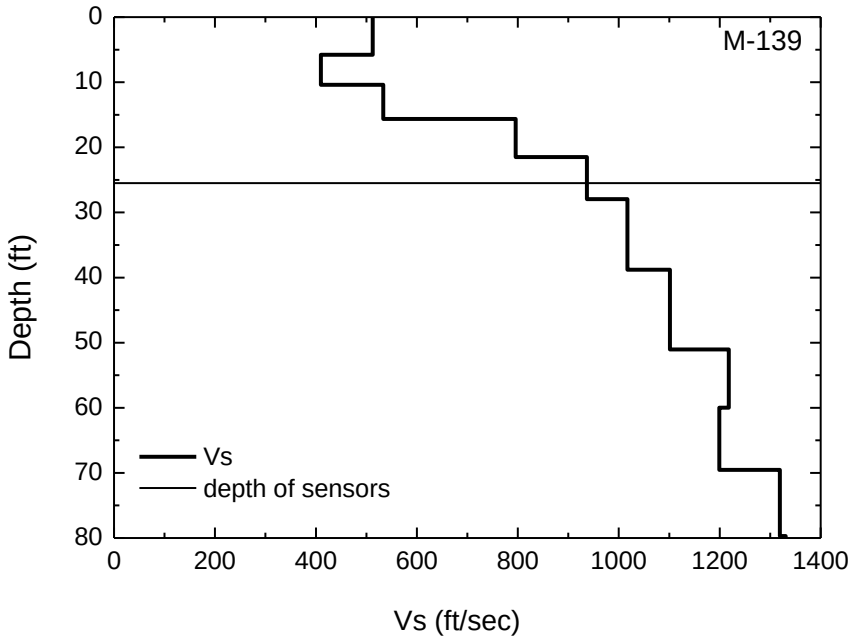

Figure 2-23 Shear wave velocity (Vs) profile for M-139 site

d) <u>US-131 Site (Abutment A)</u>

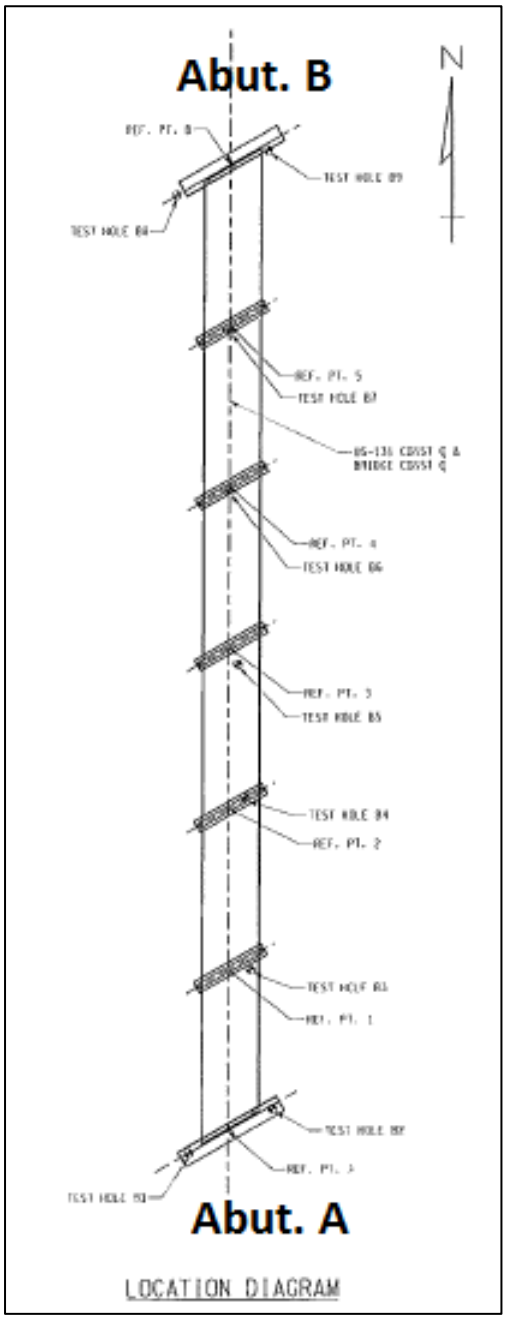

Figure 2-24 Locations of test holes at US 131 site

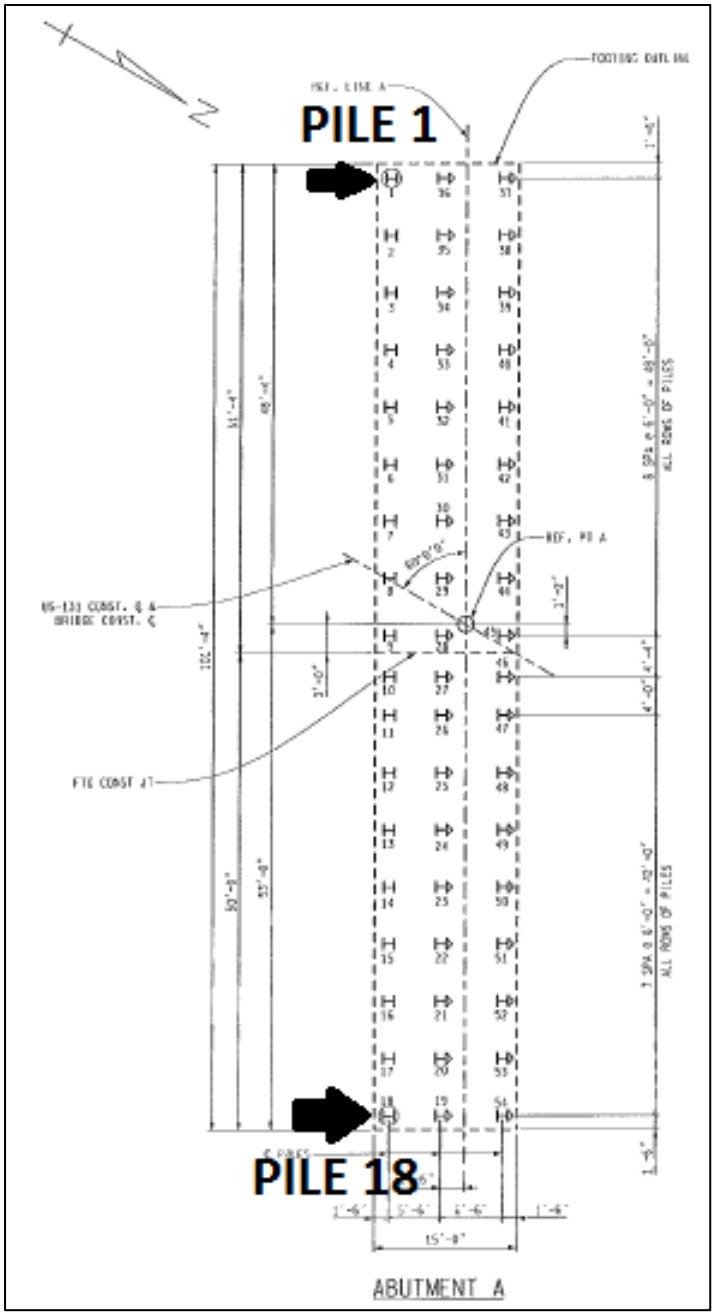

Figure 2-25 Locations of primary test pile #1 and secondary test pile #18 at US 131A site

Figure 2-26 Driving test pile #1 at US-131 A site

Figure 2-27 Test piles #1 & #18 after the end of driving at US-131 A site

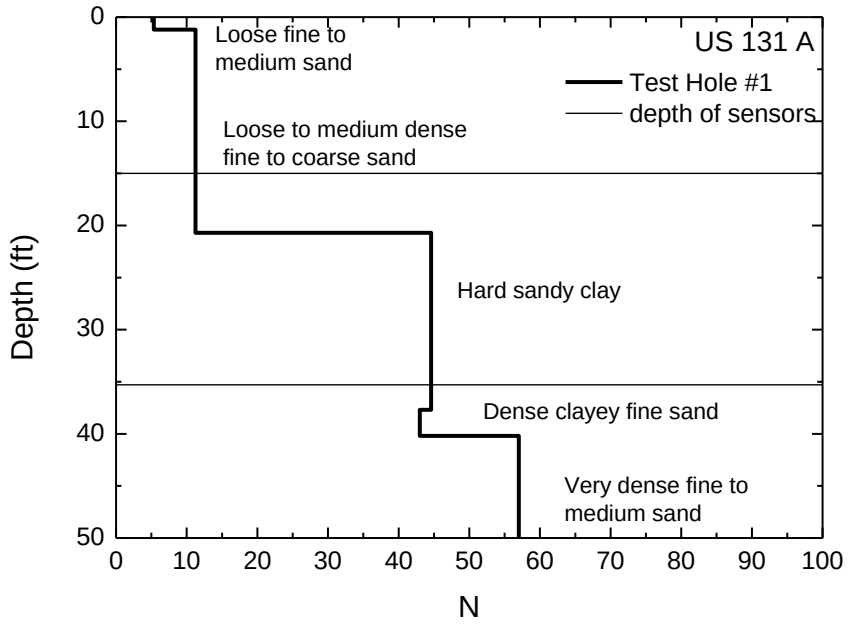

Figure 2-28 Blow count (N) profile for US-131 A site

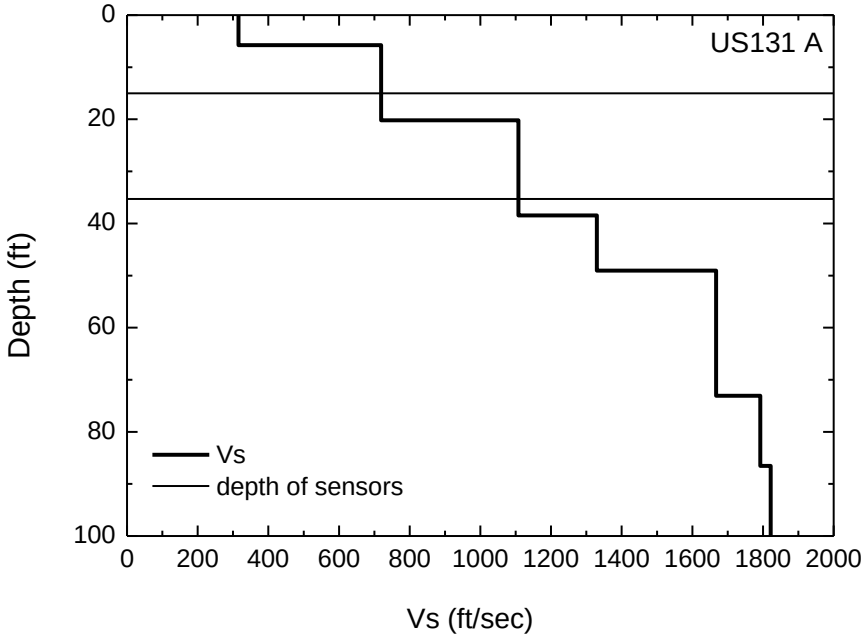

Figure 2-29 Shear wave velocity (Vs) profile for US-131 A site

e) US-131 Site (Abutment B)

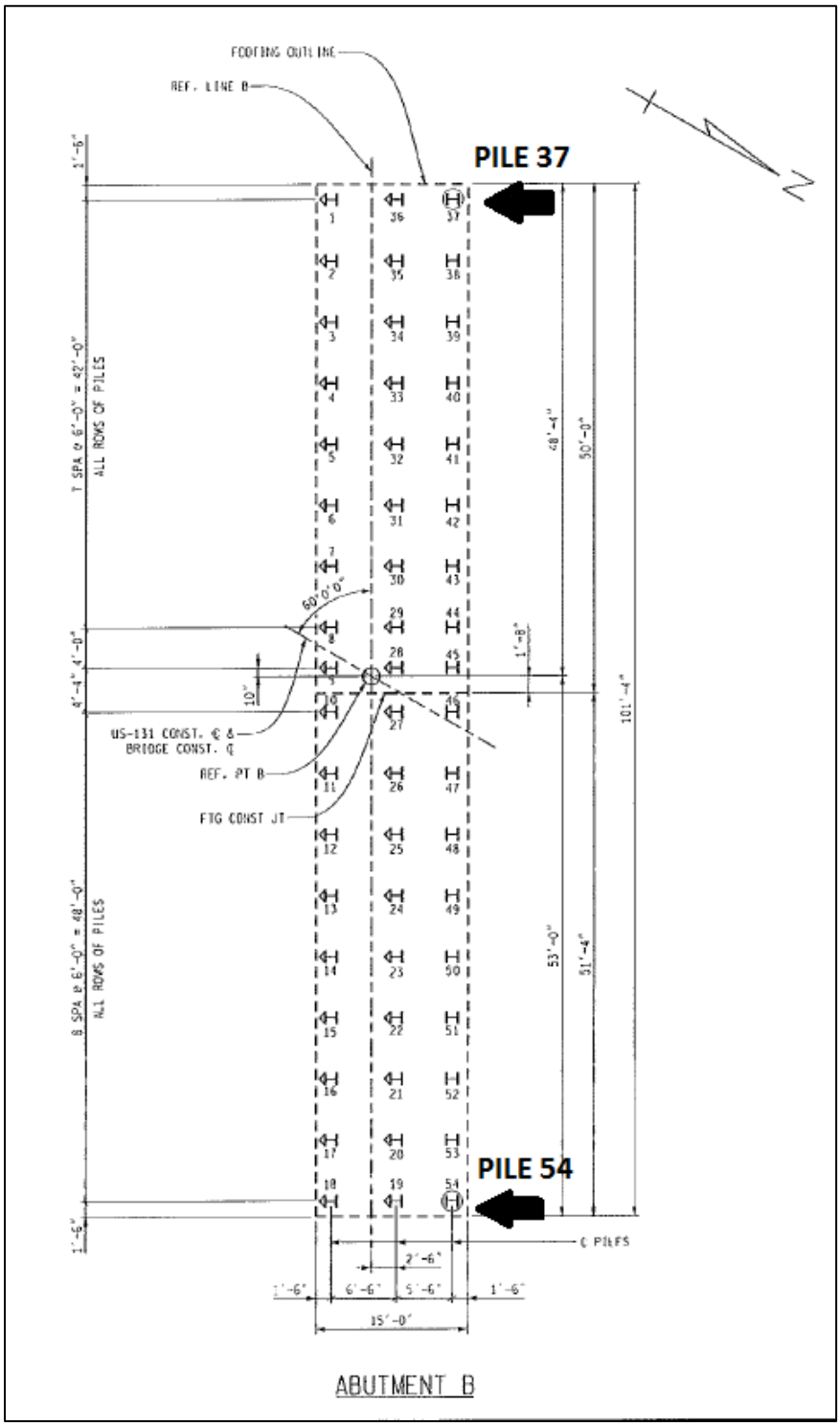

Figure 2-30 Locations of primary test pile #54 and secondary test pile #37 at US 131B site

Figure 2-31 Driving test pile #37 at US-131 B site

Figure 2-32 Cables of buried sensors at test pile #54 at US-131 B site

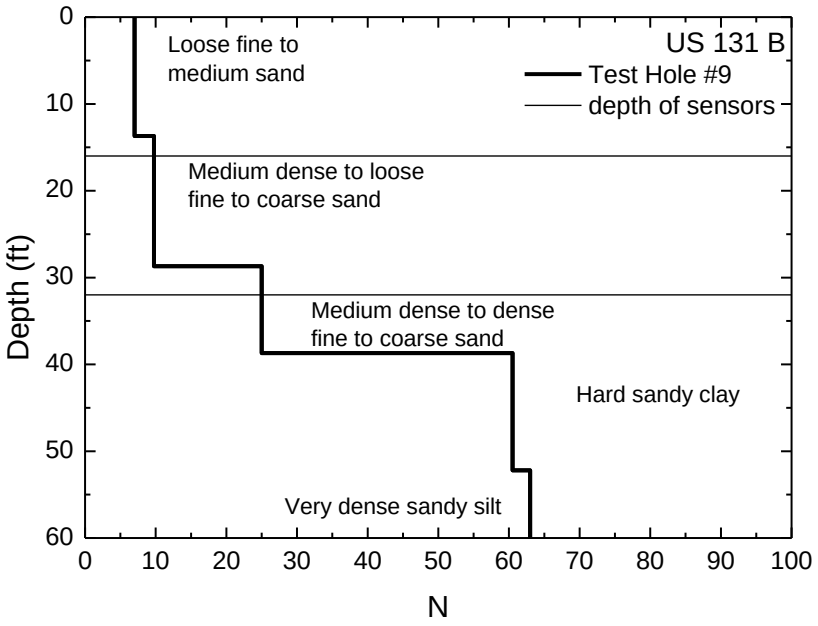

Figure 2-33 Blow count (N) profile for US-131 B site

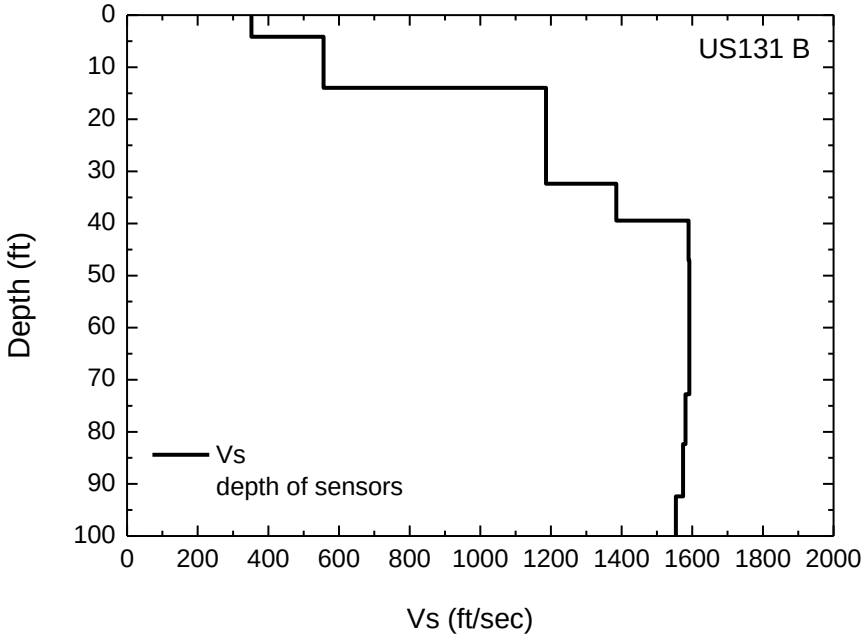

Figure 2-34 Shear wave velocity (Vs) profile for US-131 B site

3 GROUND MOTION MEASUREMENTS

3.1 Background

Each of the sites selected will be described separately with respect to data collection. Most significantly, contractors for three of the sites opted to drive a test pile rather than try to accommodate the sensor installation and controlled pile driving on a production pile. This turned out to be both good and bad. On the good side, it was much easier to spend significant time required on installation of the sensors when out of the way of the contractor's operations. On the bad side, it gave the perception to the contractor that timing of the testing was not important when it was very significant from the settlement observation viewpoint. Other significant differences resulted from the specific construction operations taking place at the site at any time, the extent to which construction had progressed, elevation of the location of the test pile with regard to the elevation of the production piles and, certainly, soil conditions at each site.

3.2 M-25 Over Harbor Beach Creek

The work at this site consisted of replacing the Harbor Beach Creek crossing while M-25 was detoured. The site soils consisted of loose sand (SP) in the upper reaches and dense silt (ML) and silty clay (CL) at depths below about 17 ft., see simplified soil profile Figure 3-2. It was the intent to place three sensor cones in the loose fine sand at a depth of about 6-7 ft. Two sensors were placed at that depth (A2 and A3), but the third (A4) could not be seated and had to be pushed to 10 feet before seating. A second level of sensors was intended to be installed at about 25 ft. Inexperience in pushing the cones and dense soil conditions led to loss/breaking of two sensor cones in the attempt to set them and none were placed at a depth of 25 ft. The resulting plan and elevation views showing the installed sensors for this site are shown in Figure 3-1. Geophones were placed along the surface of the ground at 10 ft. intervals in a straight line south from the pile to a distance of 60 ft.

The contractor opted at this site to drive a test pile which was driven from the ground elevation approximating the roadway elevation and near the location of the test hole #5, Figure 2-11. The flange side of the H-pile was facing south and all horizontal distance measurements are referenced to this pile face. The contractor had installed sheet piling to form bulkheads on each side of the creek before research engineers arrived at the site. Driving the sheet piles was not monitored so contributions to settlement of the loose sand near the surface caused by

sheet-pile driving could not be assessed. Before and after driving elevations were determined at the test pile only, showing no settlement.

Because of the loose condition of the sand near the ground surface the first few (≈3) blows drove the pile more than 12 ft., far below the sensor cones. This precluded obtaining ground motion measurements at the desired three horizontal distances from a pile tip when the pile tip was at the depth of the sensor cones (6-10 ft.). However, ground motion data was obtained for the three sensor cones at 6-10 ft. for pile tip depths from about 12 ft. to about 32 ft. Vertical accelerations from each of the three sensor cones are shown in Figure 3-3. In this figure, ground motion is plotted as g (English units: 1g = 32.2 ft./sec^2). Maximum acceleration in each foot of pile penetration is plotted at the mid-depth of each foot of pile penetration.

3.3 M 66 over Wanadoga Creek

Work at this site consisted of replacing the bridge over Wanadoga Creek, while detouring traffic on M-66 in both directions. The contractor chose to drive a test pile near the location of test hole TH#1 shown in Figure 2-15. An additional section of pile was spliced on the pile when the pile tip was at a depth of about 36 feet. The flange side of the H-pile was facing south and all horizontal distance measurements are referenced to this pile face. The simplified soil profile shown in Figure 3-5 reveals very loose to medium dense sand (SP) to a depth of about 50 ft. where sandstone was encountered. The contractor had installed sheet piling to form bulkheads on each side of the creek before research engineers arrived at the site. Driving the sheet piles was not monitored so contributions to settlement of the loose sand near the surface caused by sheet-pile driving could not be assessed.

All sensors identified with A are accelerometers, with BG and G are surface geophones and with SG are small buried geophones. Three attempts to seat triaxial accelerometer sensor cones at a depth of about 15 ft. failed but one geophone sensor (SG) cone was successfully seated at a depth of about 5 ft. Successful triaxial accelerometer sensor cone installations were achieved at a depth of about 34 ft. in the medium dense sand (SW). Figure 3-4 shows sensor cone installations in plan (Figure 3-4a) and elevation (Figure 3-4b). Vertical acceleration of the sensors versus depth of the pile tip is shown in Figure 3-6 for the three sensor cones (A1, A2, A3) at about 34 ft. deep.

Six ground surface geophones were also placed along the ground to the south of the pile at locations shown in Figure 3-7. The two closest geophones (BG1 and BG2) were triaxial configurations while the further out (G1, G2, G3, G4) were single vertical sensing geophones.

Vertical peak particle velocity (PPV) or ż (in/sec) versus depths of the tip of the pile is shown for all surface geophones in Figure 3-8.

3.4 M-139 over Dowagiac River

Work at this site consisted of replacing the bridge on M-139 over the Dowagiac River by alternately shutting one lane over the bridge while allowing traffic on the other lane. The soil profile for this site is shown in Figure 3-10 and consists principally in loose granular material (SP-SW) to a depth of about 30 ft. and sands grading to dense and very dense (SW) to a depth of about 60 ft.

The attempt to seat a sensor at a depth of 25 ft. resulted in a stoppage (unknown cause) at 11.5 ft. and 6 in. from the pile face. Installation of a second sensor cone was successful at a depth of 10.5 ft. but with great difficulty. Installation of sensor cones A3, A4, and A5, proceeded successfully providing a three sensor array at about a 25.5 ft. depth, Figure 3-9. Because of the loose condition of the near surface sand, no further attempt was made to set shallow sensor cones at intermediate and long distance from the pile. Figure 3-9 shows the plan and elevation locations of the buried sensor cones as well as the surface geophones for the M-139 site.

The contractor had installed sheet piling to form cofferdams for driving piles on both sides and in the middle of the river for the new northbound lanes before research engineers arrived at the site. Driving the sheet piles was not monitored but significant settlement was observed at the south approach to the bridge on the southbound lane due to sheet pile driving that had already occurred.

The test borings for this site were started from an elevation that represents the old bridge deck elevation. The test pile that the contractor opted to drive was driven from an elevation about 6 feet below the old bridge deck elevation. MDOT drillers made a test hole, TH#4, at this site after the test pile had been driven and near to the test pile (Figure 2-20).

Vertical acceleration of the sensors versus depth of the pile tip is shown in Figure 3-11 for the three sensor cones at about 25 ft. deep. Figure 3-12 shows the vertical surface particle velocity, ż, versus the pile tip elevation during driving.

3.5 US-131 South (Abutment A) new bridge over St. Joseph River

Work at this site consists of construction of a new, two-lane bridge over the St. Joseph River near Constantine, Michigan. The contractor had been on site and constructed several sheet-pile cofferdams before the research engineers arrived on site. The contractor chose to use a

production pile for the test pile and chose pile #1 in the abutment A foundation, Figure 2-25. Test hole #1, Figure 2-24, was closest to pile #1. A trench for construction of the abutment was excavated to the depth of the bottom of the abutment A foundation (pile cap) from which the pile would be driven. The soil profile adjusted for this excavation is shown in Figure 3-14. This site consists of about 20 ft. of medium dense sand (SW) over hard sandy clay (CL) to about 40 ft. and dense clayey fine sand (SC) to 50 ft. The pile was driven to a depth of about 45 ft.

Installation of two rows (depths) of three sensors was accomplished at this site. Figure 3-13 shows the plan and elevation views of this site with transducers identified. At this site, a geophone sensor cone, SG1, was incorporated in the mix to compare with the triaxial accelerometer sensor cone, A3 for consistency. Figure 3-15 and Figure 3-17 show ż versus depth of tip of pile for the shallow (16 ft.) sensors and deep (35 ft.) sensors respectively. Surface geophone locations are shown in Figure 3-18 and Figure 3-19 shows the PPV versus pile tip elevation for the surface geophones while driving pile #1. Similar plots are shown in Figure 3-20 and Figure 3-21 while driving pile #18.

3.6 US-131 North (Abutment B) new bridge over St. Joseph River

Work at this site consists of construction of a new, two-lane bridge over the St. Joseph River near Constantine, Michigan. The contractor had been on site and constructed several sheet-pile cofferdams before the research engineers arrived on site. The contractor chose to use a production pile for the test and chose pile #54 in the abutment B foundation, Figure 2-30. Test hole #9, Figure 2-24, was closest to pile #54. A trench for construction of the abutment was excavated to the depth of the bottom of the abutment B foundation (pile cap) from which the pile would be driven. The soil profile adjusted for this excavation is shown in Figure 3-14. This site consists of about 40 ft. of loose to medium dense sand (SW) over hard sandy clay (CL) to about 50 ft. and very dense sandy silt (ML) to a depth of about 70 ft. The pile was driven to a depth of about 55 ft.

At this site an attempt was made to determine if there was any difference between energy transfer from the pile to the surrounding soil from the open face of the H-pile and the flange face of the H-pile. Figure 3-22 shows the plan and elevation locations of the sensor cones relative to the pile to be driven. Note: the pile was driven askew of the intended orientation and that may have led to loss of the two close-in sensor cones (A1 and A2). Figure 3-24 shows ż versus pile tip depth for the four sensors at a depth of about 16 ft. and Figure 3-26 the same for sensors at a depth of 32 ft. Surface geophone locations are shown in Figure 3-27 and Figure 3-28 shows the PPV versus pile tip elevation for the surface geophones while driving pile #54. Similar plots are shown in Figure 3-29 and Figure 3-30 while driving pile #37.

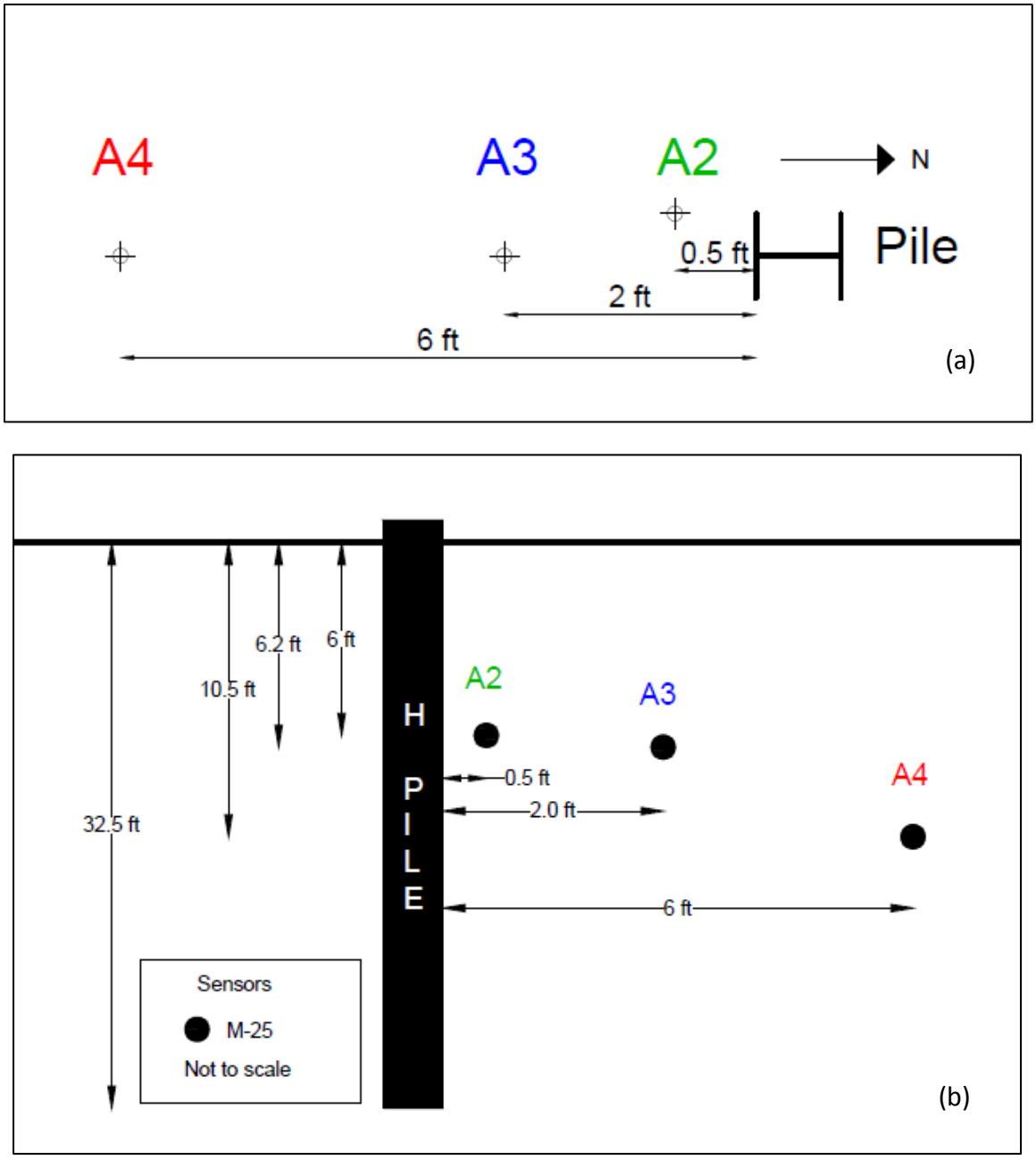

Figure 3-1 Plan (a) and elevation (b) views of embedded sensor cones at M-25 site

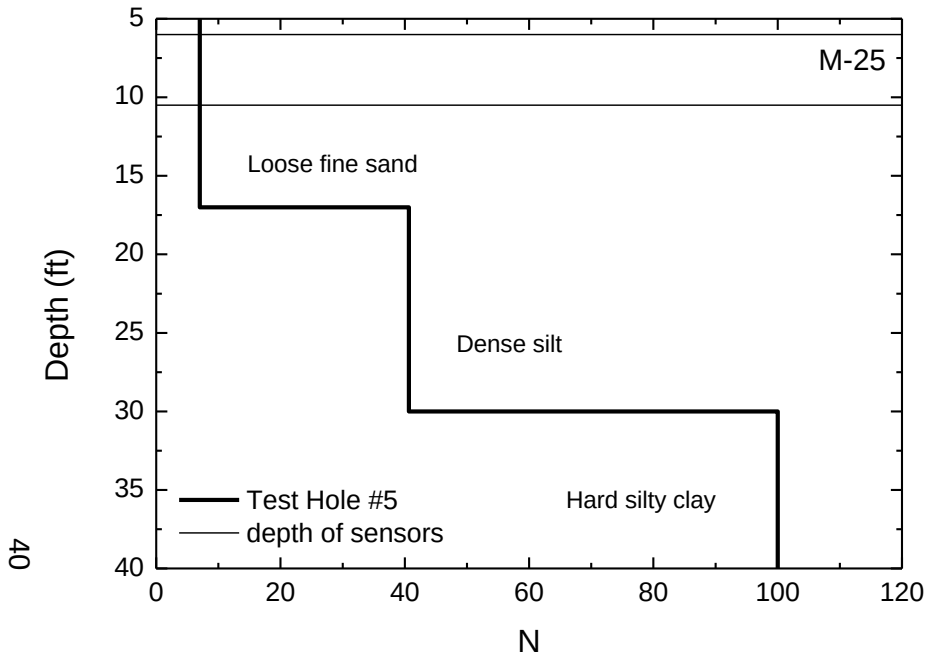

Figure 3-2 Simplified soil profile, M-25 site

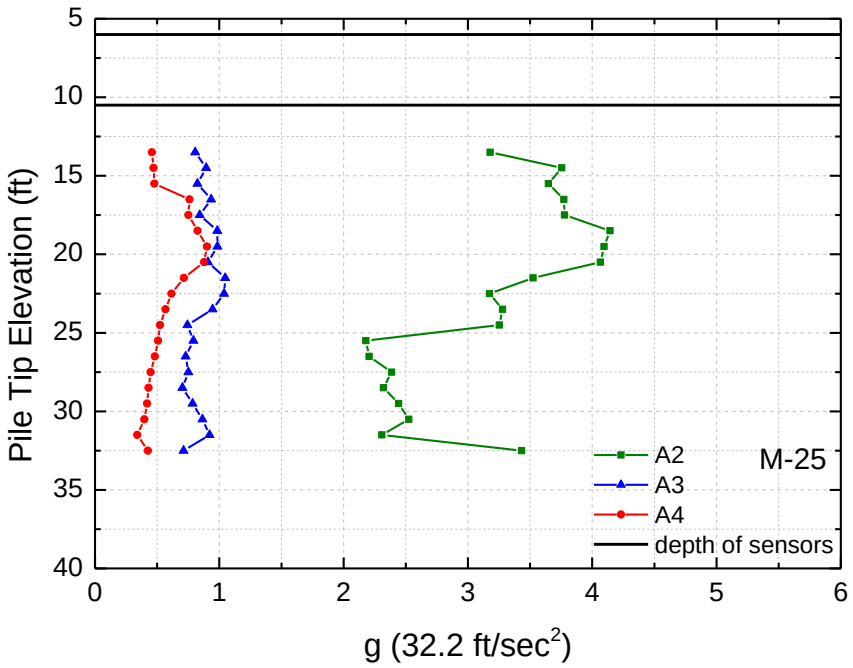

Figure 3-3 Vertical acceleration versus pile tip depth for embedded sensor cones at M-25 site

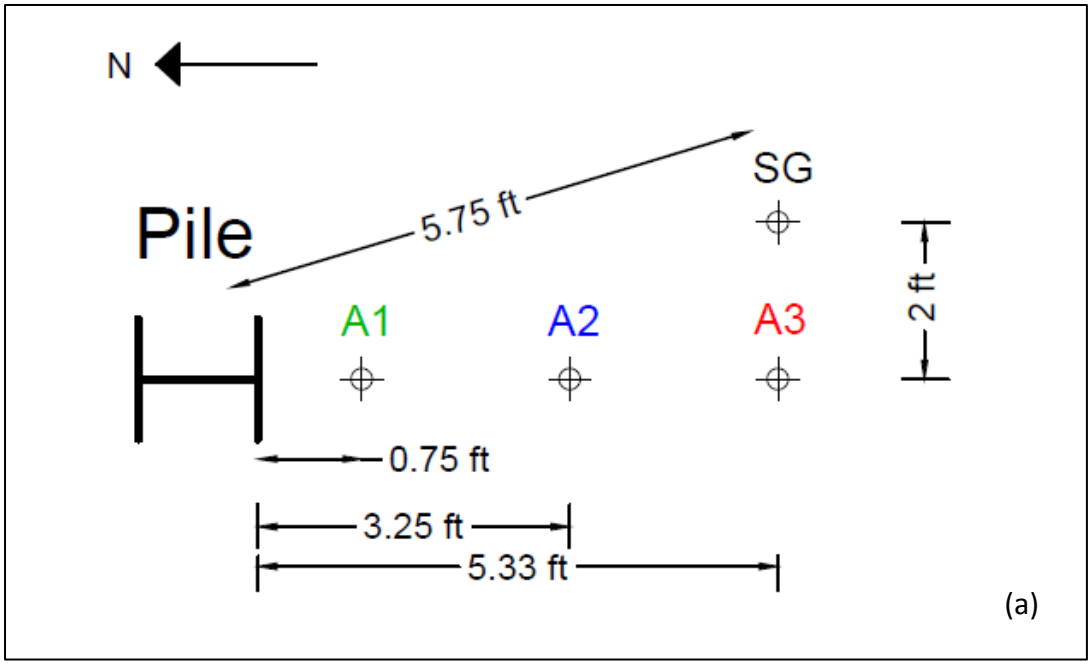

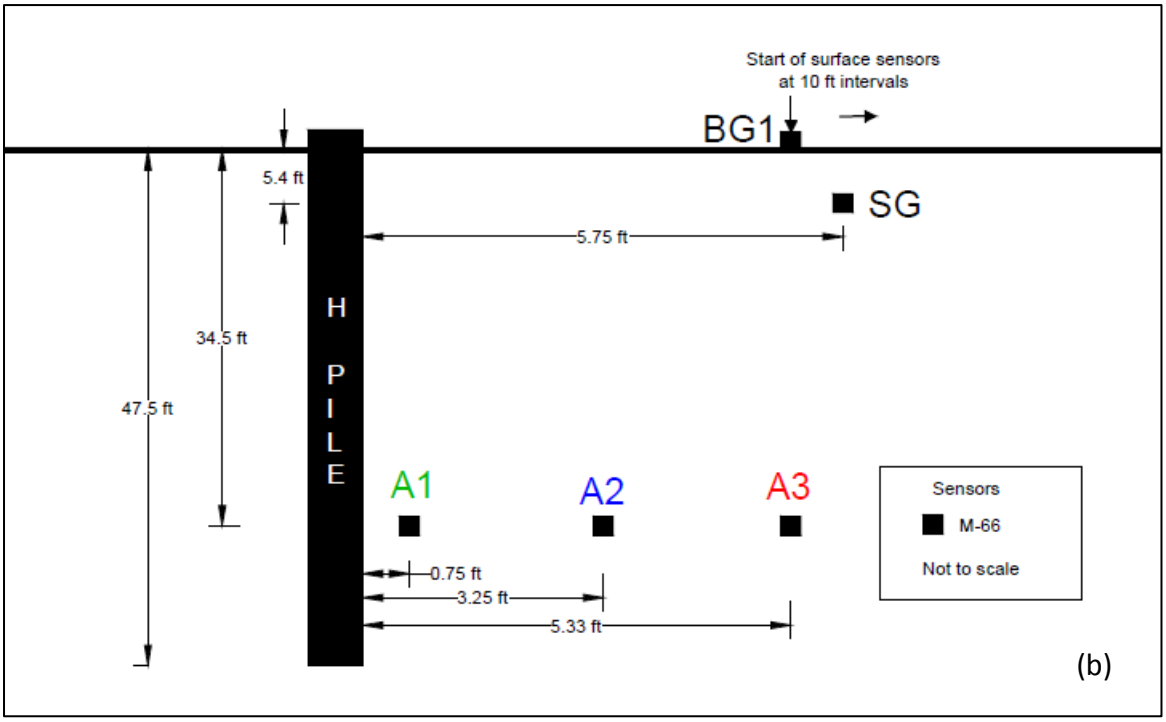

Figure 3-4 Plan (a) and elevation (b) of embedded sensor cones at M-66 site

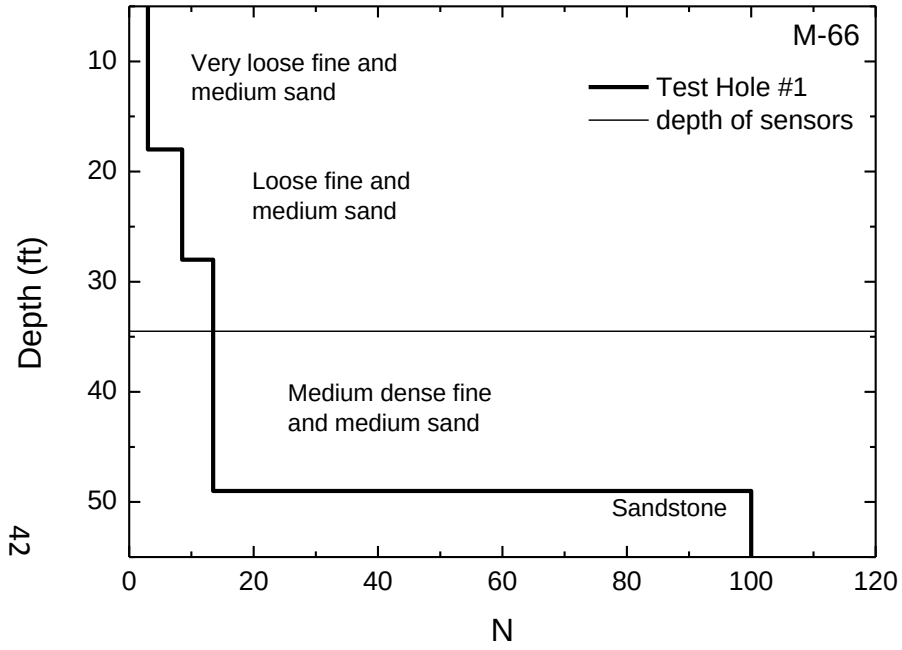

Figure 3-5 Simplified soil profile at M-66 site

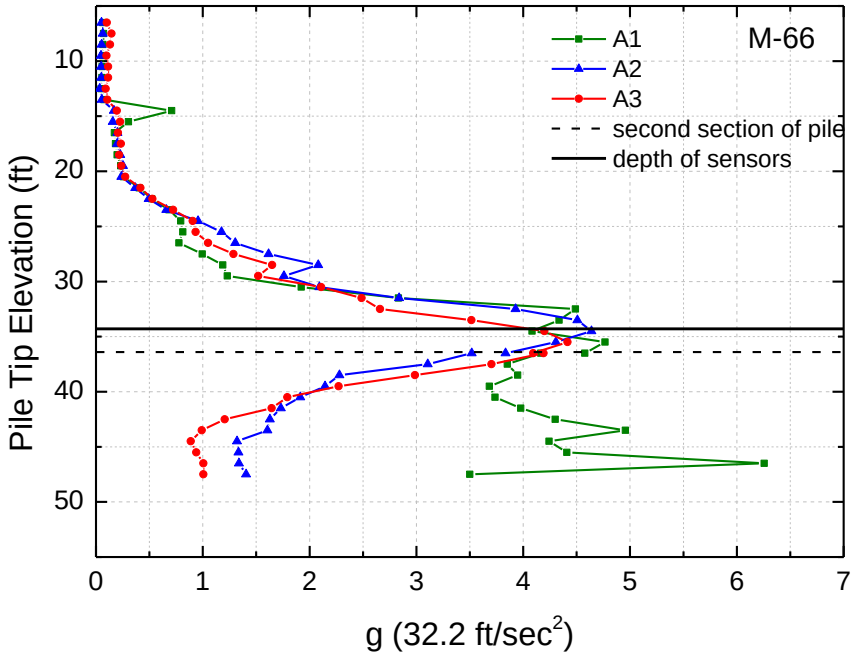

Figure 3-6 Vertical acceleration of embedded sensor cones versus pile tip depth at M-66 site

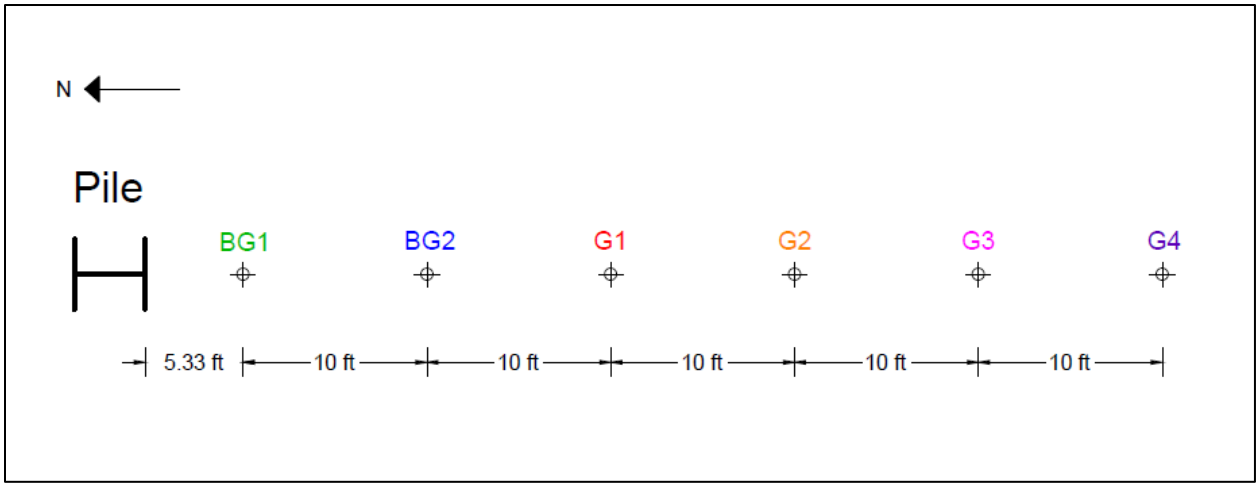

Figure 3-7 Plan view of ground surface array of geophones at M-66 site

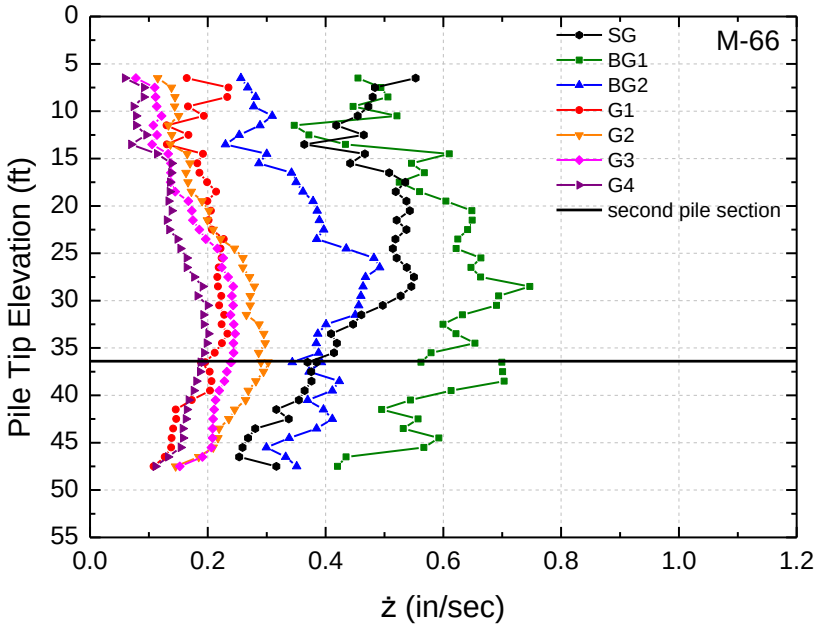

Figure 3-8 Peak vertical particle velocity, ż, versus pile tip depth for surface geophones at M-66 site

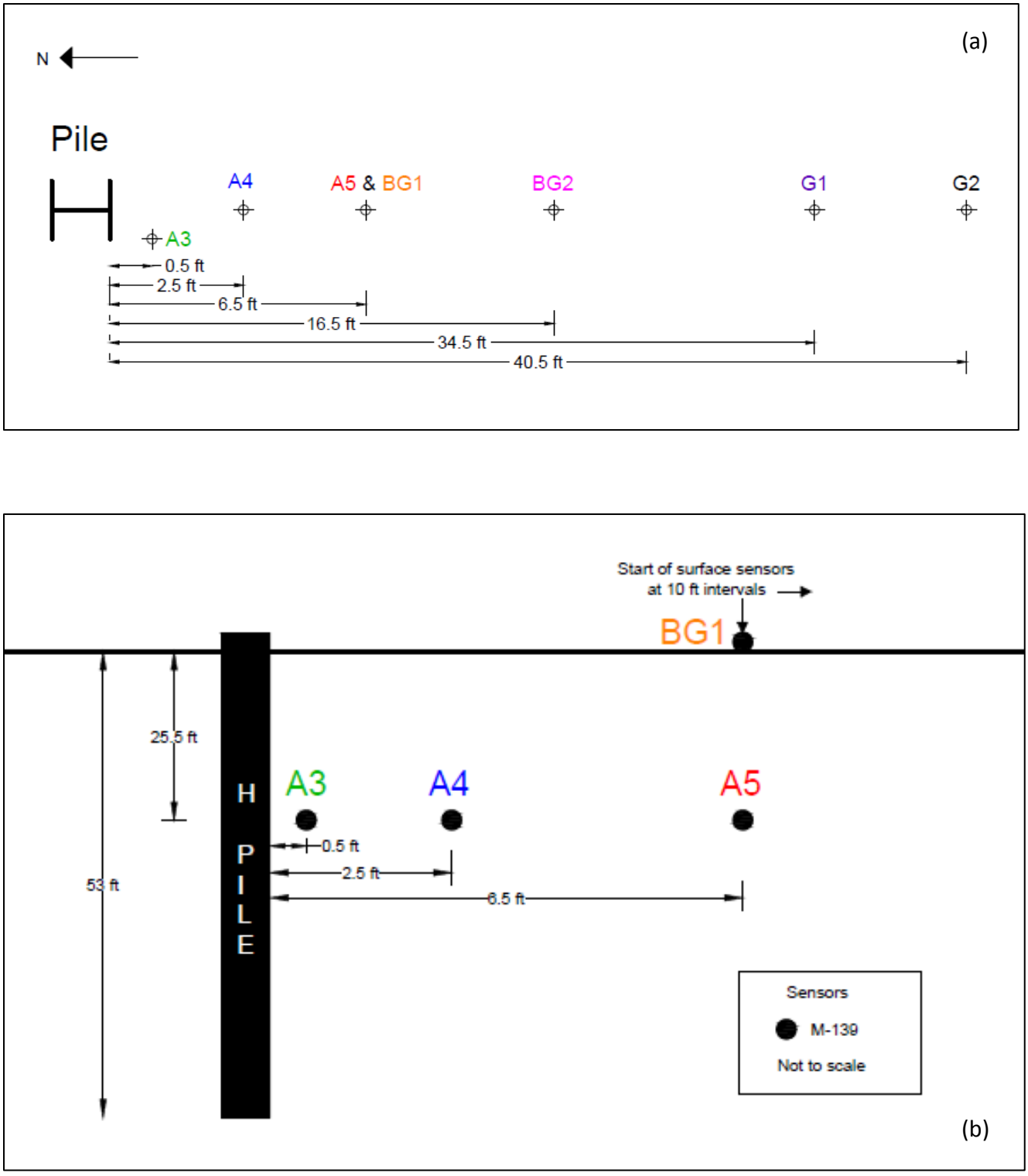

Figure 3-9 Plan (a) and elevation (b) views of embedded sensor cones and surface geophones at M-139 site

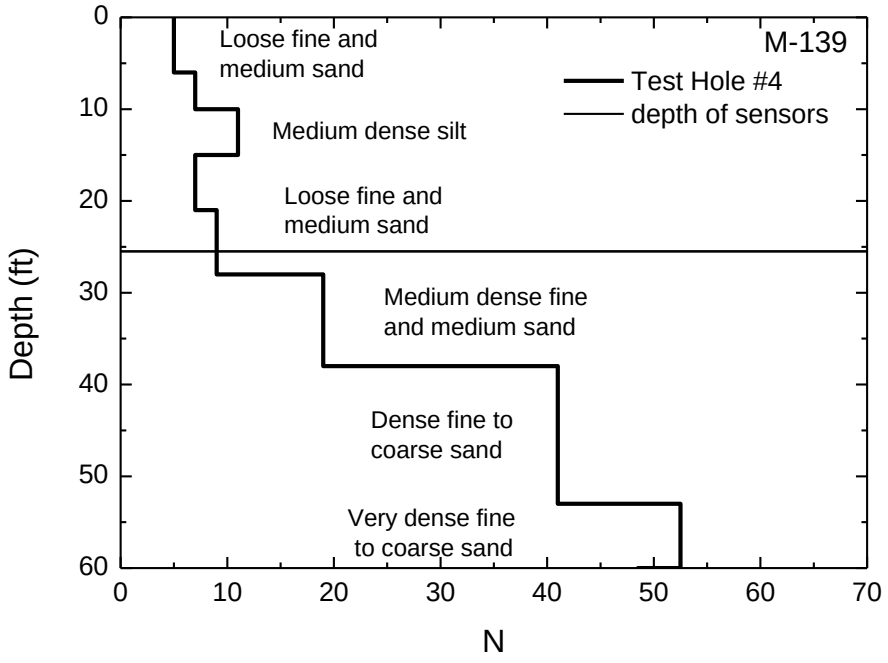

Figure 3-10 Simplified soil profile at M-139 site

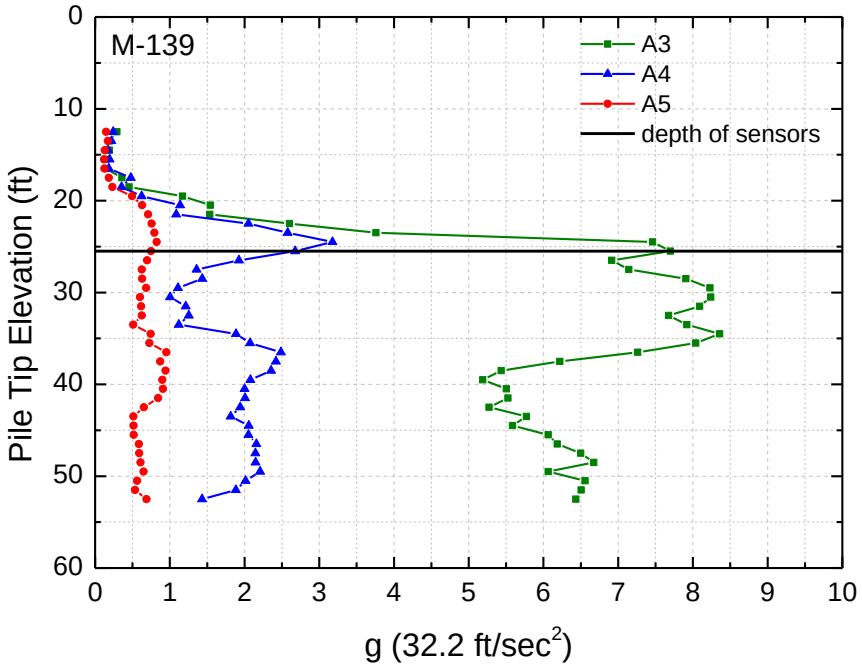

Figure 3-11 Vertical acceleration versus pile tip depth for embedded sensor cones at M-139 site

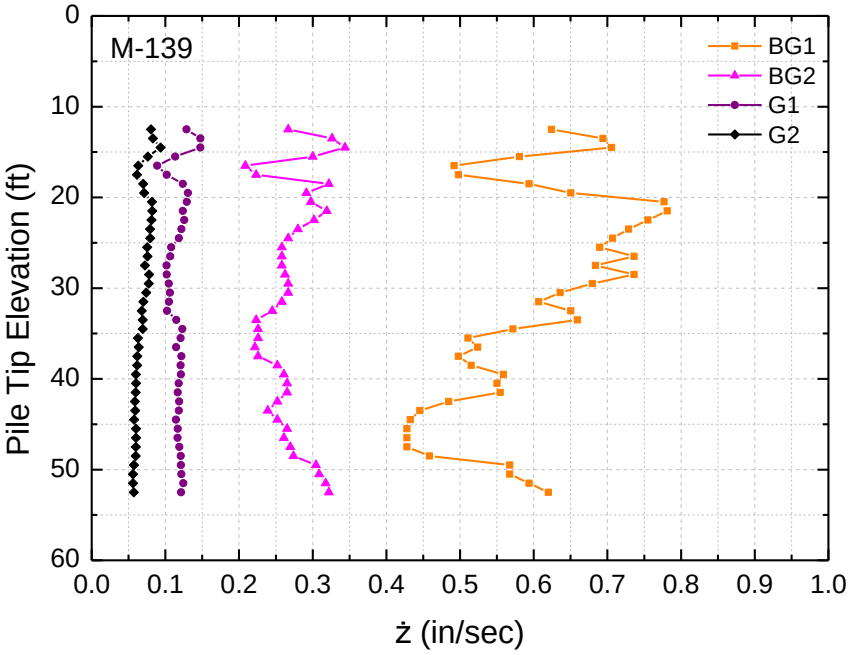

Figure 3-12 Peak vertical particle velocity versus pile tip depth for surface geophones, M-139 site

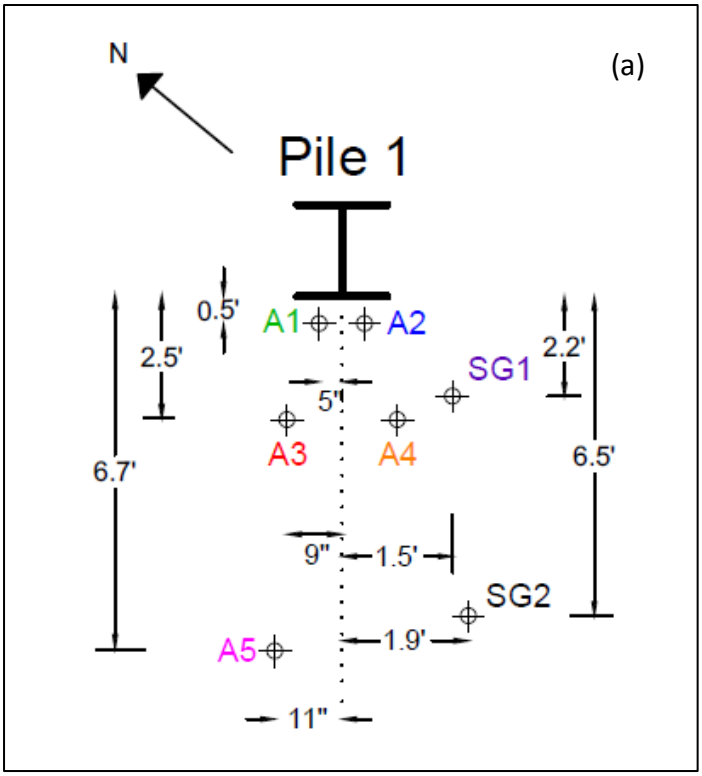

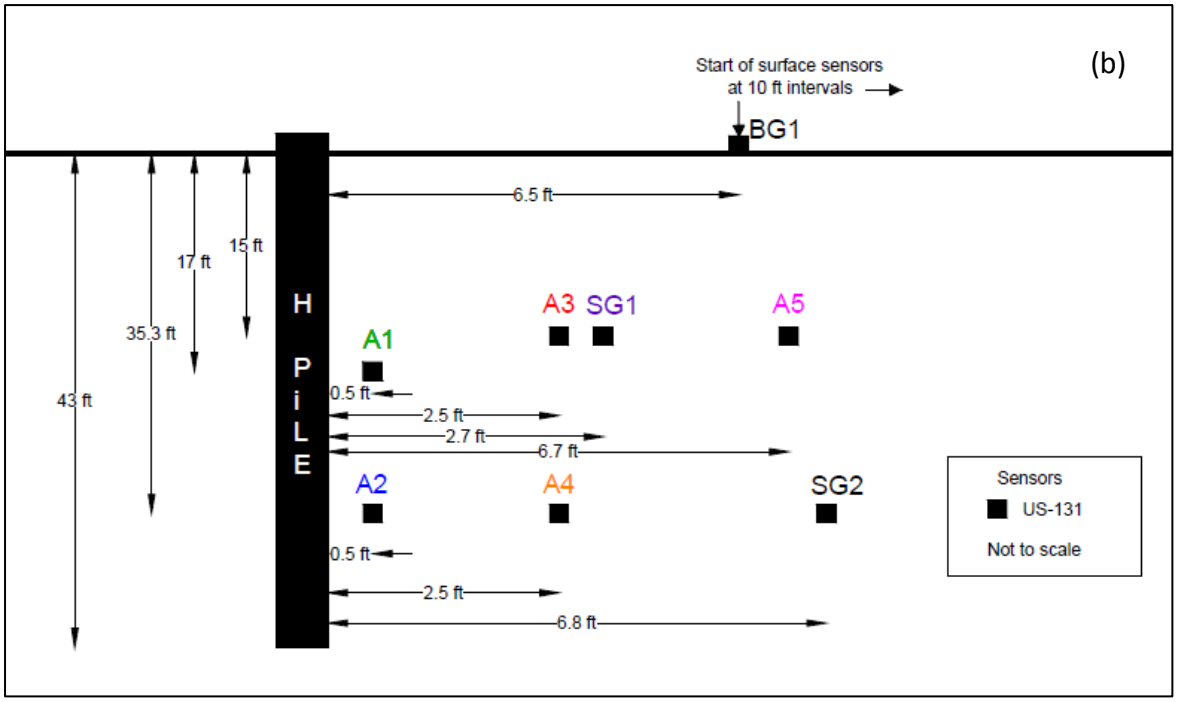

Figure 3-13 Plan (a) and elevation (b) views of embedded sensor cones at US 131A site

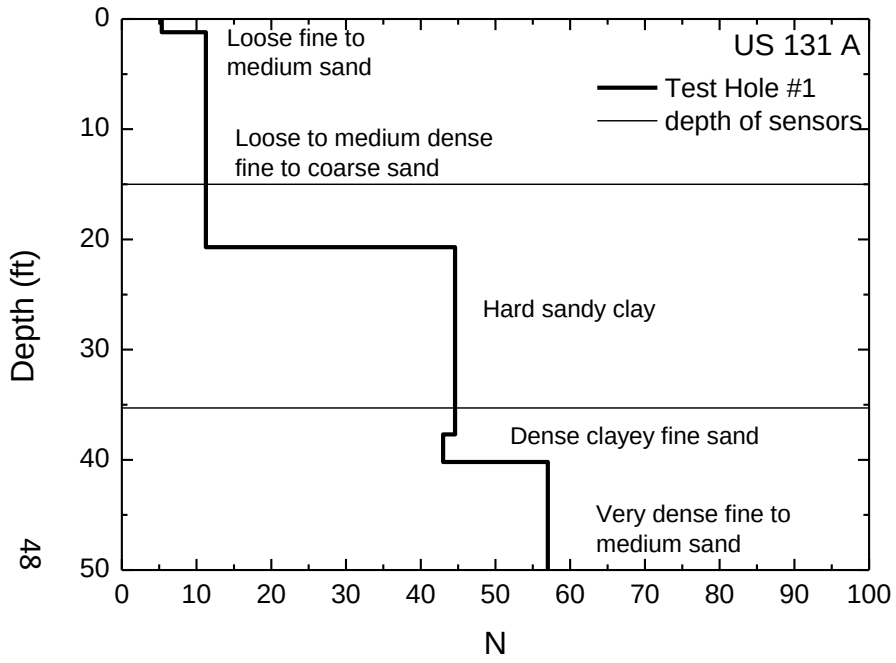

Figure 3-14 Simplified soil profile at US 131A site

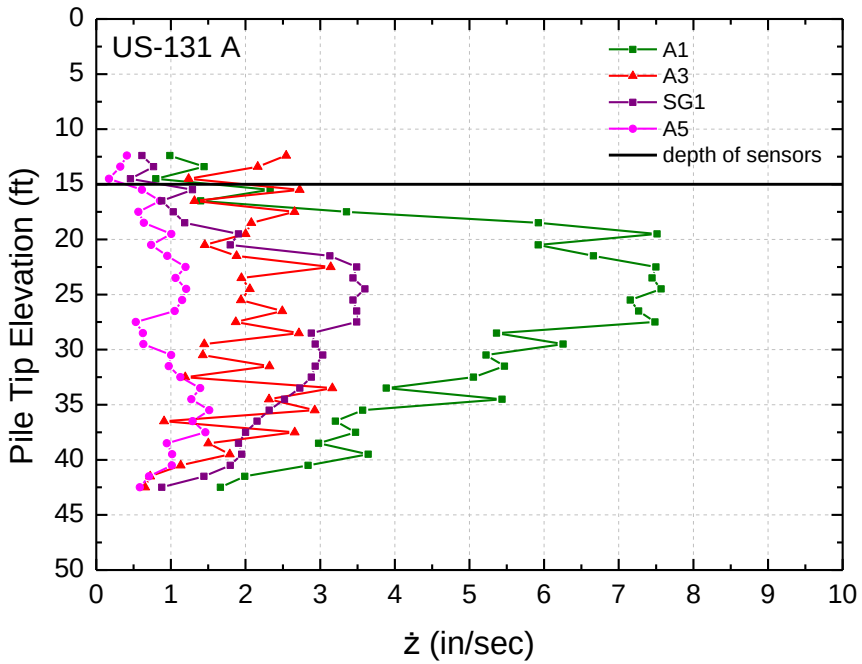

Figure 3-15 Peak vertical particle velocity versus pile tip depth for shallow embedded sensor cones at US 131 A site

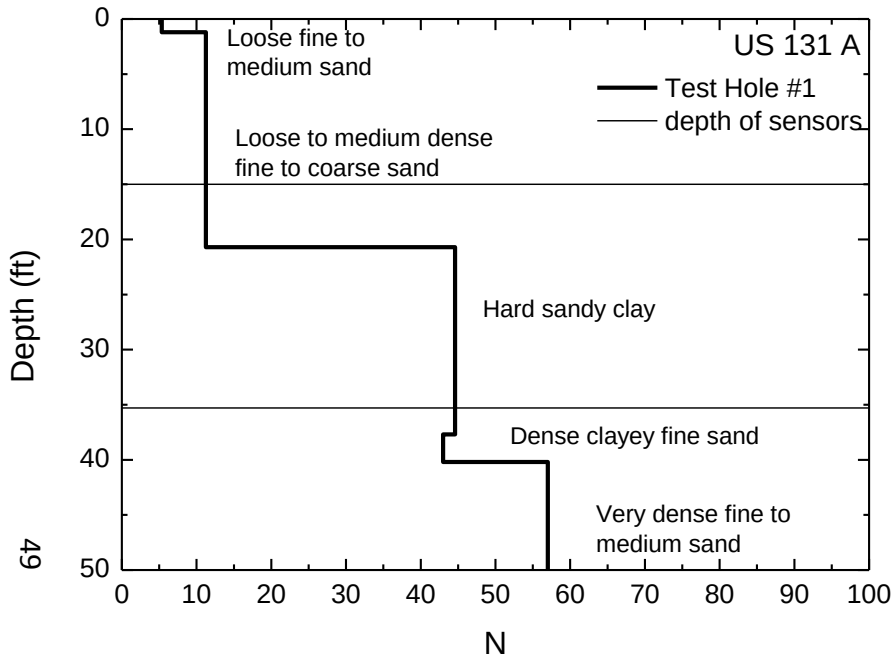

Figure 3-16 Simplified soil profile at US 131A site

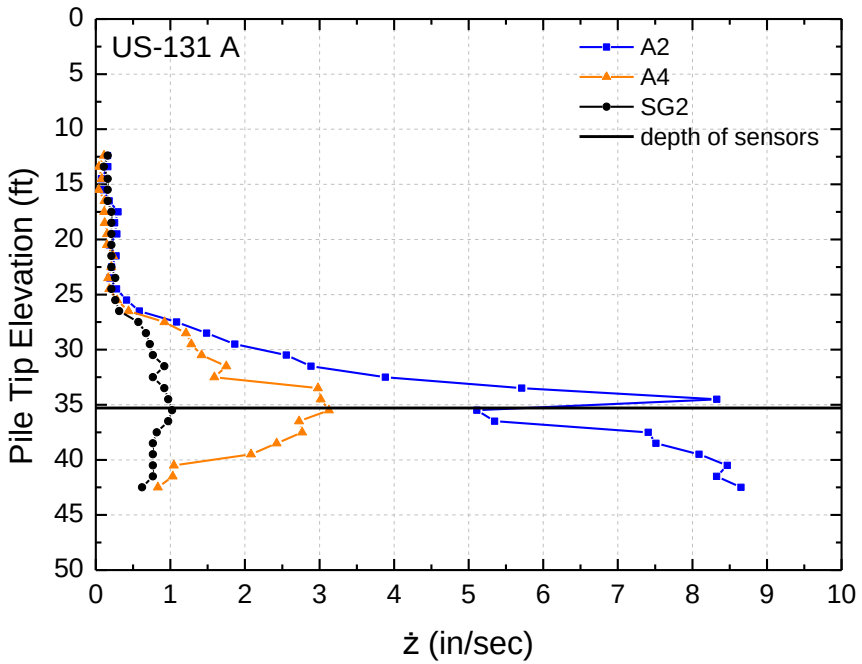

Figure 3-17 Peak vertical particle velocity versus pile tip depth for deep embedded sensor cones at US 131A site

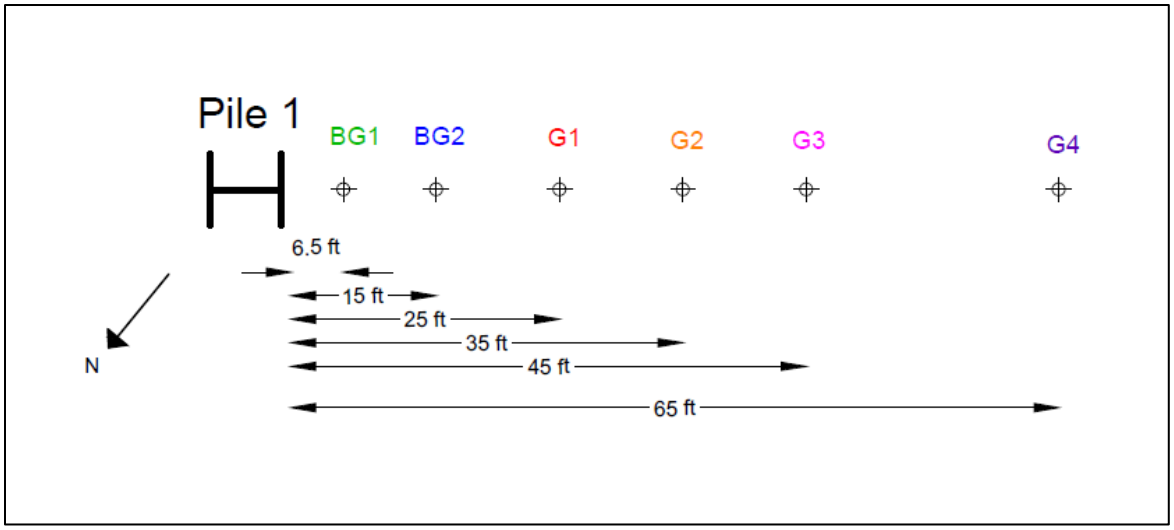

Figure 3-18 Plan view of surface geophone locations at US 131A site (Pile 1)

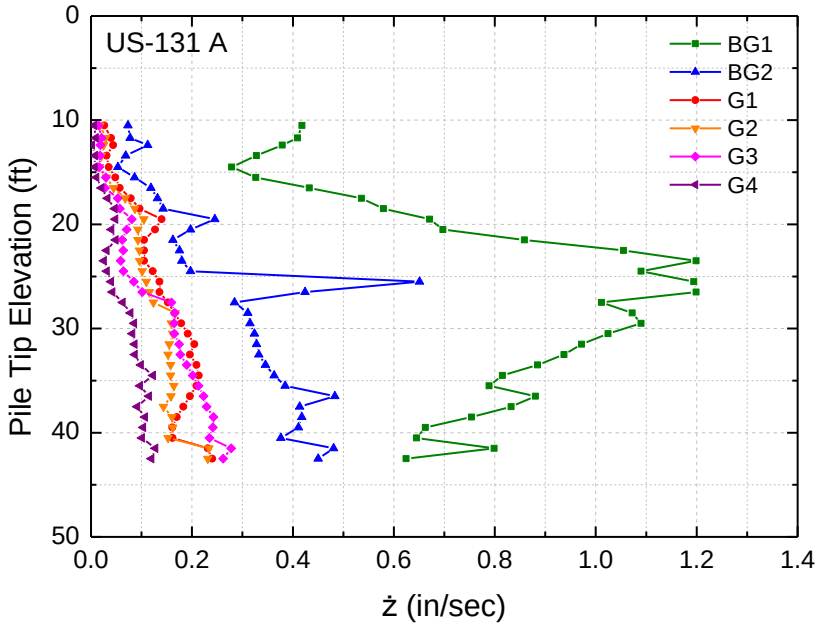

Figure 3-19 Peak vertical particle velocities versus pile tip depth for surface geophones at US 131A site (Pile 1)

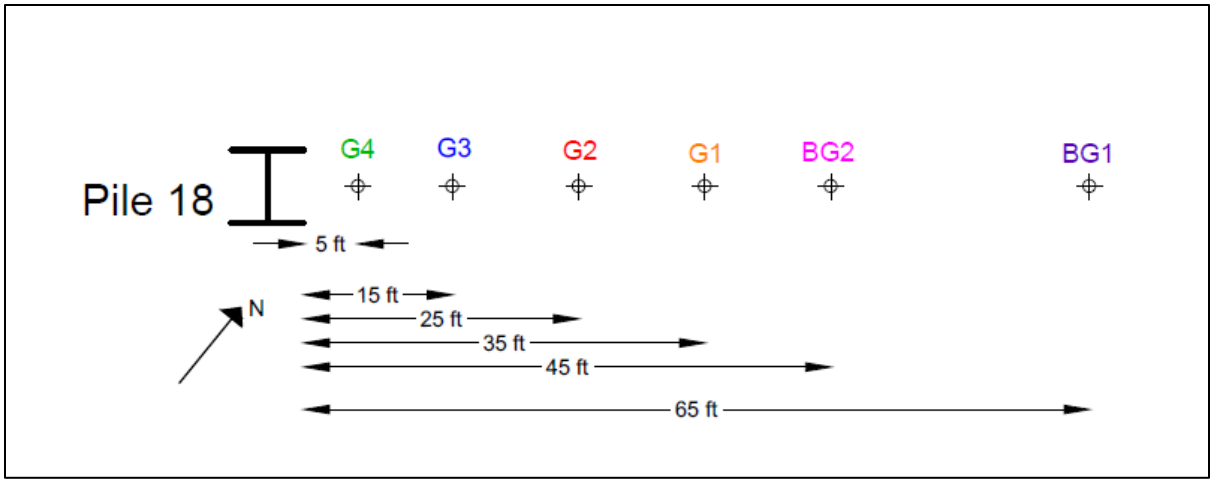

Figure 3-20 Plan view of surface geophone locations at US 131A site (Pile 18)

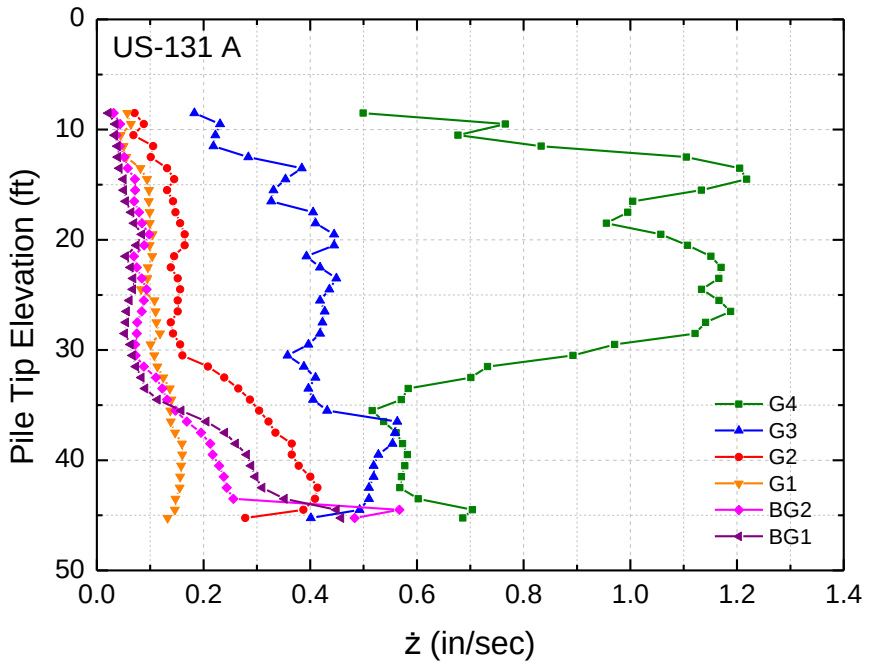

Figure 3-21 Peak vertical particle velocities versus pile tip depth for surface geophones at US 131A site (Pile 18)

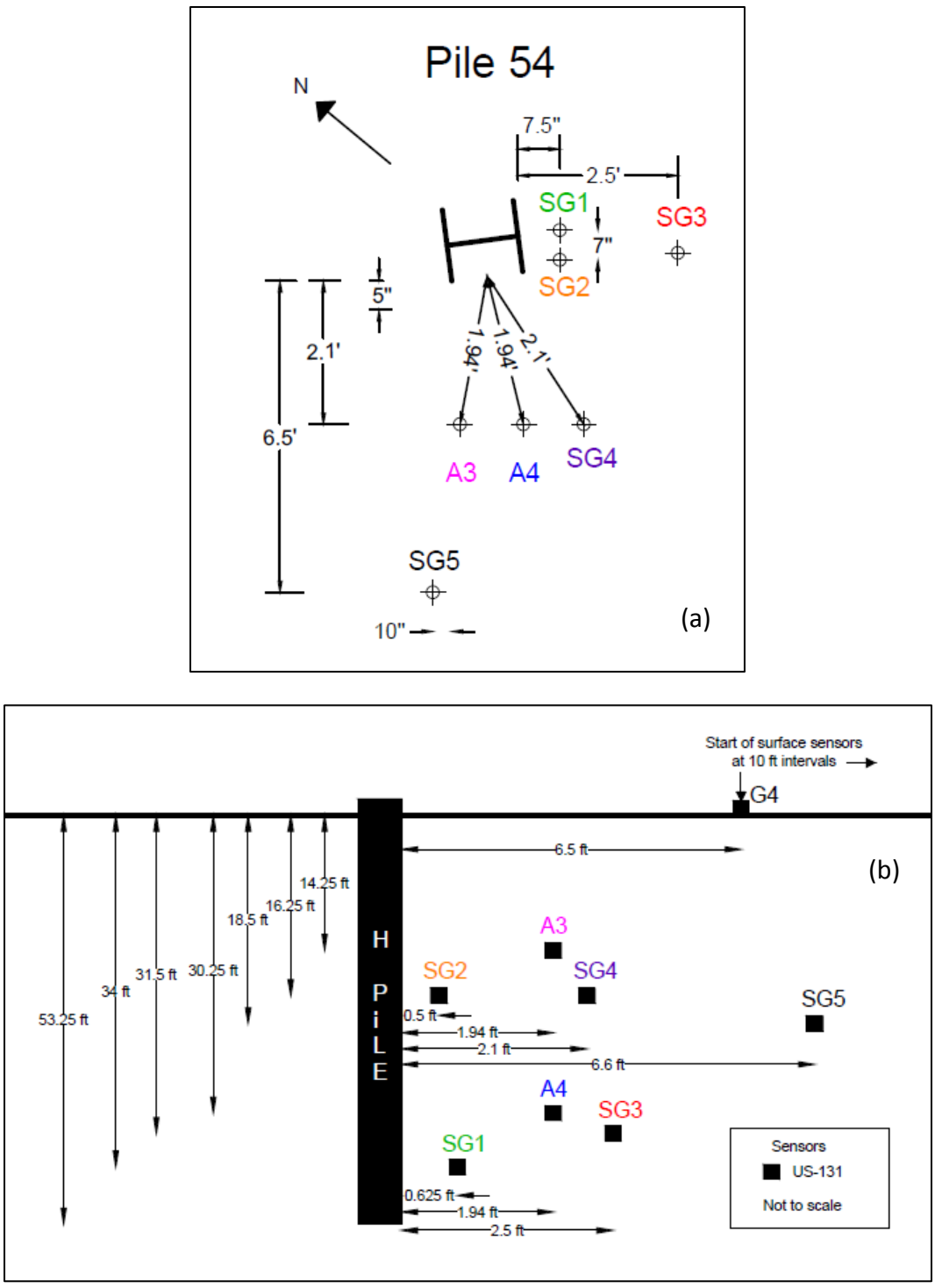

Figure 3-22 Plan (a) and elevation (b) views of embedded sensor cones at US 131B site

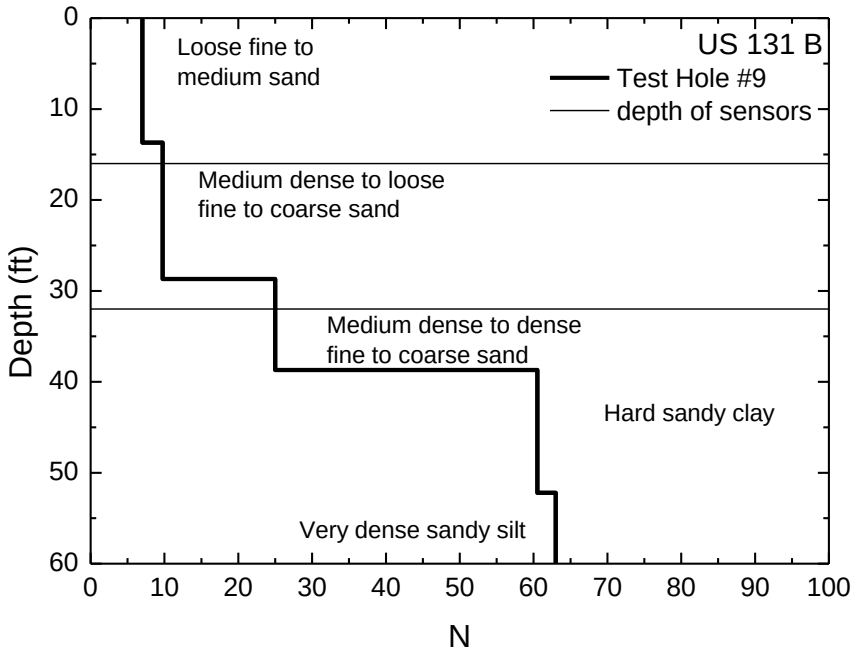

Figure 3-23 Simplified soil profile at US 131B site

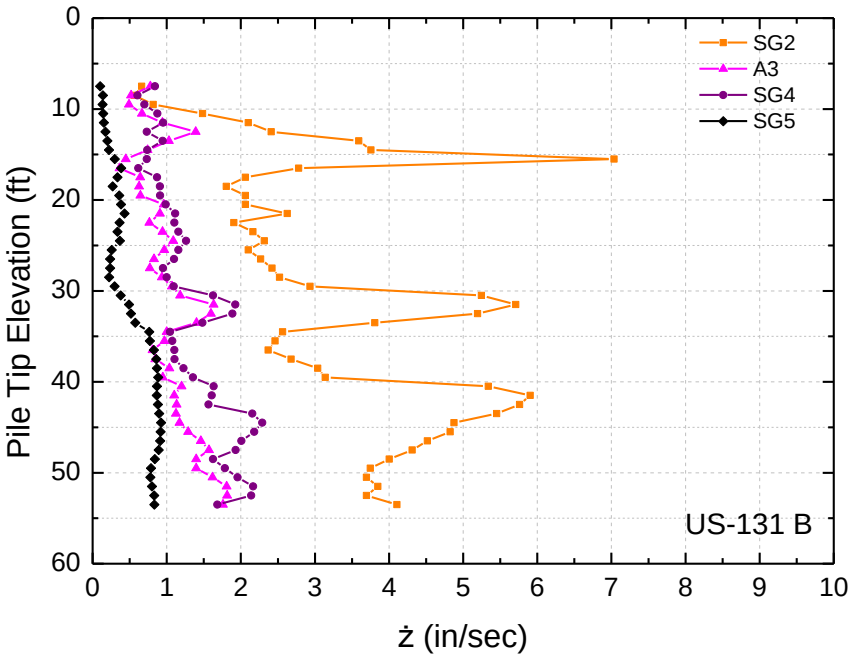

Figure 3-24 Peak vertical particle velocity versus pile tip depth for shallow sensor cones at US 131B site

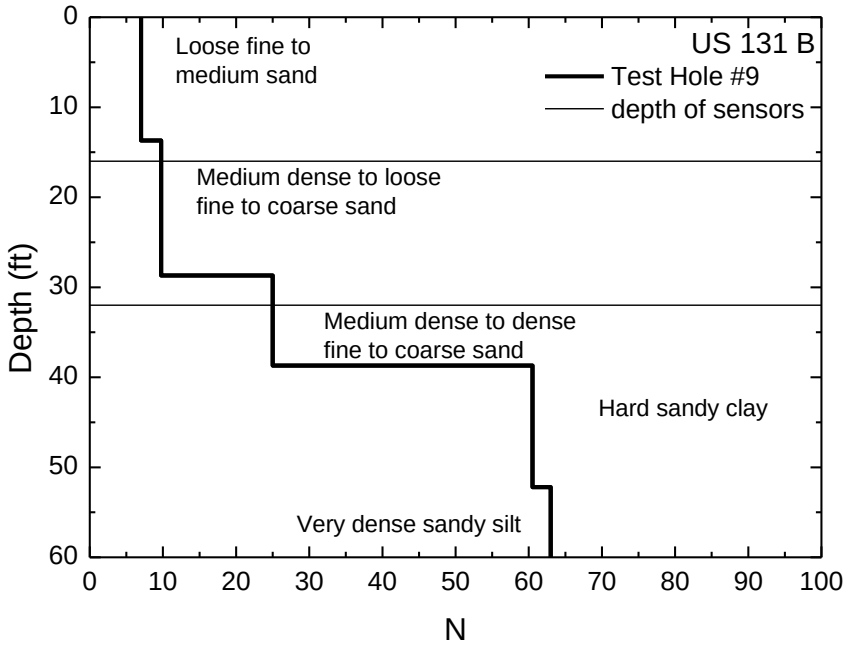

Figure 3-25 Simplified soil profile at US 131B site

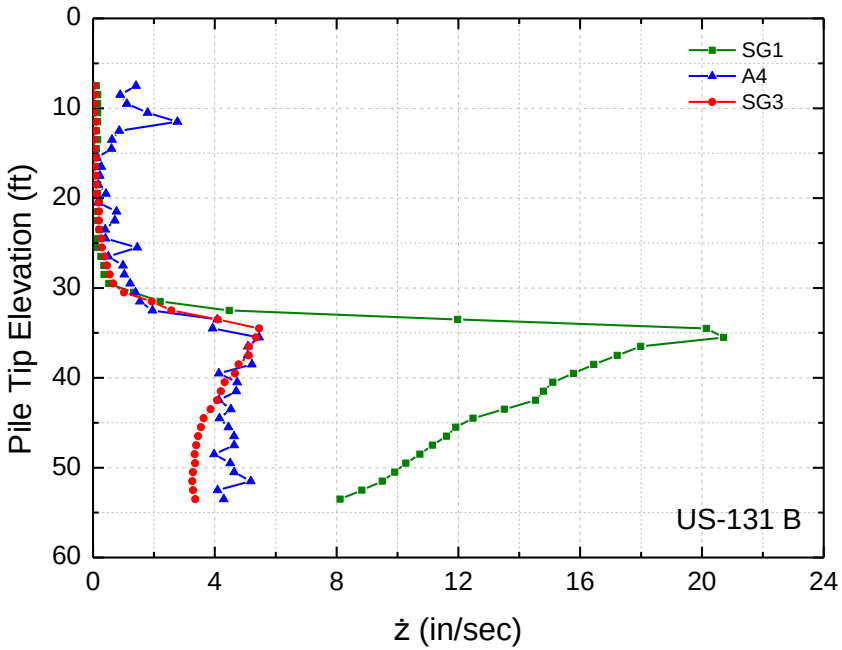

Figure 3-26 Peak vertical particle velocity versus pile tip depth for deep sensor cones at US 131B site

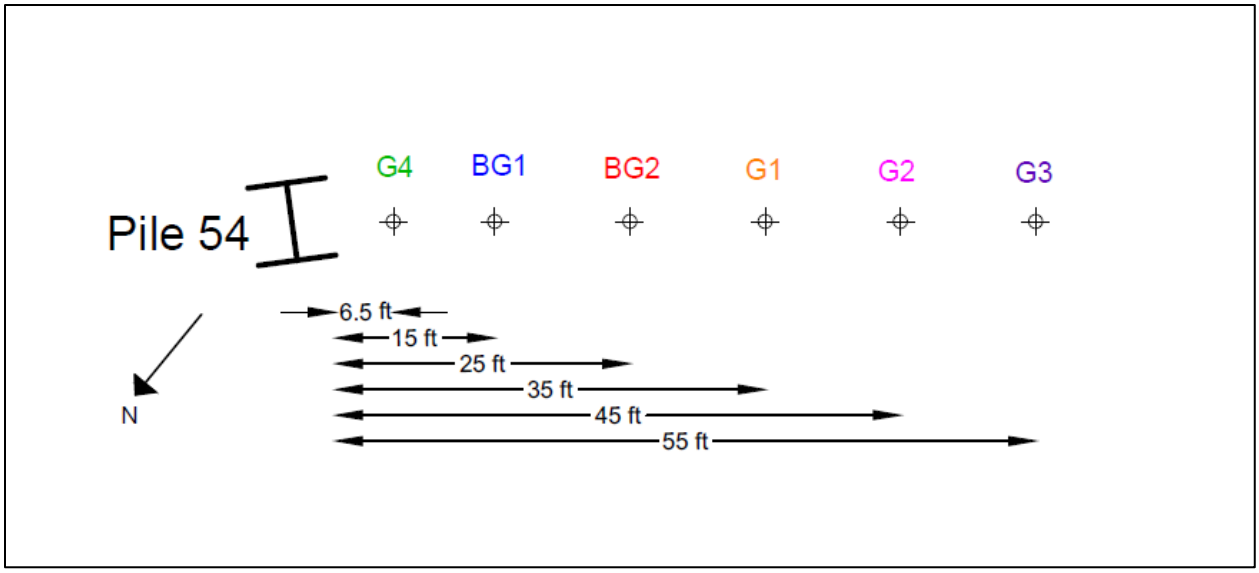

Figure 3-27 Surface geophone array at US 131B site (Pile 54)

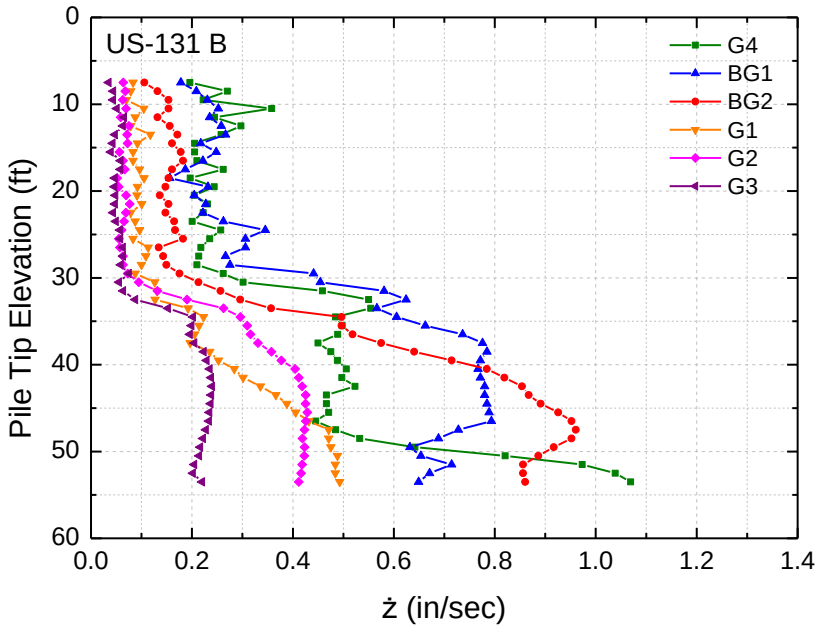

Figure 3-28 Peak vertical particle velocity versus pile tip depth for surface geophones at US 131B site (Pile 54)

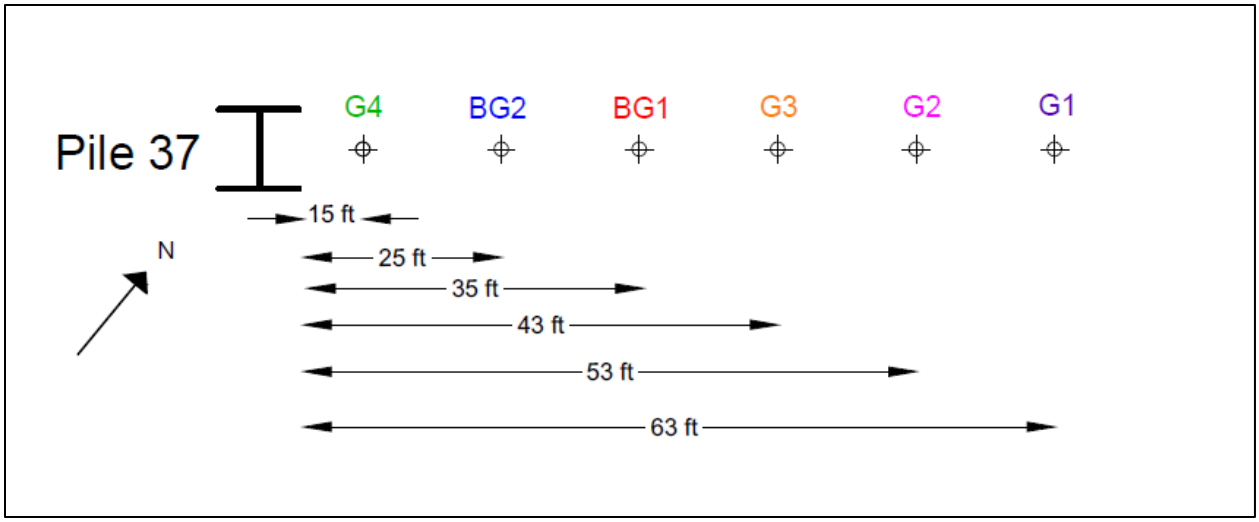

Figure 3-29 Surface geophone array at US 131B site (Pile 37)

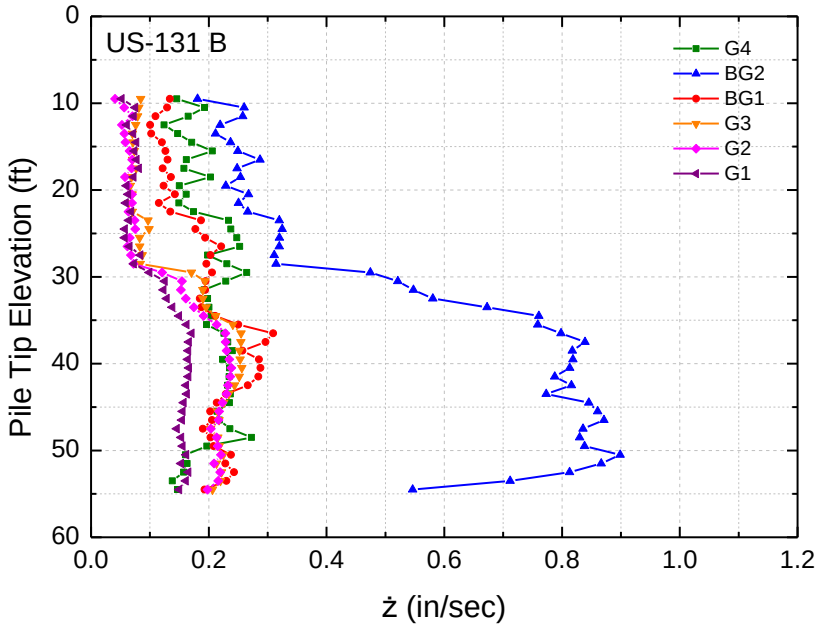

Figure 3-30 Peak vertical particle velocity versus pile tip depth for surface geophones at US 131B site (Pile 37)

4 ANALYSIS OF RESULTS

4.1 Ground motion measured at sensors during pile driving – Buried transducers

The first level of data analysis involves examining the amplitude of ground motion (acceleration and/or particle velocity) recorded at each sensor while the piles were being driven. In some cases the ground motion for every blow has been plotted while in most cases the maximum or average ground motion in each one foot increment of pile tip penetration has been plotted as a function of pile tip penetration. Where data has been collected as acceleration, it has been, in some cases, integrated to particle velocity for plotting and comparisons.

Figure 4-1 to Figure 4-7 are representative of these plots for five sites (M-25, M-66, M139, US 131 A and US 131 B) respectively. In each of these plots, the depth of the sensors at a common depth is shown by a horizontal line. Most of these plots reveal expected behavior, i.e. sensors nearest to the face of the pile show largest ground motion amplitudes, while those farthest from the face of the pile show smallest ground motion amplitudes. One exception is shown on Figure 4-2 for the M-66 site where the sensor closest to the pile does not show the largest amplitude until the pile is driven after the splice. The reason for this anomalous behavior is not known, but most likely is a function of poor coupling between the ground and the sensor.

4.2 Ground motion measured at sensors during pile driving – Surface transducers

Similar plots for ground motion at the surface geophones as the pile tip is driven into the ground are fundamental parts of the data set. Figure 4-8 to Figure 4-13 are representative of these plots for four sites (M-66, M-139, US 131 A and US 131 B) respectively. Trends in these plots are as expected with closest to the pile having higher amplitudes of ground motion.

4.3 Ground motion versus diagonal distance from pile tip to sensor

Another way of examining ground motion data is a plot of particle motion versus diagonal distance from pile tip to motion sensor. Figure 4-14 to Figure 4-45 are representative of these

plots for four sites (M-66, M-139, US 131 A and US 131 B) respectively. These figures are best read by starting in the lower right corner and following the data points upward to the left which represents the pile tip coming closer to the location of the sensor from the top (i.e., pile tip above sensor) until the pile tip reaches the depth of the sensor, then follow the data points to the right as the pile tip departs downward from the depth of the sensor. The sensor in each grouping that is closest to the pile shows the greatest difference in behavior when the pile tip is above the sensor compared with when the pile tip is below the sensor.

The difference in behavior when the pile tip is above the sensor depth is that the energy from the pile tip (P-wave) is most important when the pile tip is above the sensor, i.e. when there is no part of the pile shaft adjacent to or below the sensor. When the pile reaches the sensor and continues below, the shaft (S-wave) has a significant contribution to the ground motion of the sensor and continues to have influence for the remainder of the driving while the pile tip is getting further from the sensor and having lesser influence at the sensor. These observations are consistent with the hypothesis presented earlier (Figure 1-1) for ground motion caused by pile driving.

4.4 Coefficient of attenuation for body waves from pile driving

There are at least two ways of expressing attenuation of vibrations emanating from a pile while it is being driven: Bornitz equation (1.1) (Bornitz, 1931) and Power equations. For either method, the amount of data collected in this project includes only a small variety of soils and only two pile/pile driver combinations. So whatever approach is selected it will represent only a first approximation. The power equation approach was discarded when it was evident that there was no common coefficient or common power that could be found from the limited data available from these tests. So, the Bornitz equation approach was pursued.

On a basic level, it must be recognized that the Bornitz equation was developed for sinusoidal motion at a single frequency. The ground motion measured here from each pile hammer blow does not create a sinusoidal wave at one frequency at a buried sensor; see Figure 4-46 and Figure 4-49, for example. Furthermore, the vibrations emanating from the pile are composed of components of at least three types of waves: body waves from the pile tip, cylindrical waves from the pile shaft, and Rayleigh type waves at the ground surface. Even the Rayleigh waves are not pure because they are made up of waves from a vertical linear source, the pile, not a point or circle source on the surface. Consequently, it is incorrect to describe the vibrations from pile driving as conforming to conditions represented by the Bornitz equation. However, it is possible to adopt the form of the Bornitz equation to describe attenuation in this case. Because the Bornitz equation is widely known and the symbol for coefficient of attenuation of the Bornitz equation, α, is widely recognized it is proposed that the form of the

Bornitz equation be preserved but the coefficient of attenuation for this condition be defined as the Cyrillic я. The Cyrillic я is pronounced, ya. Using this symbol there should be no confusion about applying coefficients of attenuation, α, from other sources or applications to this application of vibrations from driven piles. Coefficient я is determined from the tests conducted as part of the research project. The equation will be written:

$$\dot{z}_2 = \dot{z}_1(r_1/r_2)^{0.5} \exp[-я(r_2-r_1)] \qquad (4.1)$$

where:

r_1 = distance from source to point of known amplitude, (ft.)
r_2 = distance from source to point of unknown amplitude, (ft.)
$\dot{z}_1$ = amplitude of motion at distance r_1 from source, (in./sec)
$\dot{z}_2$ = amplitude of motion at distance r_2 from source, and (in./sec)
я = coefficient of attenuation for vibrations from driven pile. (1/ft.)
exp = base of natural logarithm, e

Another feature of the Bornitz coefficient of attenuation, α, is that it is frequency dependent. After considerable evaluation of the frequency content of the ground motion measured in these tests, it has been concluded that dominant frequencies in these records are more likely a function of the type of pile being driven and the pile driver than related to attenuation of vibrations. Again, only two pile sections and two pile driving hammers were used in these tests, so only a limited use value of я can be derived. Coefficient я, herein, will be used without adjustment for frequency.

The coefficients of attenuation, я, from these tests were determined by fitting equation (4.1) through pairs of points of measured amplitude at the same depth. Several possibilities for this calculation were developed from the collected data. An example of the data and analyses for я for US 131 A site and for the shallow sensor array is shown in Table 4-2. It can be seen that in Table 4-2, an amplitude of motion is given for a fictitious distance called pile face or “pile”. It was not considered feasible to determine the ground vibration precisely at the pile-soil interface, but Massarsch and Fellenius (2008) presented an equation for predicting the maximum amplitude of soil motion at the pile-soil interface that depends on shearing strength, shear wave velocity and mass density of the soil:

$$\dot{z} = \tau/V_s \rho \qquad (4.2)$$

where $\dot{z}$ is the peak particle velocity (in./sec) in the soil at the pile-soil interface, τ is the shearing strength (lb./in^2) of the soil at the depth in question, V_s is the shear wave velocity (ft./sec) in the soil at the contact with the pile and ρ is the mass density (lb.sec^2/ft.^{4}) of the soil.

All of the terms on the right side of equation 4.2 can be estimated from the SPT blow count, N. Equation 4.2 can then be used to calculate the particle velocity at the interface between pile and soil. It was assumed that the particle velocity from equation 4.2 was valid at about one in. or about 0.1 ft. from the surface of the pile. The particle velocity calculated from equation 4.2 and the soil conditions at each site was inserted in Table 4-1 to Table 4-3 as the particle velocity at 0.1 ft. from the pile.

Attenuation curves with values from Table 4-1 are plotted in Figure 4-47 with the sensor closest to the pile as the base point for site M-139. Using the Bornitz equation, one point has to be assumed as the base point for calculation of particle velocity at any other point. The region in which soil conditions including shear wave velocity and particle motion change most rapidly is nearest to the pile so our closest measurement point is used as the base for attenuation calculations. In Figure 4-47, amplitudes at two known points, A3 and A4, were used to plot the red line. It can be seen that the red line fits all points quite well. Then the я from Table 4-1 for points A3 and A5 was plotted again using point A3 as the reference point and blue line resulted, again a good match for all points. Finally, the я from Table 4-1 for points A4 and A5 was used to plot the black line again using A3 as the base point and all data points were again fitted well. The quality of the fit was judged visually as sufficient data for a statistical evaluation of the fit are not available. For the M-139 site, pile type, pile hammer, and soil profile, a value of я of 0.11 was chosen as representative for this data.

Similar results are shown for US 131A site in Table 4-2 and Figure 4-50. An average я value of 0.18 was chosen as representative for this data. For US 131B site, Table 4-3 is a tabulation of the я values and Figure 4-53 shows the plot of attenuation curves. For this site я was valued at 0.089. The sands in the reach of the pile driven in each of the three sites used in the above analysis had blow counts, N, of 9, 11, and 10 respectively. The H-pile sections at all three sites was a HP 14x73 and were driven with Pileco D30-32 (M-139) or Delmag D30-32 (US 131 A&B). It was judged that the soil conditions, pile type and pile driving hammers were essentially the same so lumping then together for an average is valid. Then, the average value of я for these sites was 0.13 with two significant figures, but on the basis of the sparse data, it might be prudent to consider only one significant figure to this data, i.e. я=0.1.

4.5 Attenuation of surface waves from pile driving

Attenuation curves of peak particle velocity versus distance from pile face for surface geophones are presented in Figure 4-54 and Figure 4-55 for sites M-66 and M-139 respectively, Figure 4-56 and Figure 4-57 for US-131 A and Figure 4-58 and Figure 4-59 for US-131 B. Values of α for each plot have been determined and the resulting curve drawn through the point

representing the geophone closest to the pile face. Five of six values of α were 0.02 to 0.03 while one value was 0.1. The high value of 0.1 occurred on the line from the pile #1 to the pile #18 at US 131A. The reverse line produced an α of 0.03, which is similar to the other measured attenuation coefficients. Horizontal heterogeneity is very important in the case of surface wave attenuation from piles as the pile tip goes deeper into the ground. There is not sufficient soil profile data to judge the heterogeneity at this site so it cannot be determined if that or other reasons explain the difference in α from two directions along the same line. The measured of α of 0.02 matches α from Woods (1997) for a blow count, N, of 10 and frequency of 25 Hz.

Table 4-1 *я* coefficients for M-139 site

M-139	Distance from pile (ft)	ż (in/sec)	Sensor Depth 25.5 ft	*я* (1/ft)
PILE	0.1	18		
A3	0.5	4.79	**A3-A4**	0.22
A4	2.5	1.39	**A4-A5**	0.025
A5	6.5	0.78	**A3-A5**	0.089
			average	0.11

Table 4-2 *я* coefficients for US-131 A site

US-131 A	Distance from pile (ft)	ż (in/sec)	Sensor Depths 15-17 ft	*я* (1/ft)
PILE	0.1	22		
A1	0.5	5.92	**A1-SG1**	0.35
SG1	2.7	1.19	**SG1-A5**	0.035
A5	6.7	0.65	**A1-A5**	0.15
			average	0.18
SG1	94.4	0.04	**SG1-SG1**	0.018

Table 4-3 я coefficients for US-131 B site

US-131 B	Distance from pile (ft)	ż (in/sec)	Sensor Depths 16.25-18.5 ft	я (1/ft)
PILE	0.1	10.5		
SG2	0.5	2.06	**SG2-SG4**	0.091
SG4	2.1	0.87	**SG4-SG5**	0.088
SG5	6.5	0.34	**SG2-SG5**	0.089
			average	0.089
SG5	90.65	0.02	**SG5-SG5**	0.021

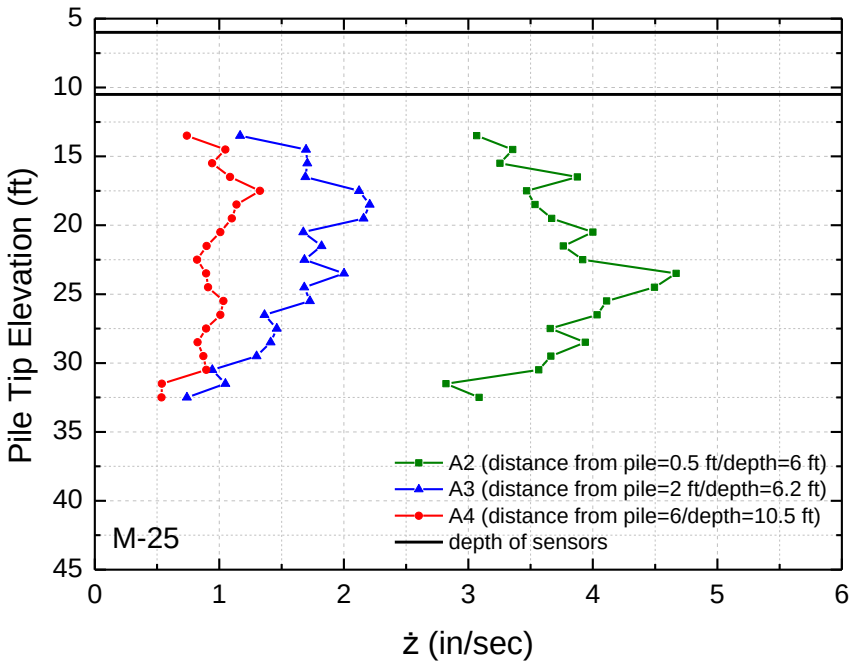

Figure 4-1 Peak vertical particle velocity, ż, versus pile tip depth for embedded sensor cones at M-25 site

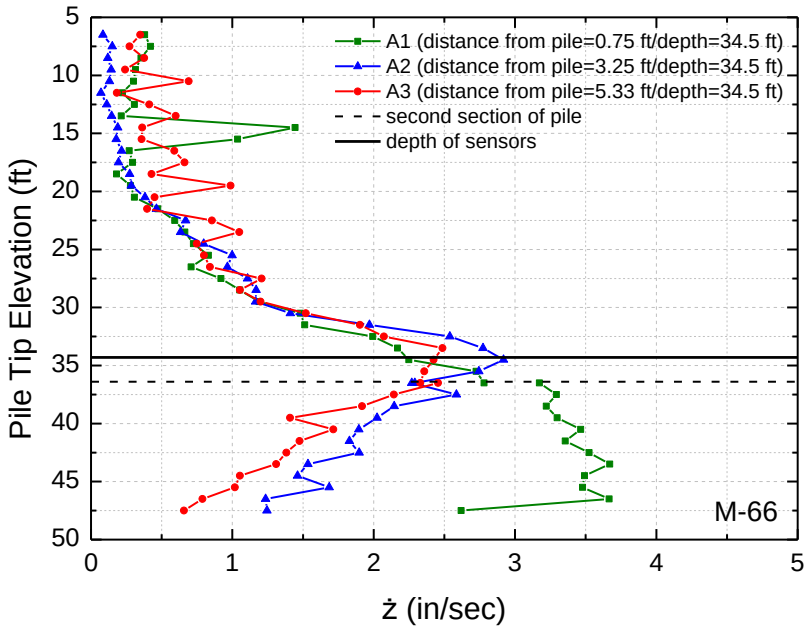

Figure 4-2 Peak vertical particle velocity, ż, versus pile tip depth for embedded sensor cones at M-66 site

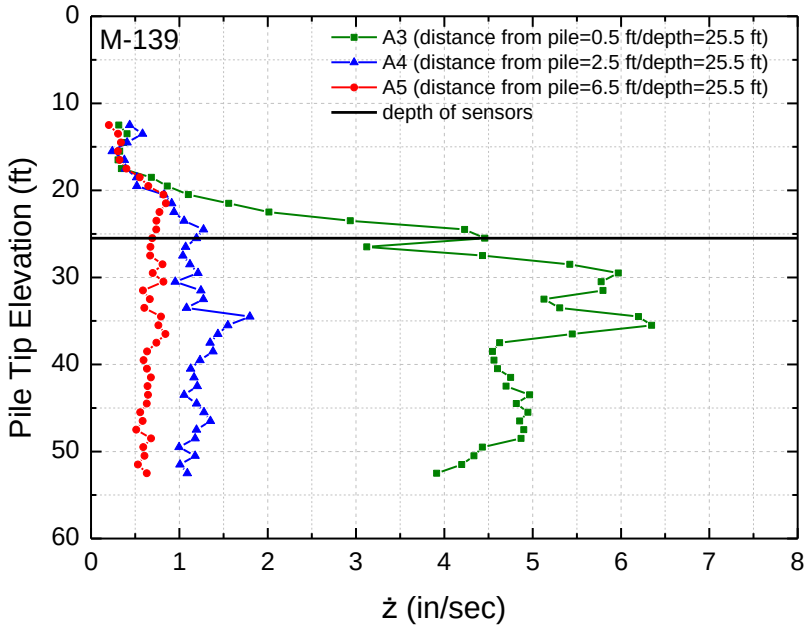

Figure 4-3 Peak vertical particle velocity, ż, versus pile tip depth for embedded sensor cones at M-139 site

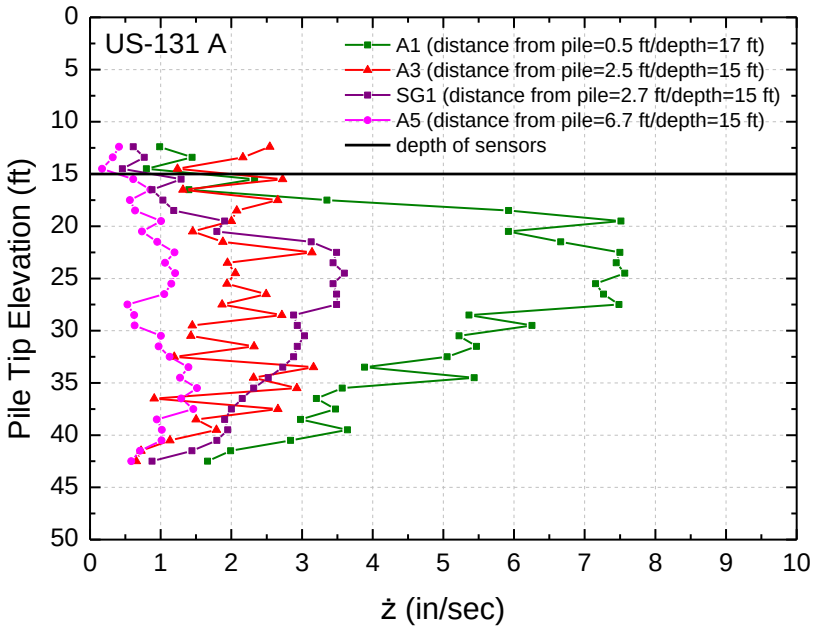

Figure 4-4 Peak vertical particle velocity, ż, versus pile tip depth for shallow embedded sensor cones at US 131A site

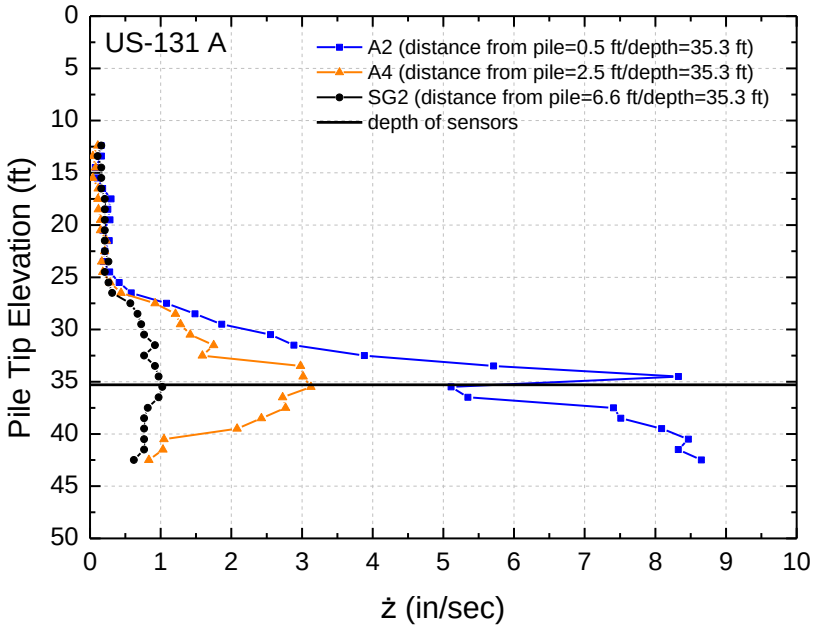

Figure 4-5 Peak vertical particle velocity, ż, versus pile tip depth for deep embedded sensor cones at US 131A site

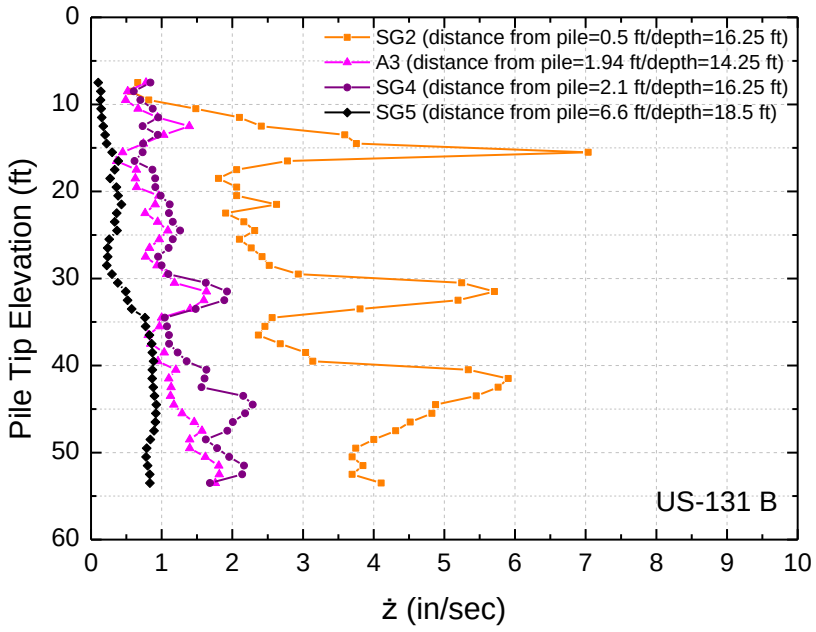

Figure 4-6 Peak vertical particle velocity, ż, versus pile tip depth for shallow embedded sensor cones at US 131B site

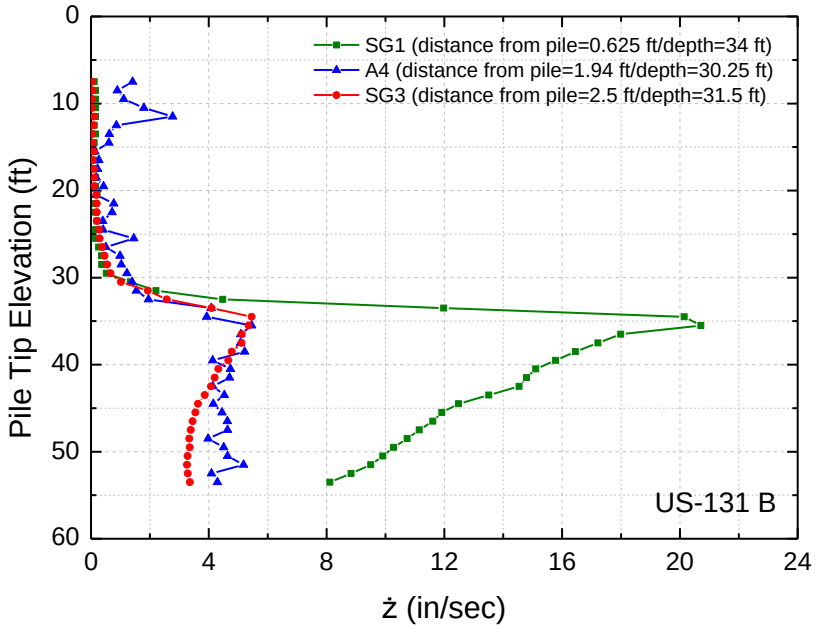

Figure 4-7 Peak vertical particle velocity, ż, versus pile tip depth for deep embedded sensor cones at US 131B site

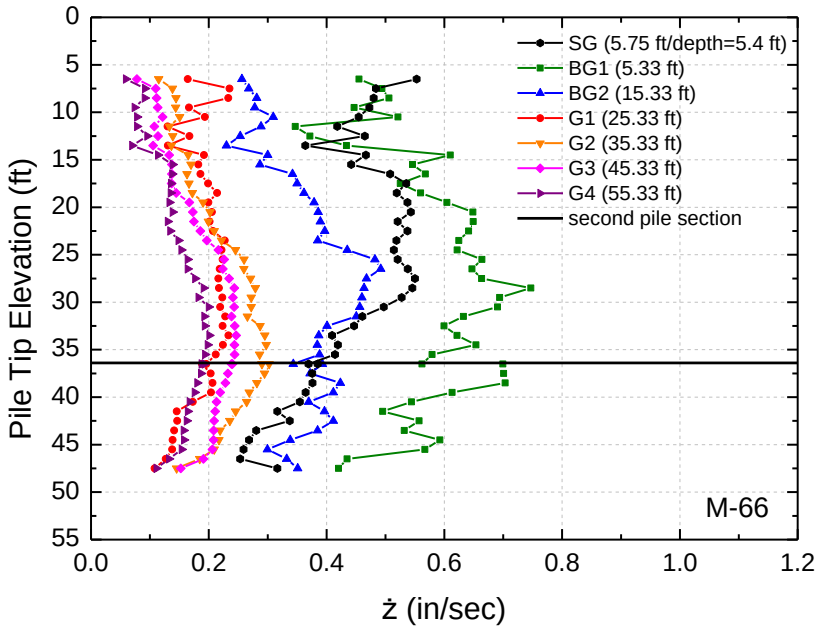

Figure 4-8 Peak vertical particle velocity, ż, versus pile tip depth for surface geophones at M-66 site

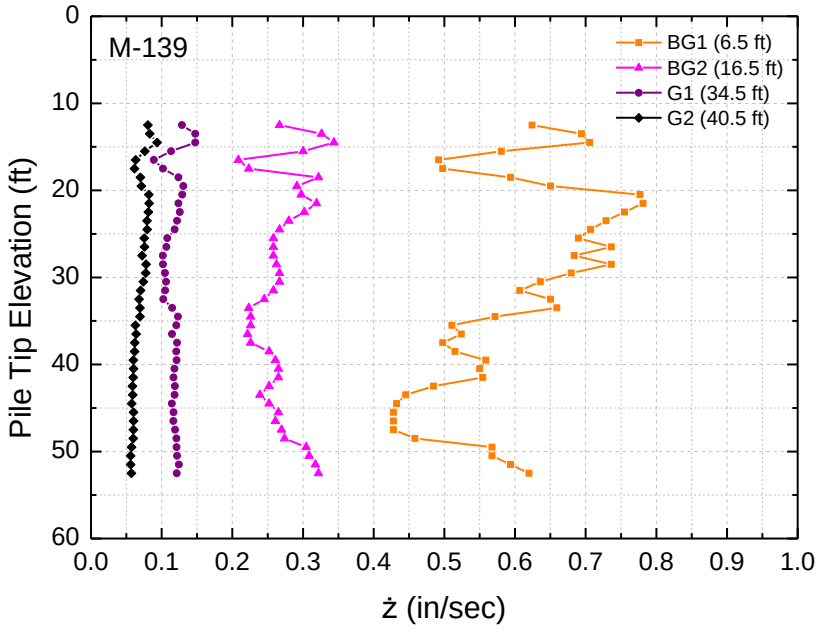

Figure 4-9 Peak vertical particle velocity, ż, versus pile tip depth for surface geophones at M-139 site

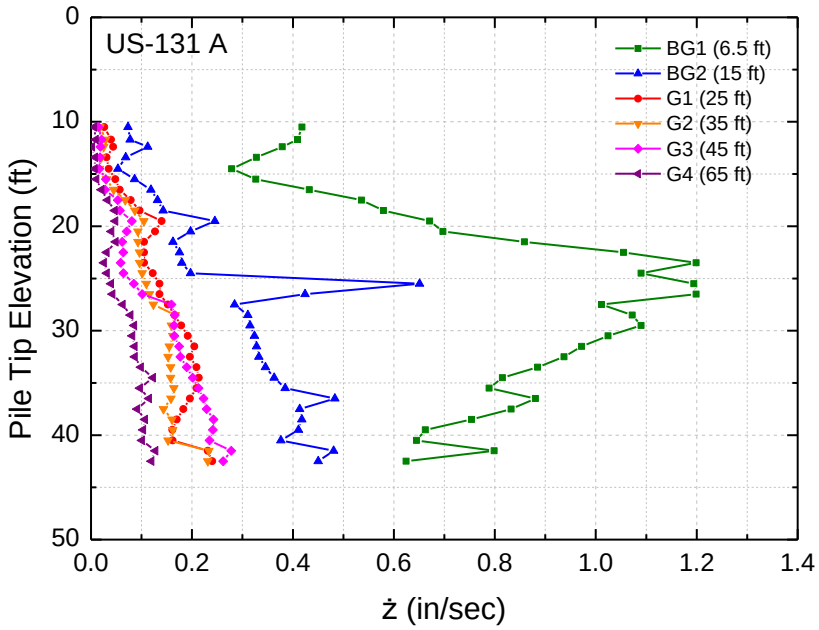

Figure 4-10 Peak vertical particle velocity, ż, versus pile tip depth for surface geophones at US 131A site (Pile 1)

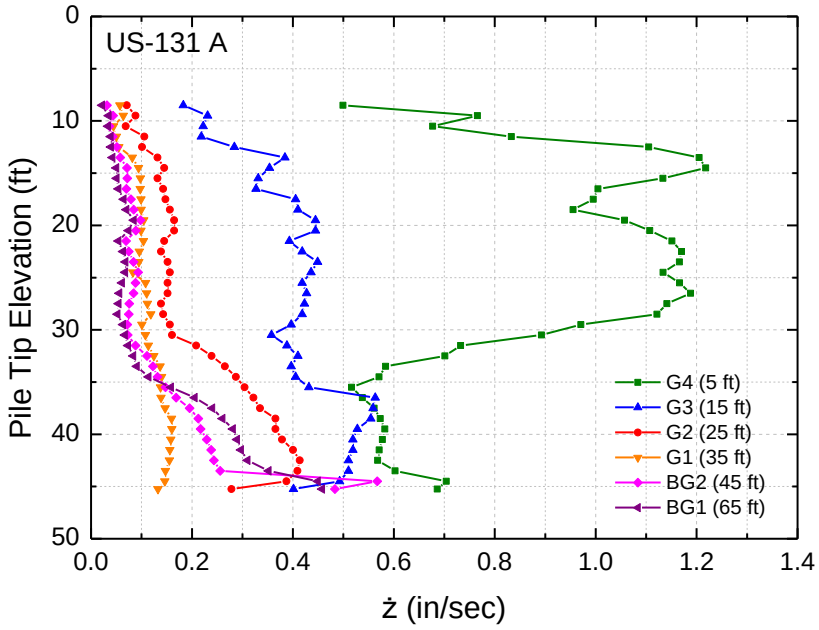

Figure 4-11 Peak vertical particle velocity, ż, versus pile tip depth for surface geophones at US 131A site (Pile 18)

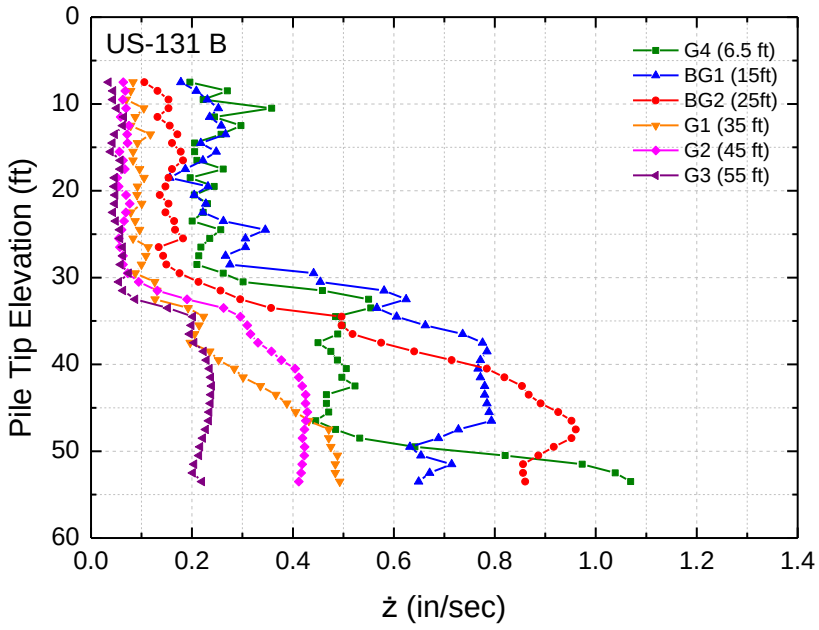

Figure 4-12 Peak vertical particle velocity, ż, versus pile tip depth for surface geophones at US 131B site (Pile 54)

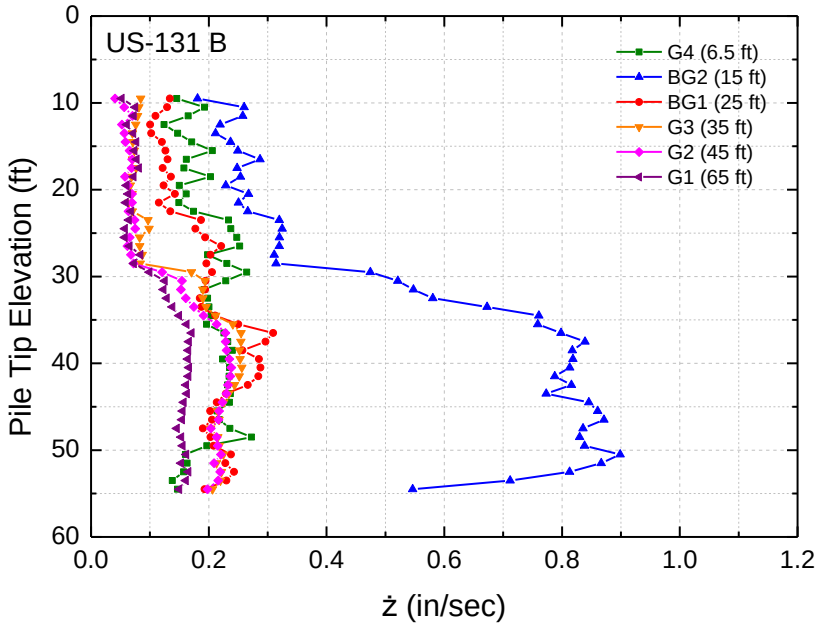

Figure 4-13 Peak vertical particle velocity, ż, versus pile tip depth for surface geophones at US 131B site (Pile 37)

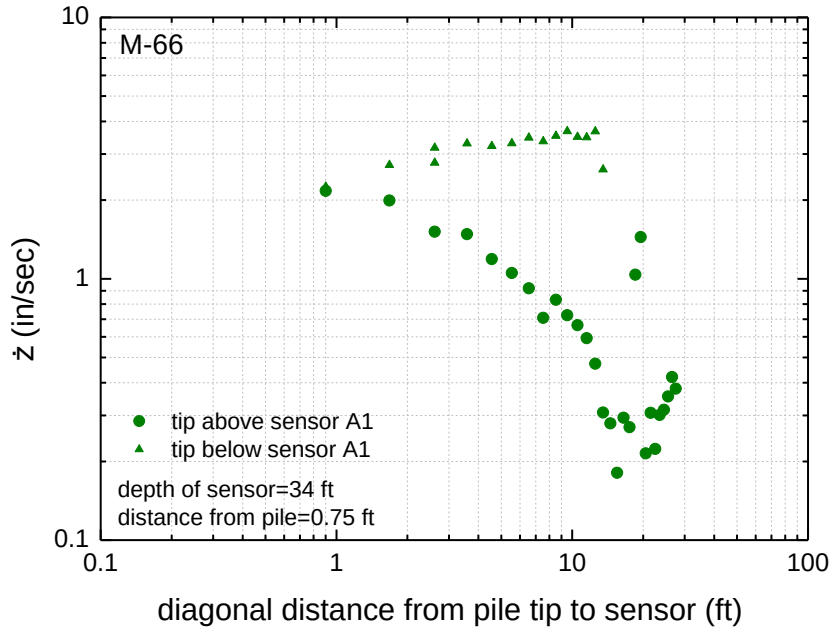

Figure 4-14 Peak vertical particle velocity, ż, versus diagonal distance from pile to sensor A1

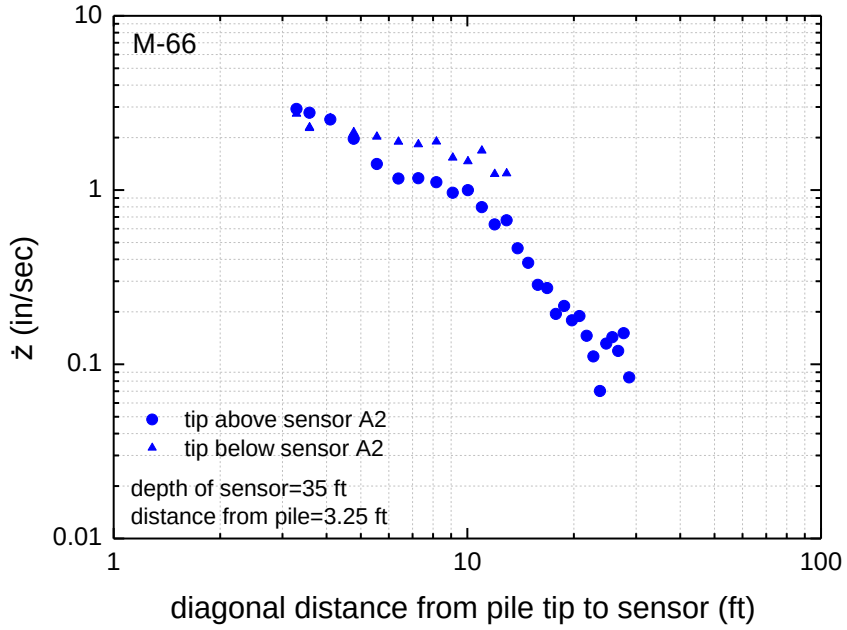

Figure 4-15 Peak vertical particle velocity, ż, versus diagonal distance from pile to sensor A2

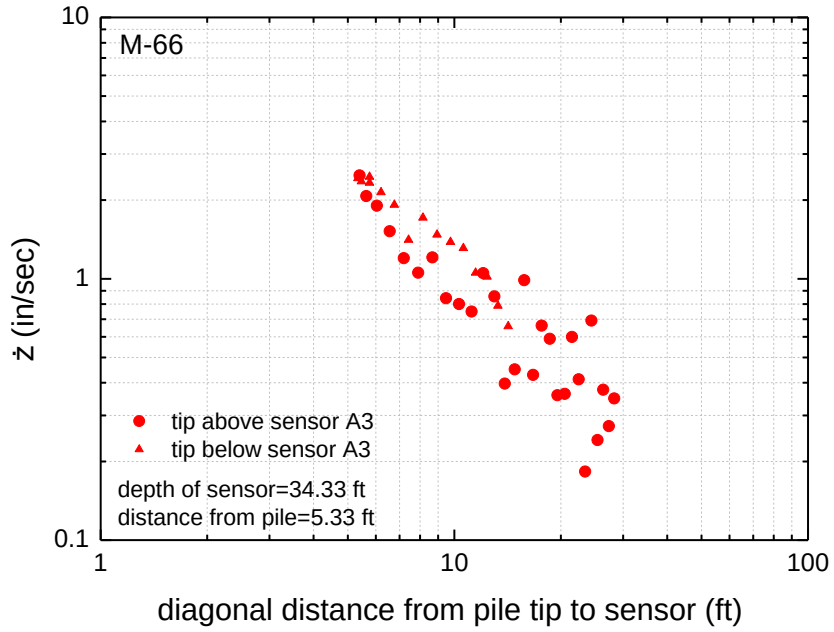

Figure 4-16 Peak vertical particle velocity, ż, versus diagonal distance from pile to sensor A3

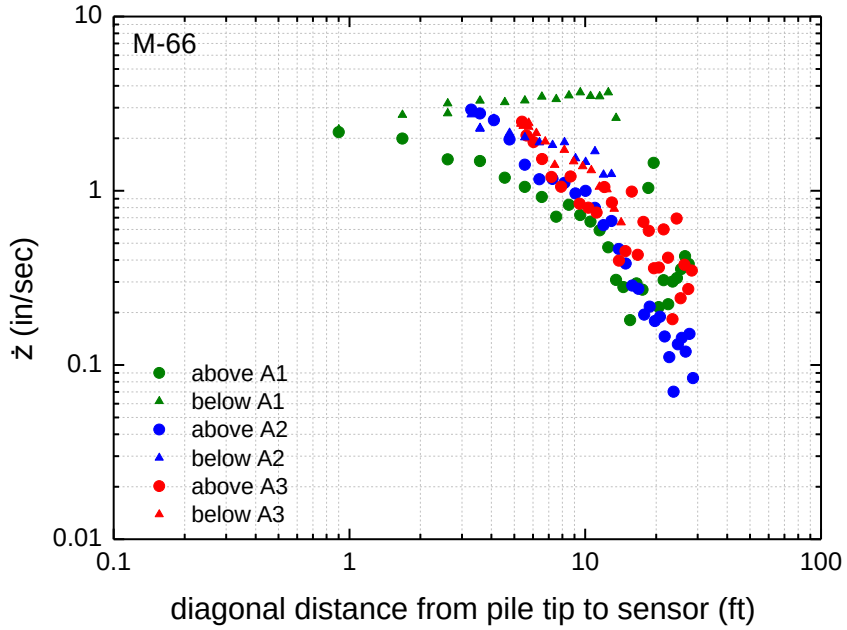

Figure 4-17 Peak vertical particle velocity, ż, versus diagonal distance from pile to all sensors

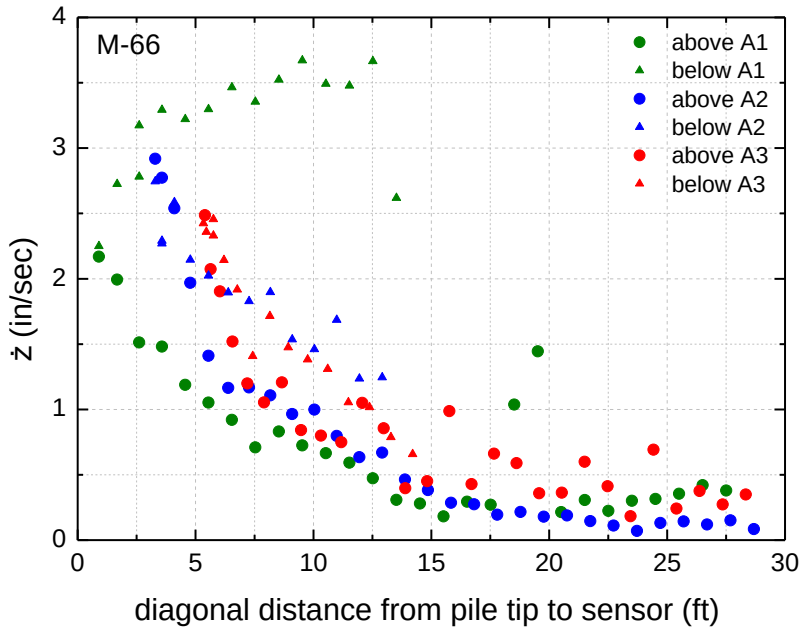

Figure 4-18 Peak vertical particle velocity, ż, versus diagonal distance from pile to all sensors

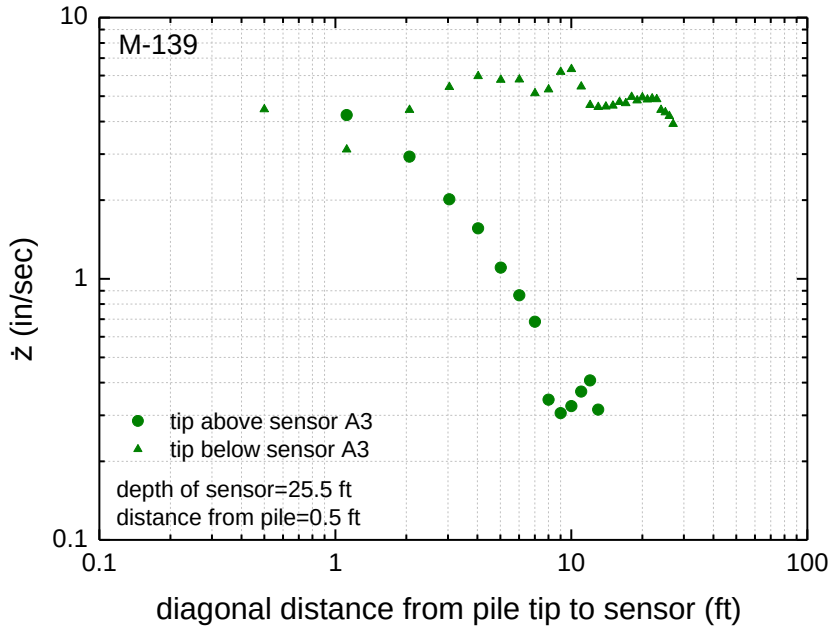

Figure 4-19 Peak vertical particle velocity, ż, versus diagonal distance from pile to sensor A3

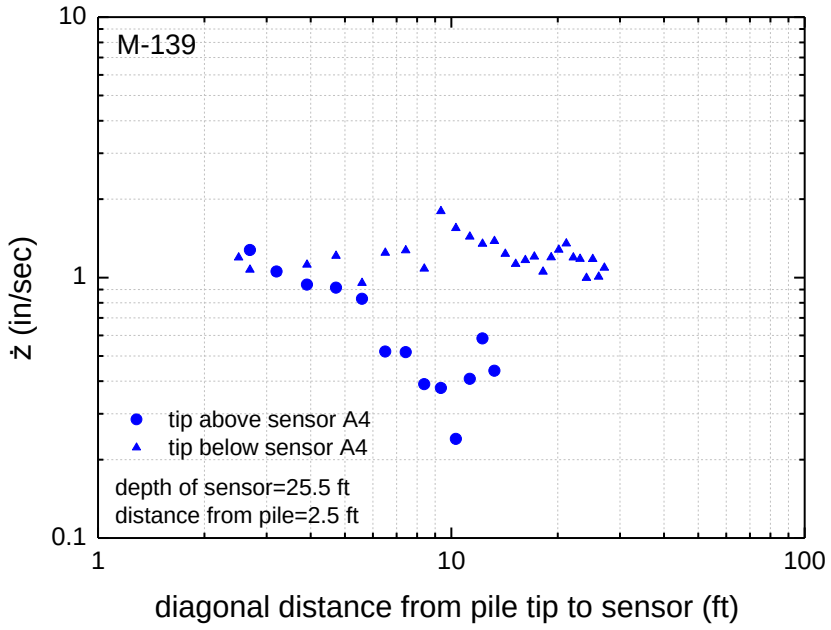

Figure 4-20 Peak vertical particle velocity, ż, versus diagonal distance from pile to sensor A4

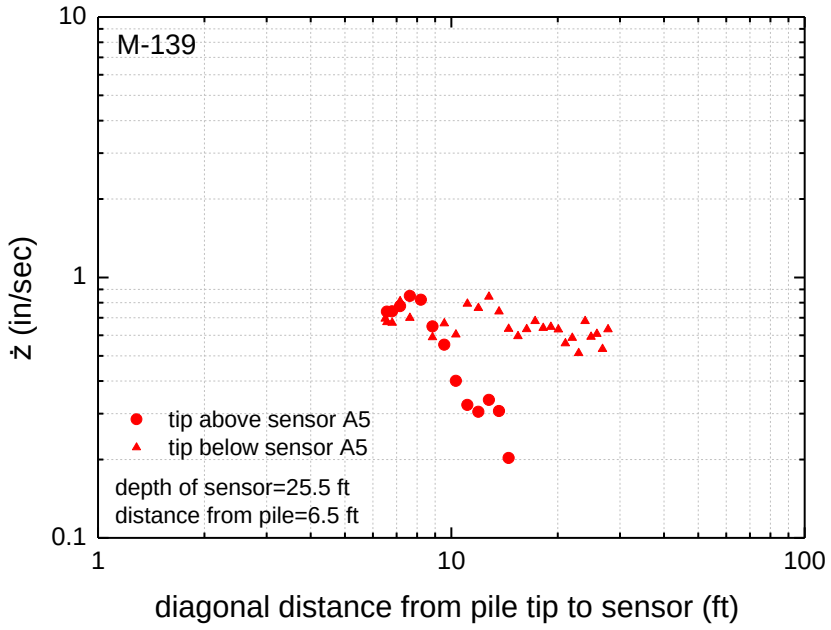

Figure 4-21 Peak vertical particle velocity, ż, versus diagonal distance from pile to sensor A5

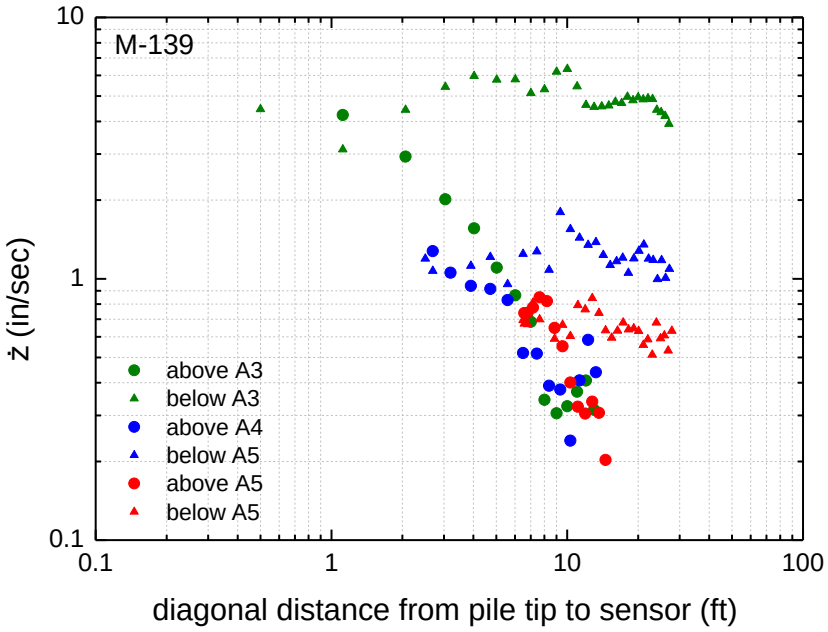

Figure 4-22 Peak vertical particle velocity, ż, versus diagonal distance from pile to all sensors

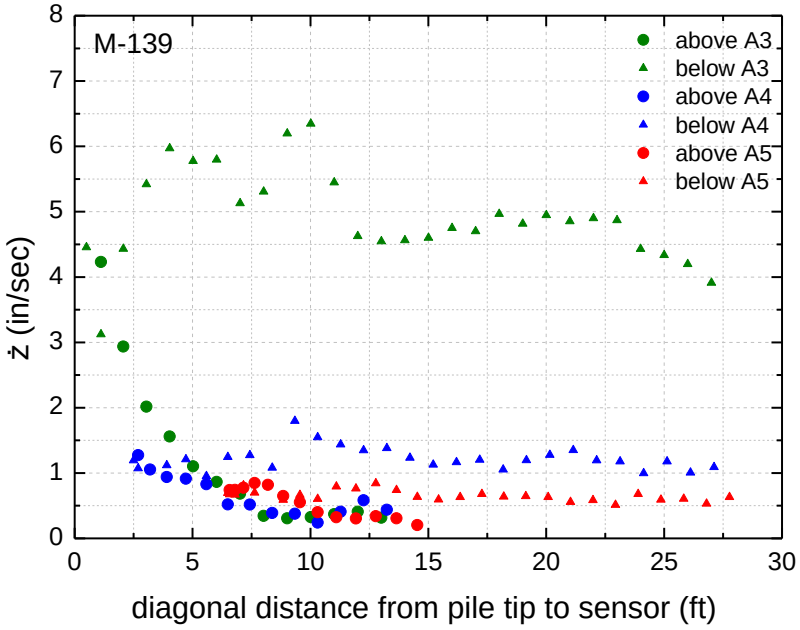

Figure 4-23 Peak vertical particle velocity, ż, versus diagonal distance from pile to all sensors

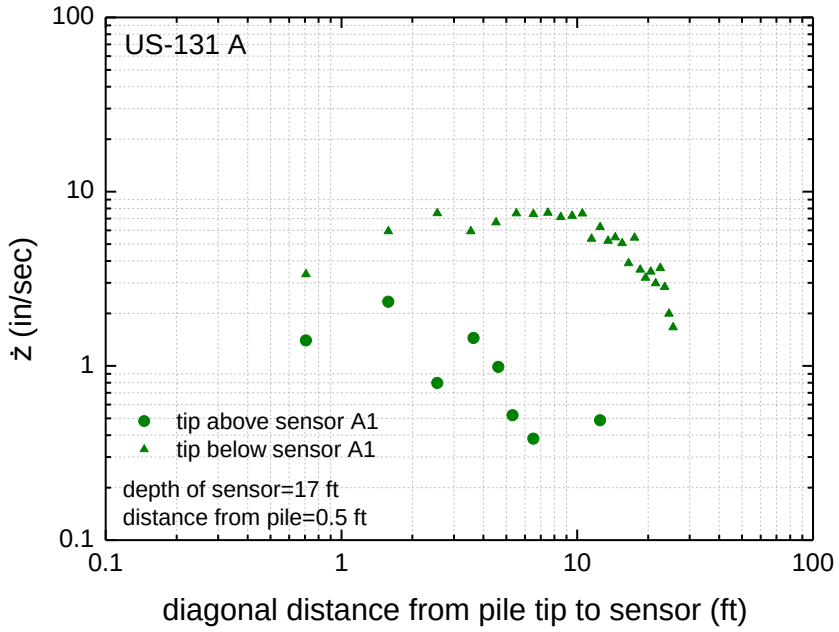

Figure 4-24 Peak vertical particle velocity, ż, versus diagonal distance from pile 1 to sensor A1

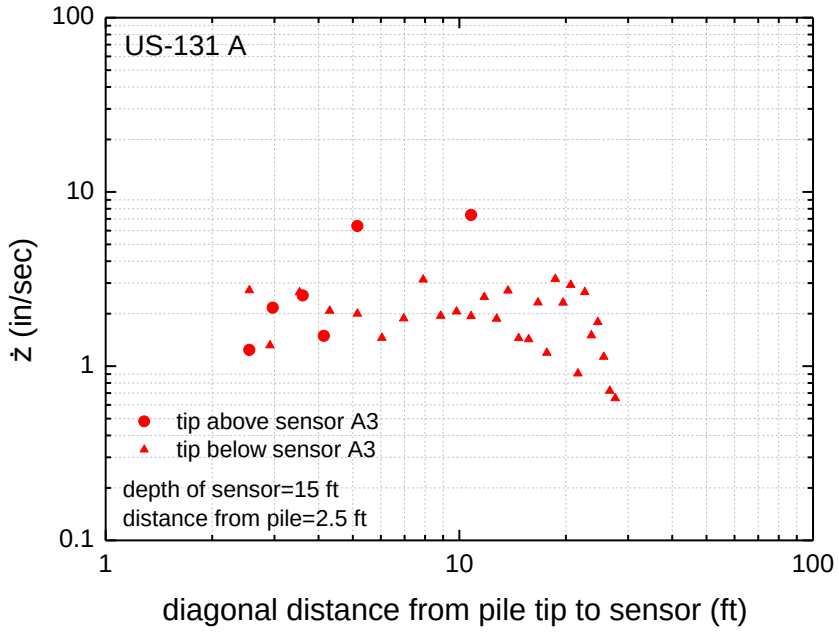

Figure 4-25 Peak vertical particle velocity, ż, versus diagonal distance from pile 1 to sensor A3

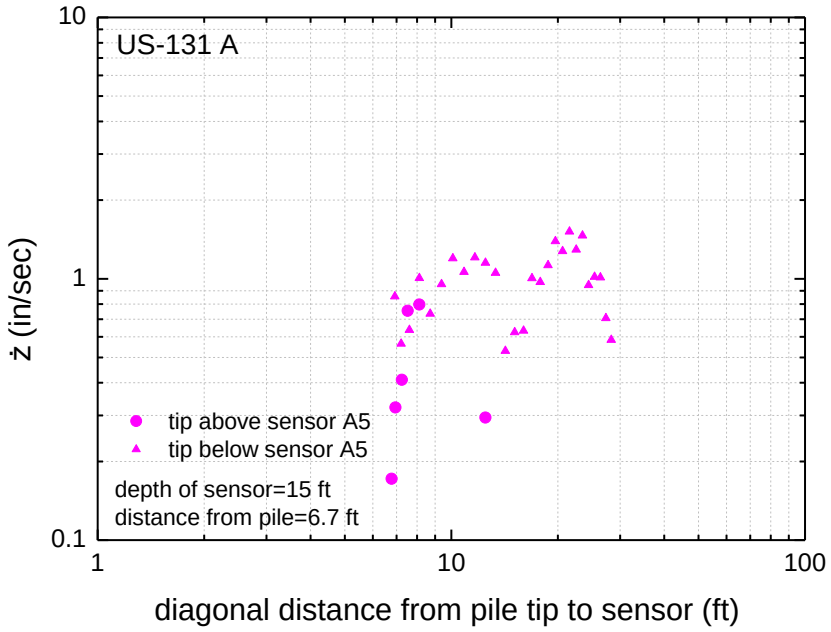

Figure 4-26 Peak vertical particle velocity, ż, versus diagonal distance from pile 1 to sensor A5

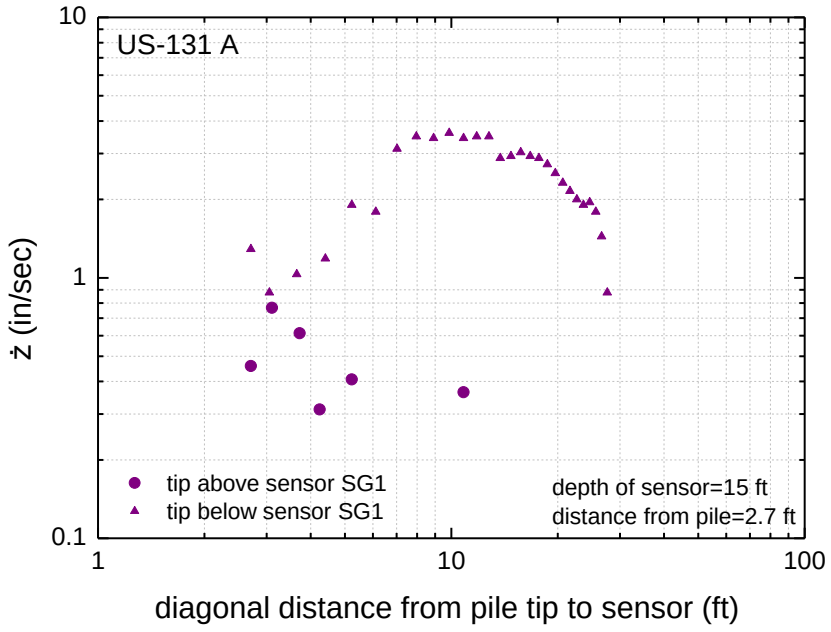

Figure 4-27 Peak vertical particle velocity, ż, versus diagonal distance from pile 1 to sensor SG1

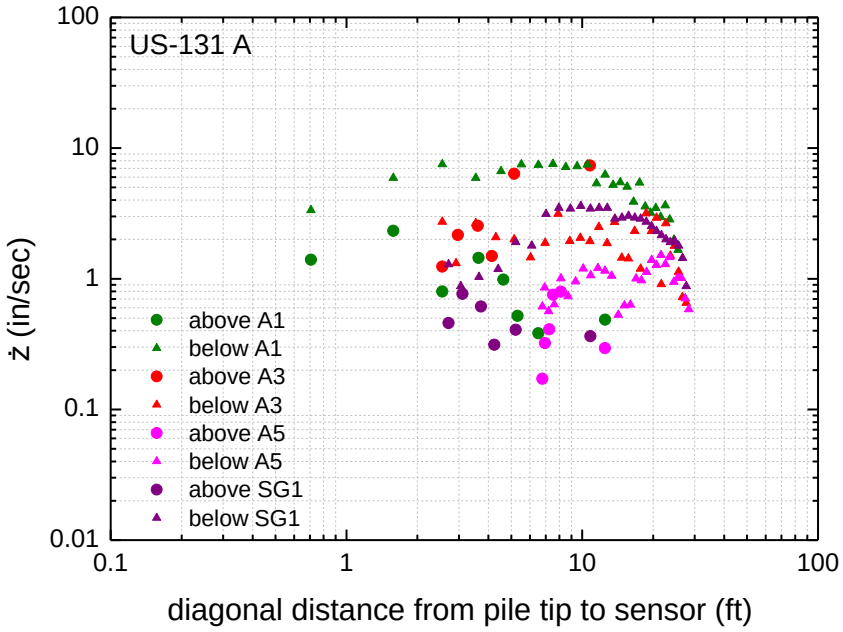

Figure 4-28 Peak vertical particle velocity, ż, versus diagonal distance from pile 1 to all sensors

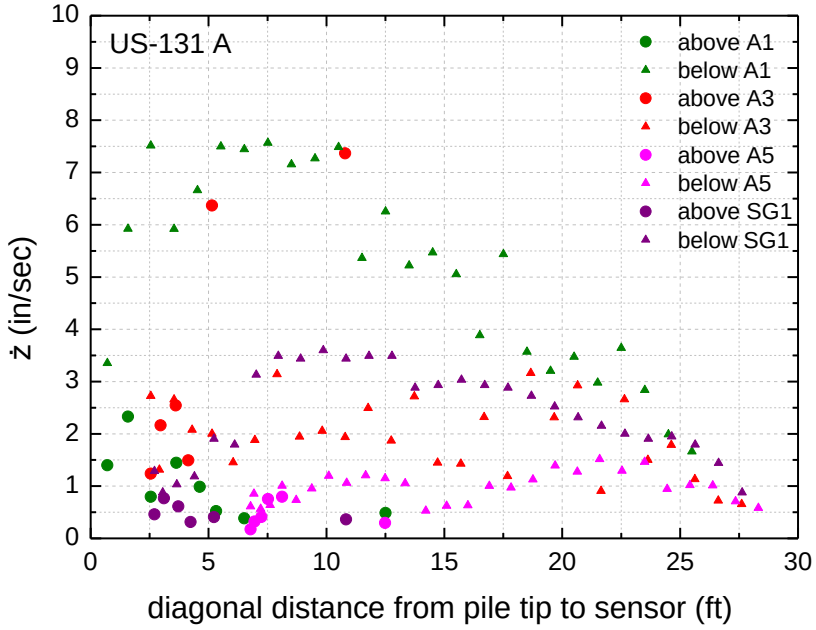

Figure 4-29 Peak vertical particle velocity, ż, versus diagonal distance from pile 1 to all sensors

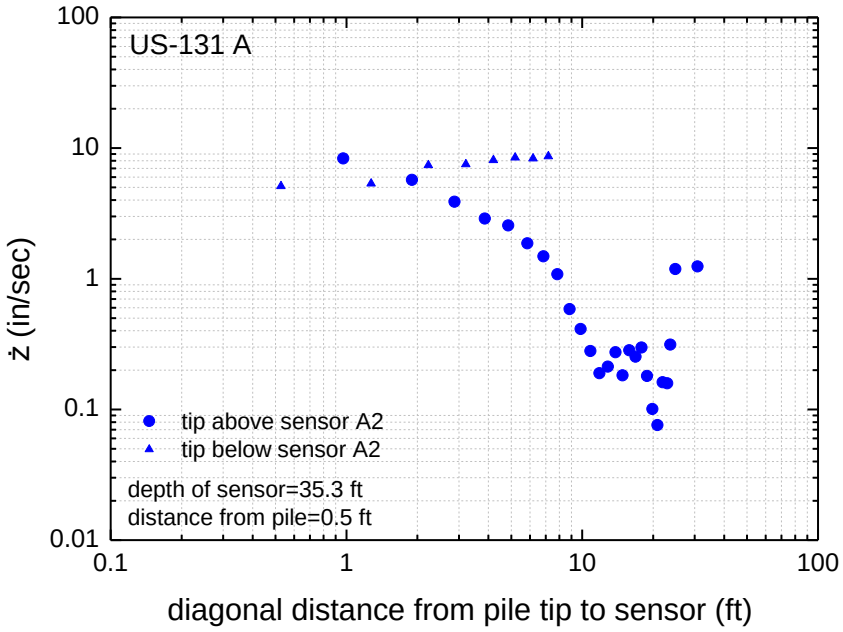

Figure 4-30 Peak vertical particle velocity, ż, versus diagonal distance from pile 1 to sensor A2

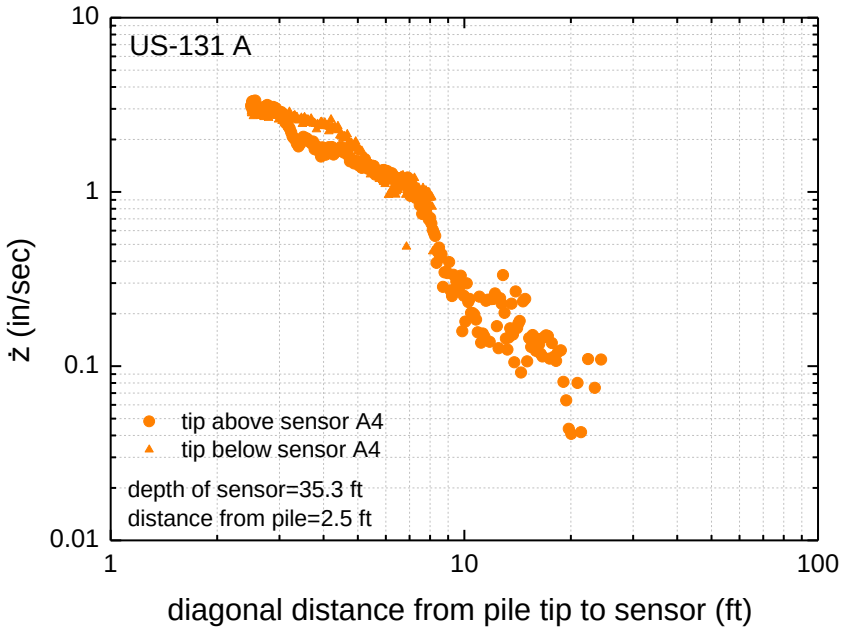

Figure 4-31 Peak vertical particle velocity, ż, versus diagonal distance from pile 1 to sensor A4

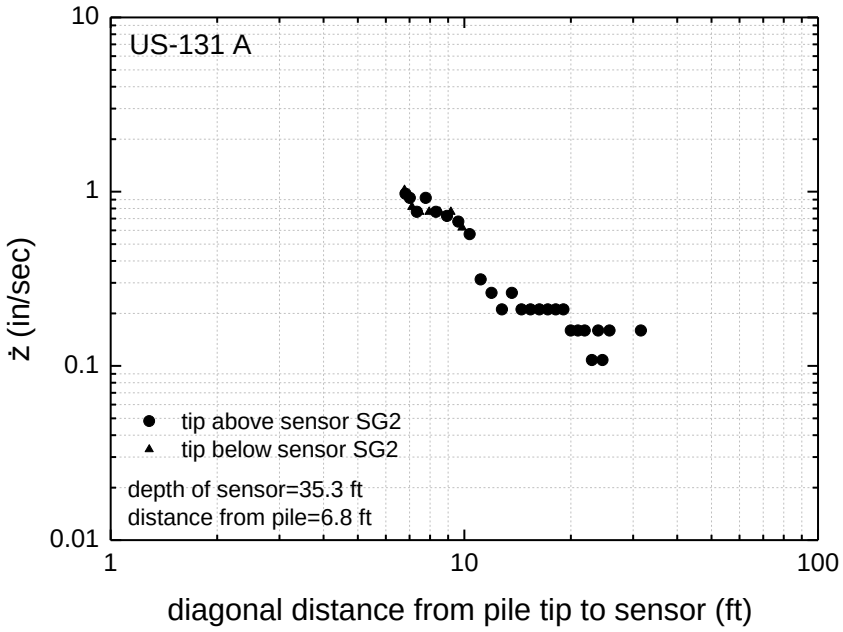

Figure 4-32 Peak vertical particle velocity, ż, versus diagonal distance from pile 1 to sensor SG2

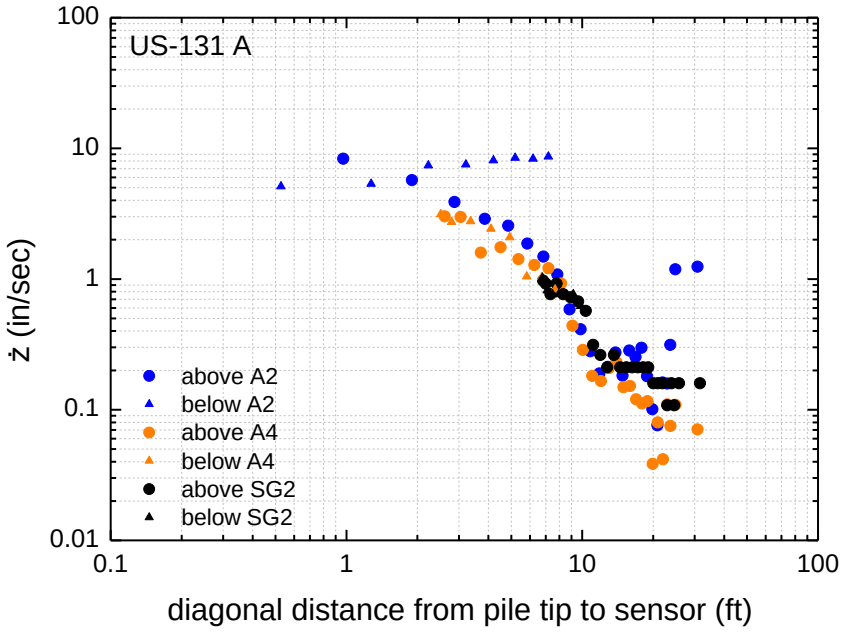

Figure 4-33 Peak vertical particle velocity, ż, versus diagonal distance from pile 1 to all sensors

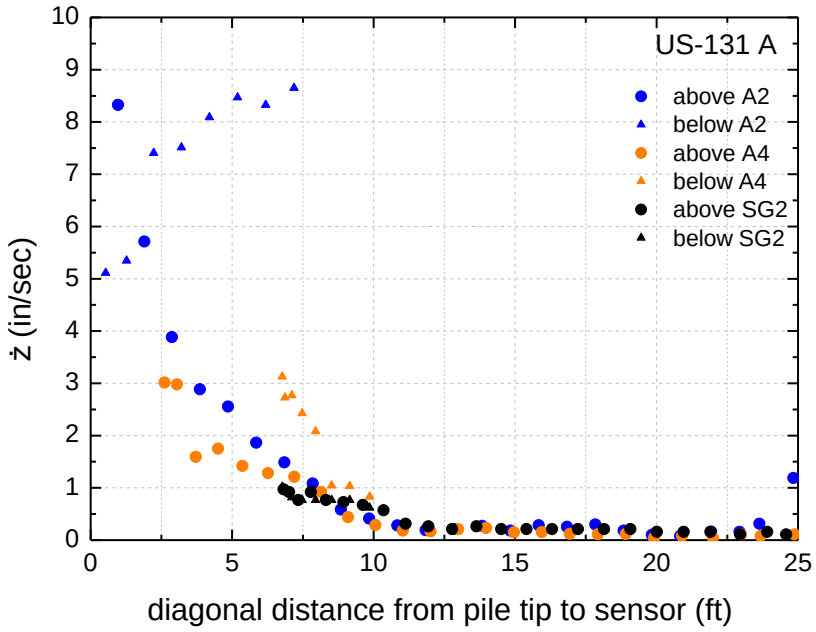

Figure 4-34 Peak vertical particle velocity, ż, versus diagonal distance from pile 1 to all sensors

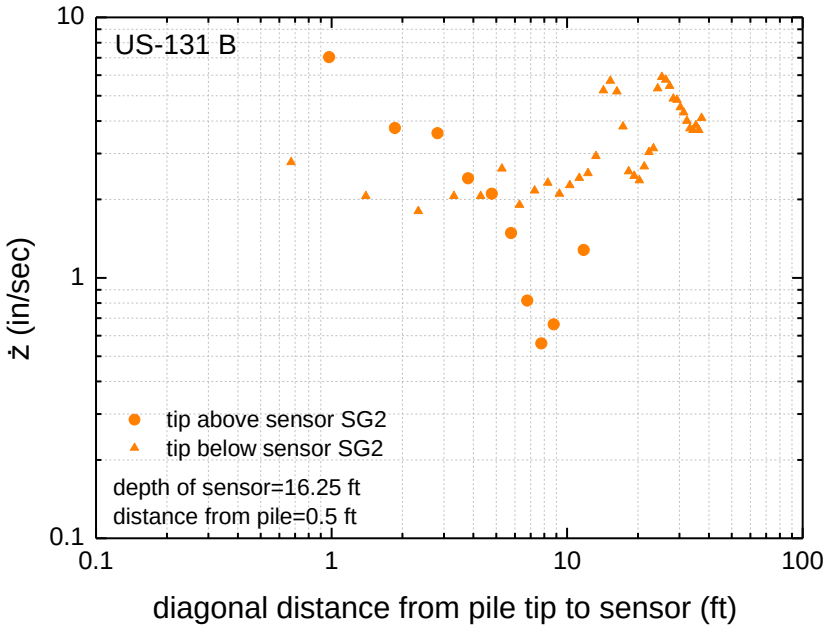

Figure 4-35 Peak vertical particle velocity, ż, versus diagonal distance from pile 54 to sensor SG2

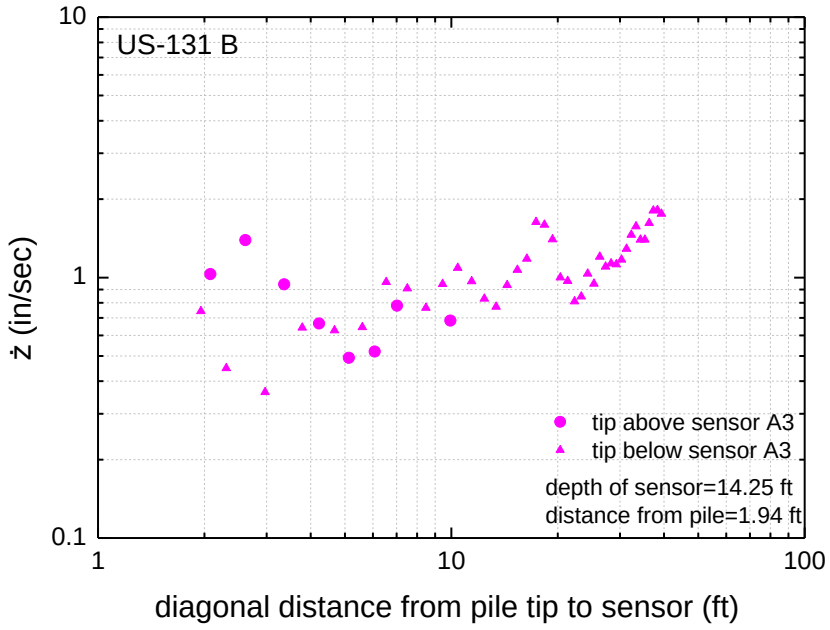

Figure 4-36 Peak vertical particle velocity, ż, versus diagonal distance from pile 54 to sensor A3

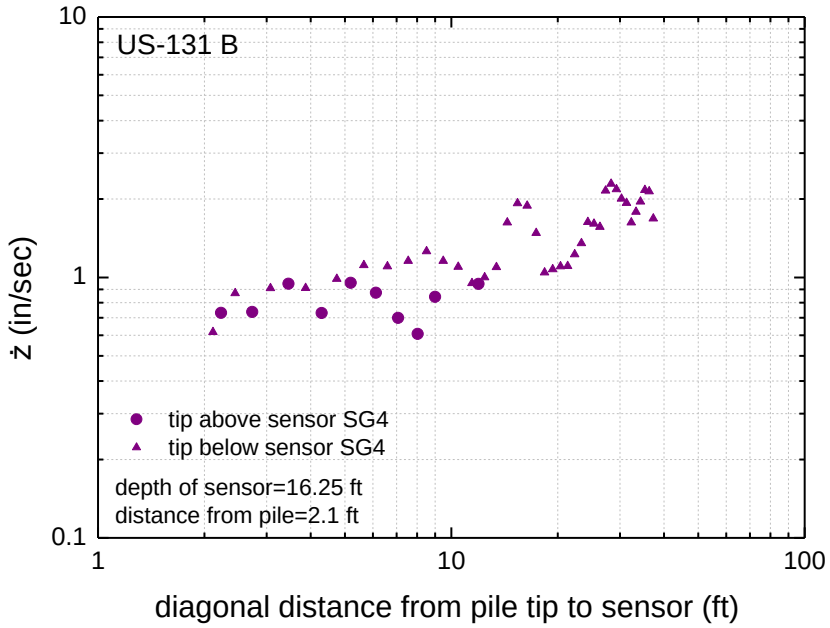

Figure 4-37 Peak vertical particle velocity, ż, versus diagonal distance from pile 54 to sensor SG4

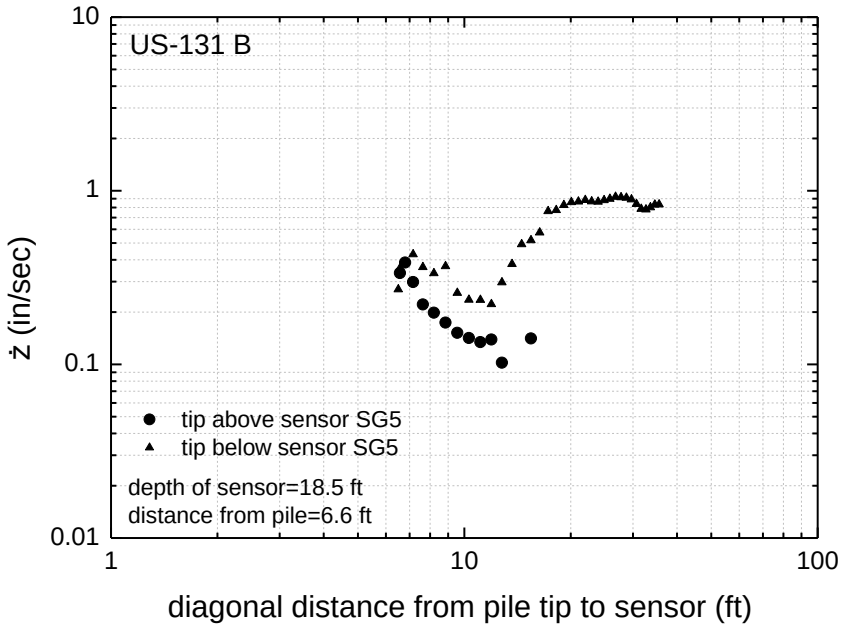

Figure 4-38 Peak vertical particle velocity, ż, versus diagonal distance from pile 54 to sensor SG5

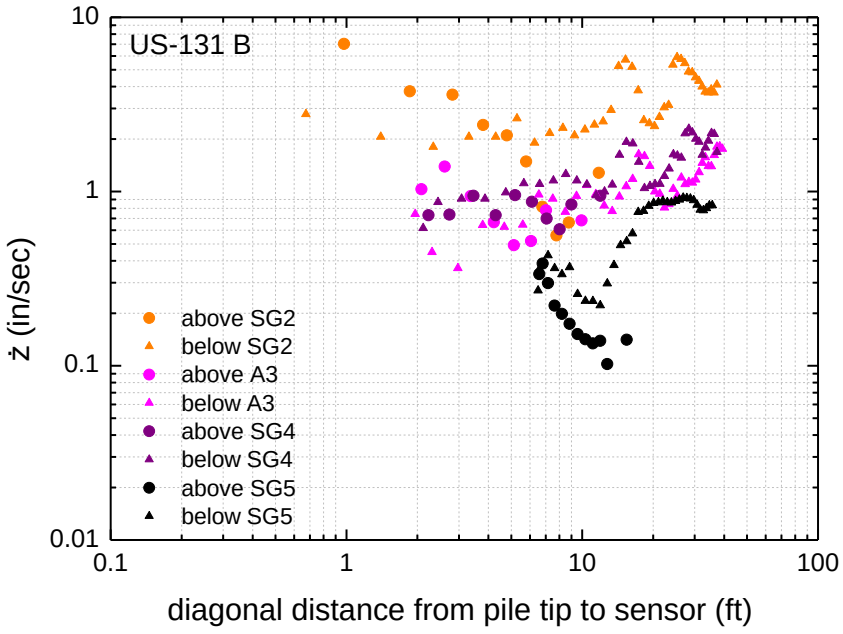

Figure 4-39 Peak vertical particle velocity, ż, versus diagonal distance from pile 54 to all sensors

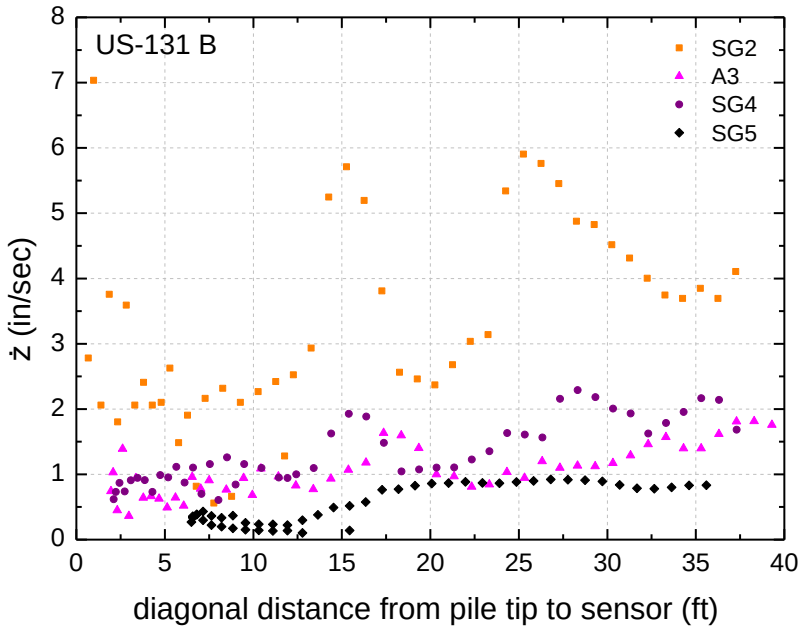

Figure 4-40 Peak vertical particle velocity, ż, versus diagonal distance from pile 54 to all sensors

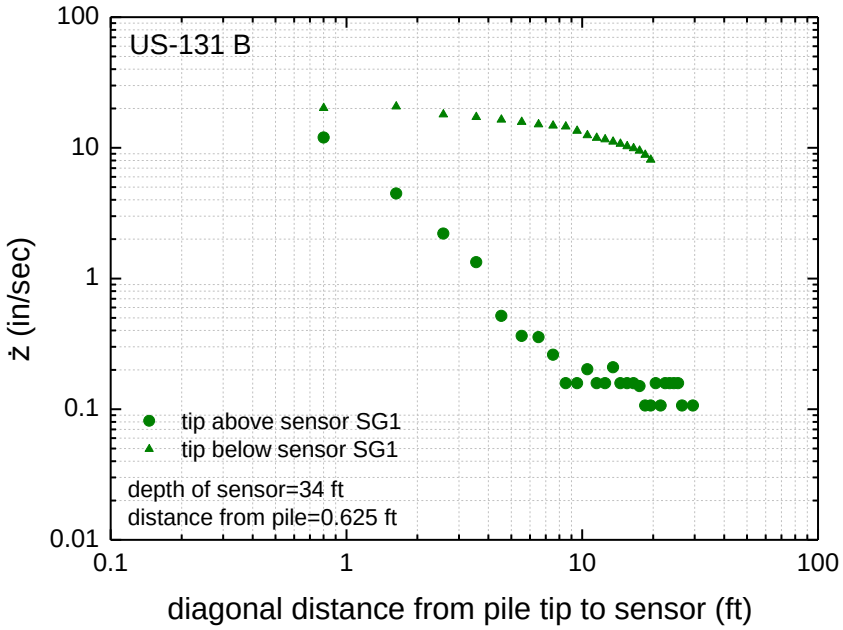

Figure 4-41 Peak vertical particle velocity, ż, versus diagonal distance from pile 54 to sensor SG1

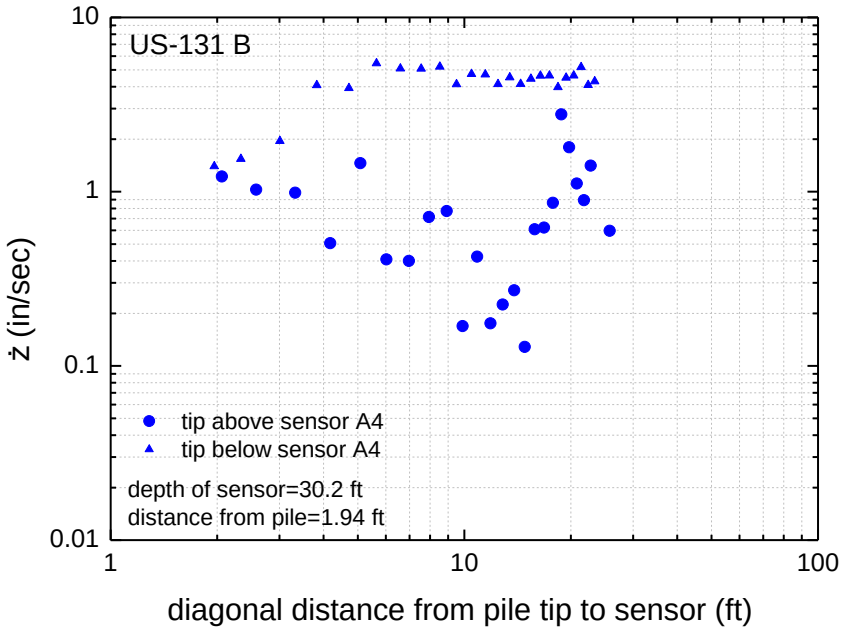

Figure 4-42 Peak vertical particle velocity, ż, versus diagonal distance from pile 54 to sensor A4

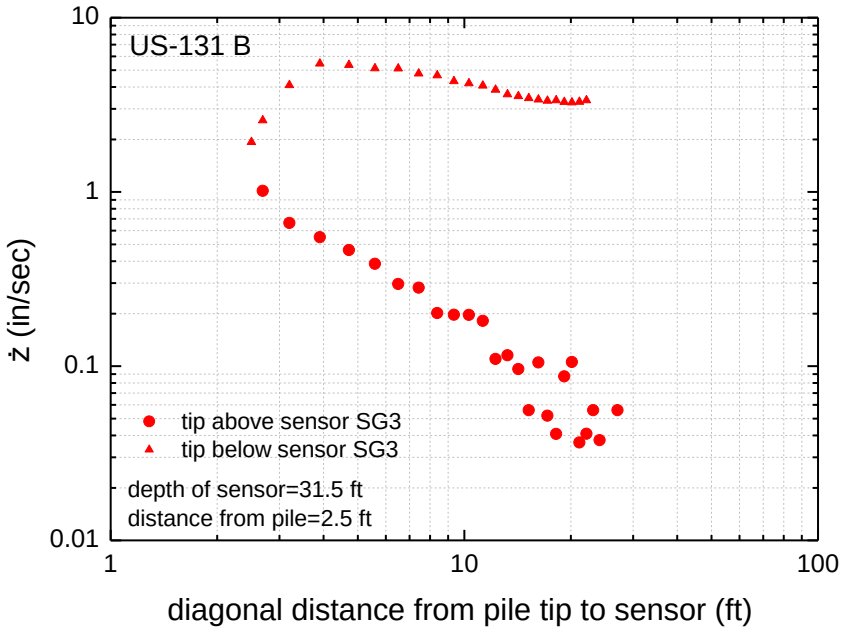

Figure 4-43 Peak vertical particle velocity, ż, versus diagonal distance from pile 54 to sensor SG3

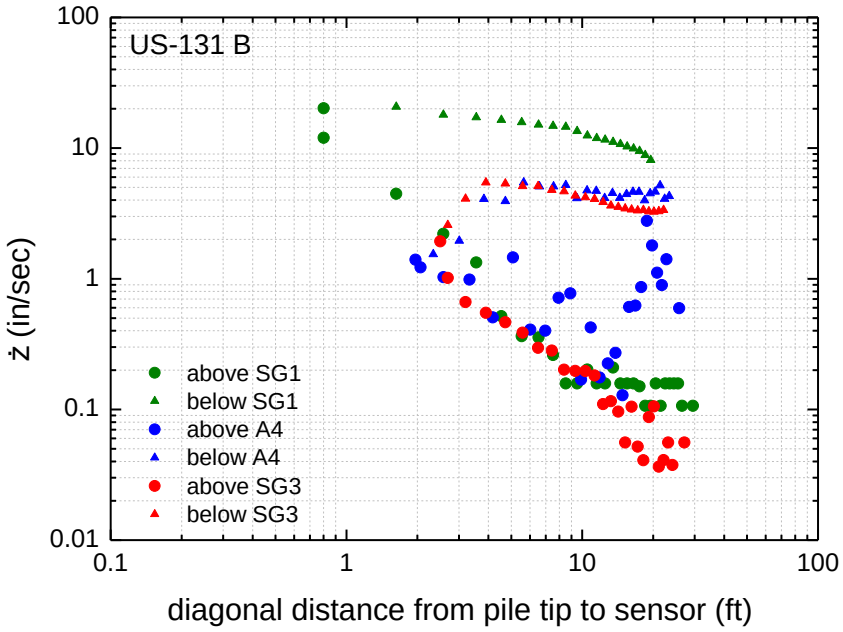

Figure 4-44 Peak vertical particle velocity, ż, versus diagonal distance from pile 54 to all sensors

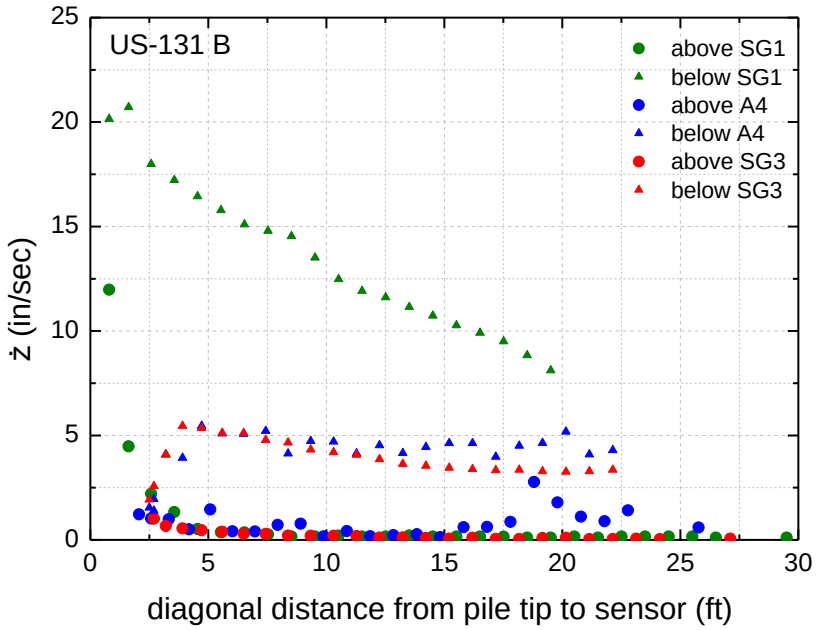

Figure 4-45 Peak vertical particle velocity, ż, versus diagonal distance from pile 54 to all sensors

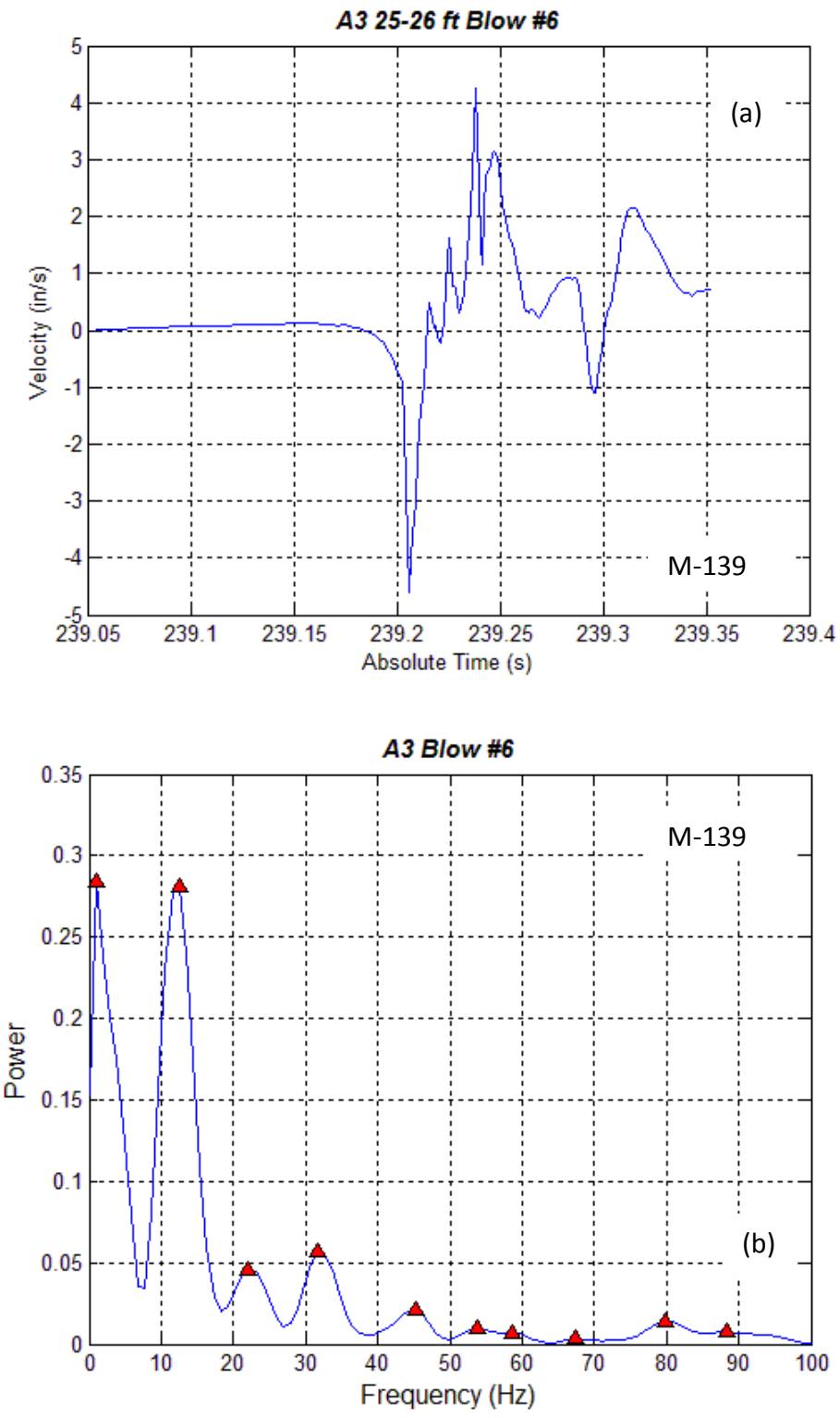

Figure 4-46 Single pile hammer blow signal (a) and frequency content (b), M-139 site

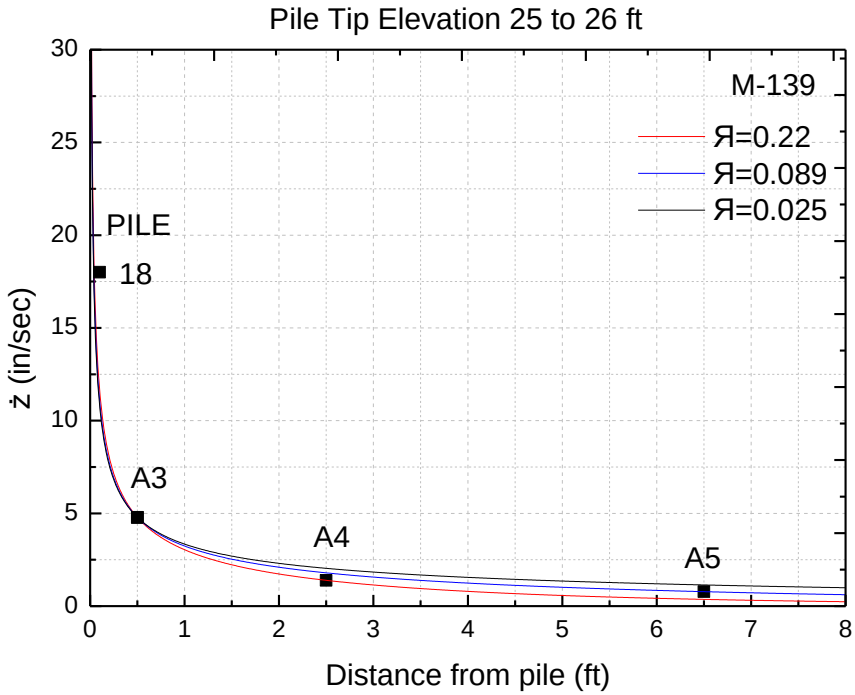

Figure 4-47 Attenuation curves with A3 as base point, M-139 site

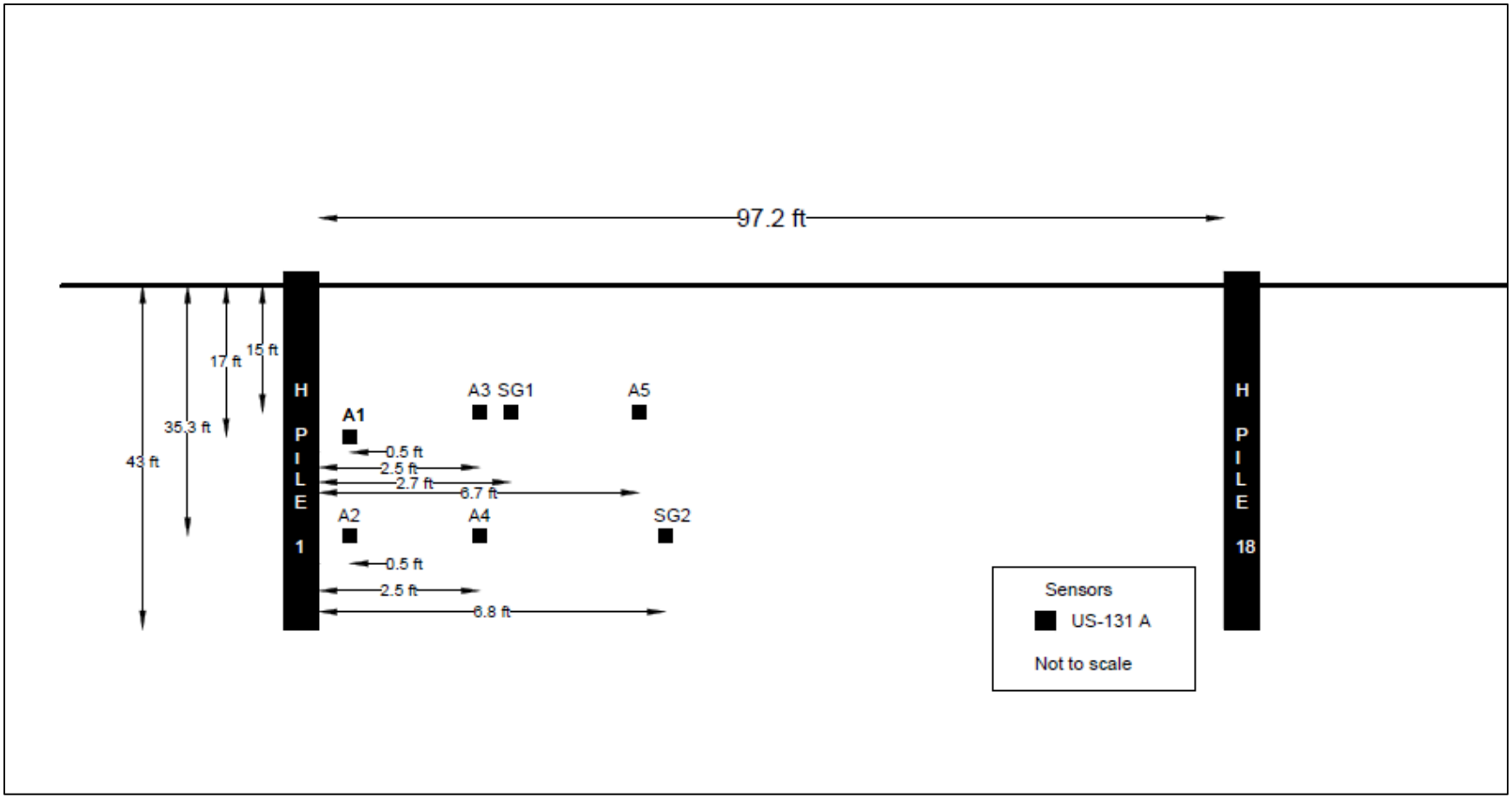

Figure 4-48 Cross section of two piles tested at US-131 A site

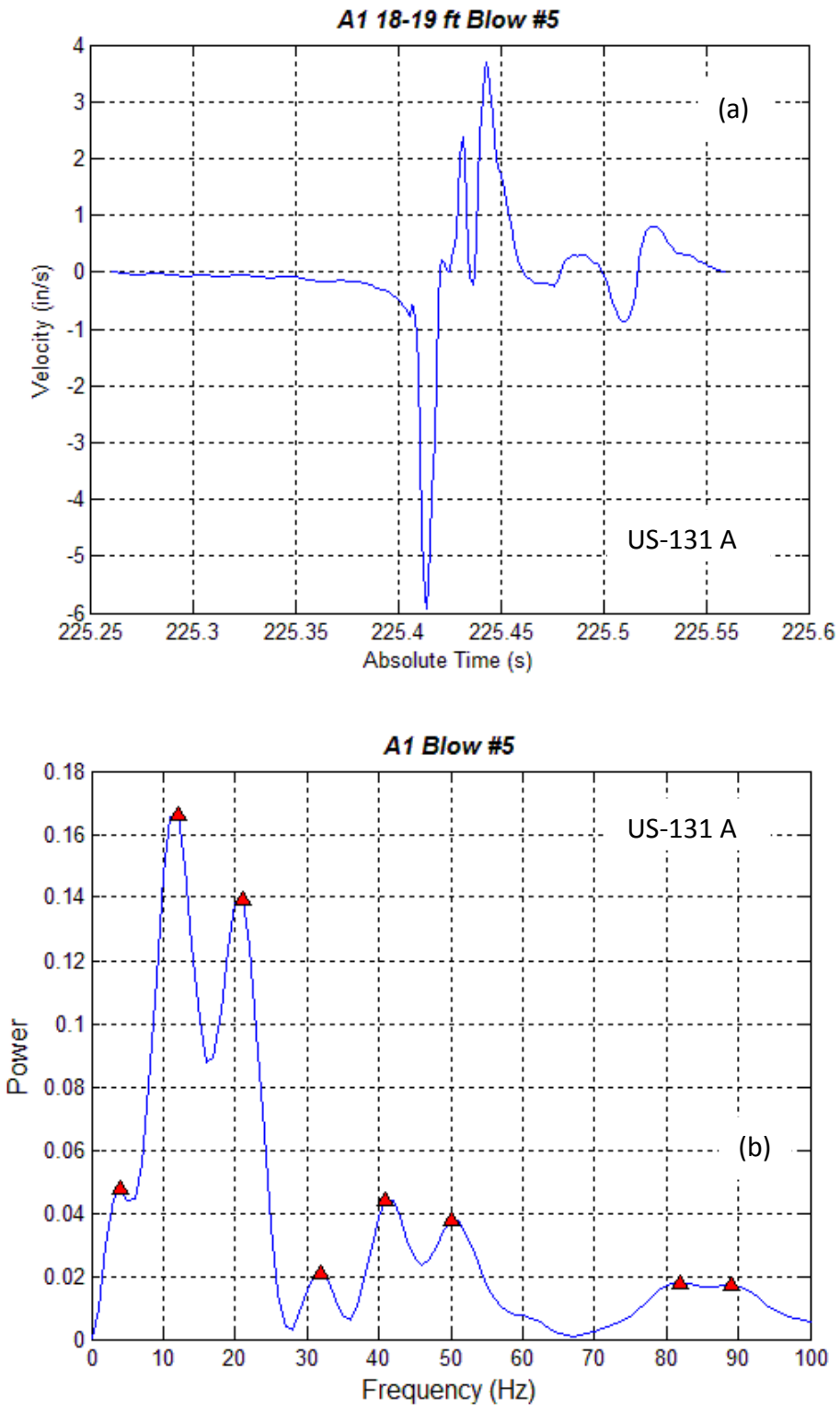

Figure 4-49 Single pile hammer blow signal (a) and frequency content (b), US-131 A site

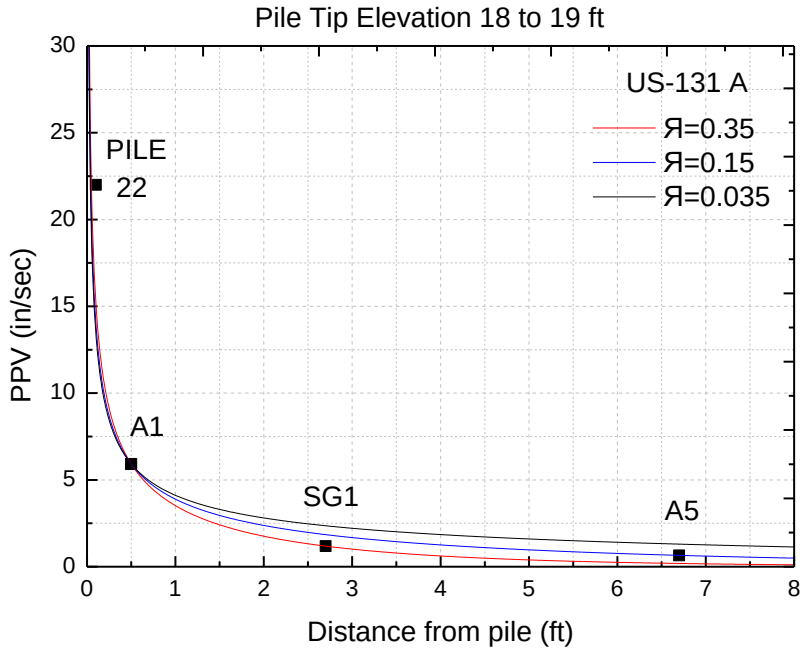

Figure 4-50 Attenuation curves with A1 as base point, US-131 A site (Pile 1)

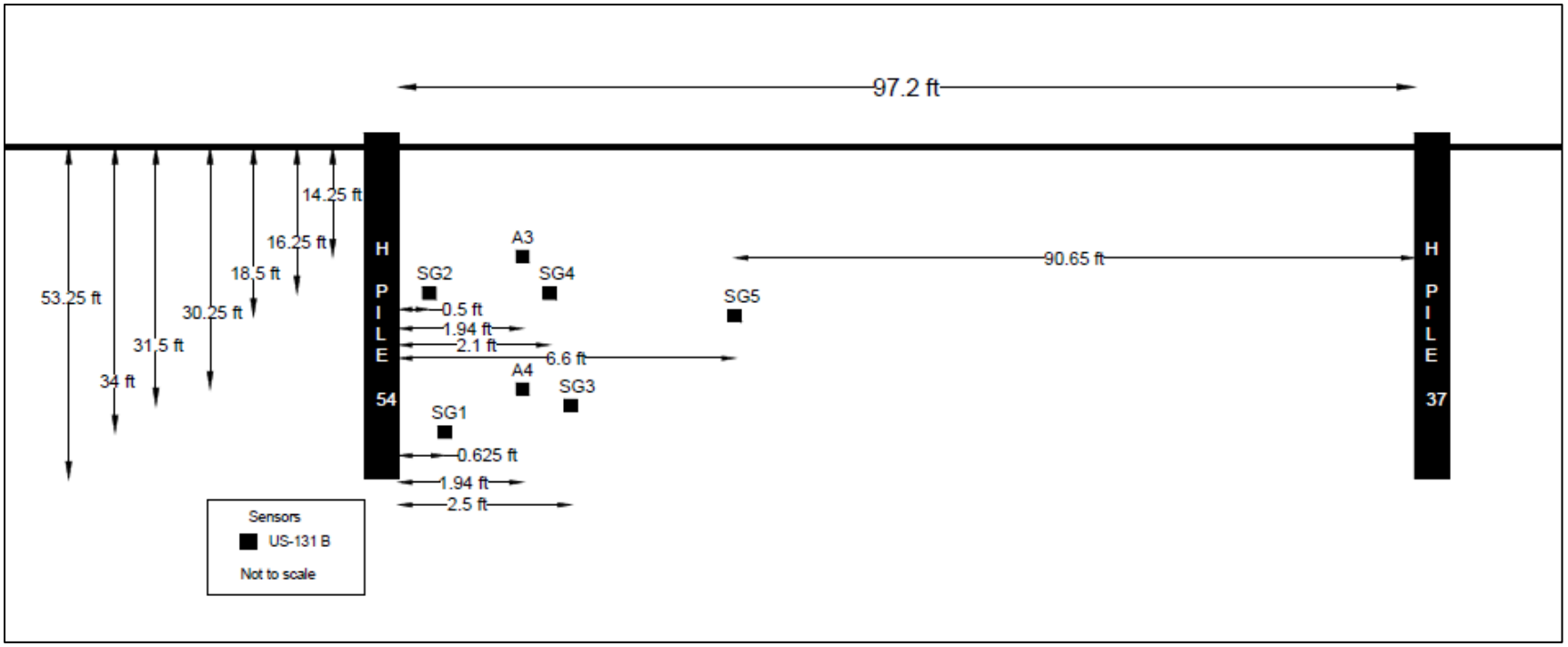

Figure 4-51 Cross section of two piles tested at US-131 B site

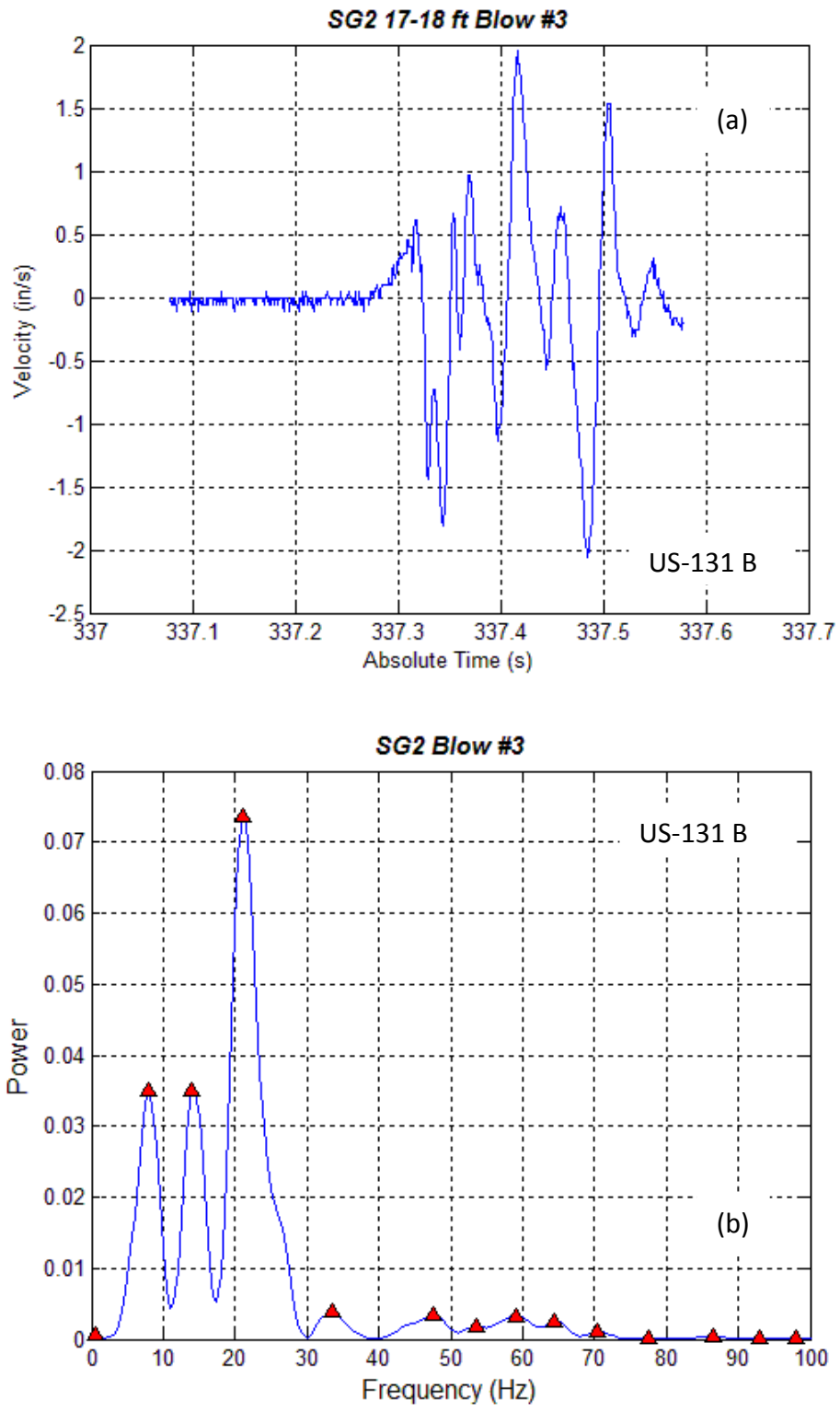

Figure 4-52 Single pile hammer blow signal (a) and frequency content (b), US-131 B site

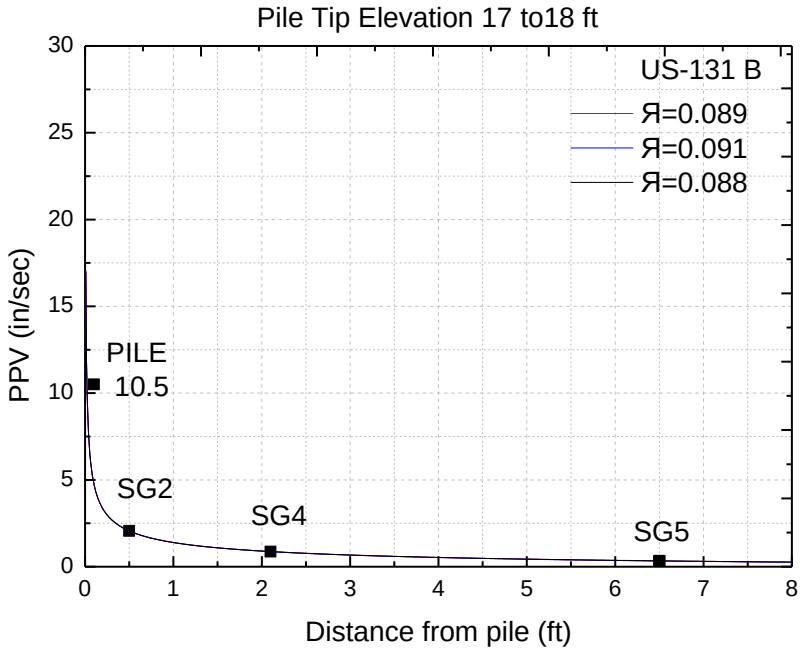

Figure 4-53 Attenuation curves with SG2 as base point, US-131 B site (Pile 54)

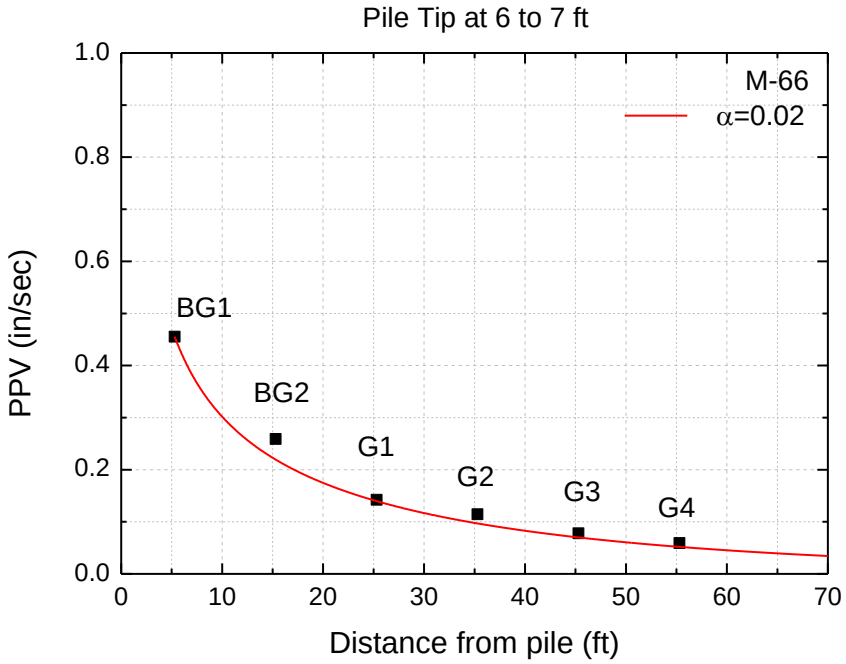

Figure 4-54 Attenuation curves for surface geophones, M-66 site

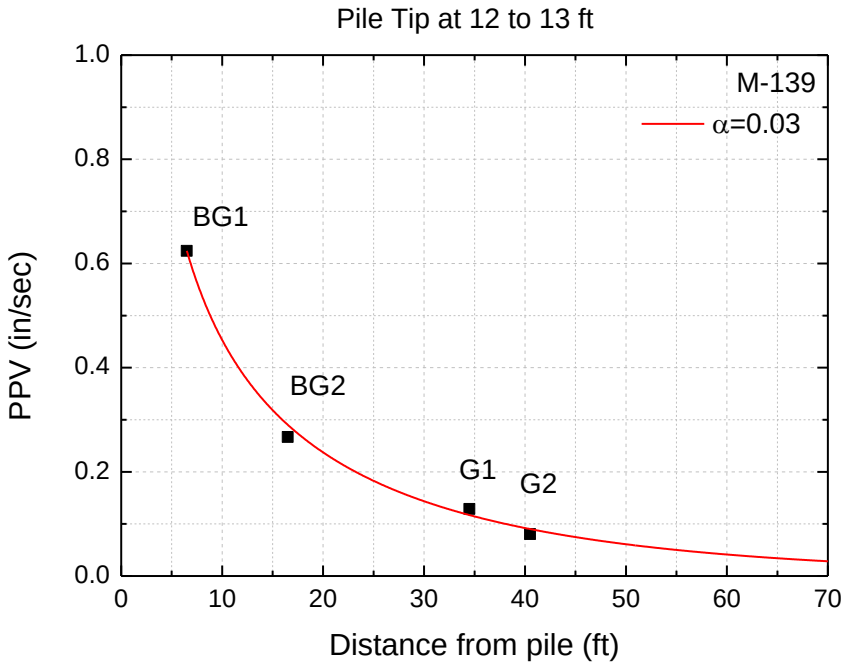

Figure 4-55 Attenuation curves for surface geophones, M-139 site

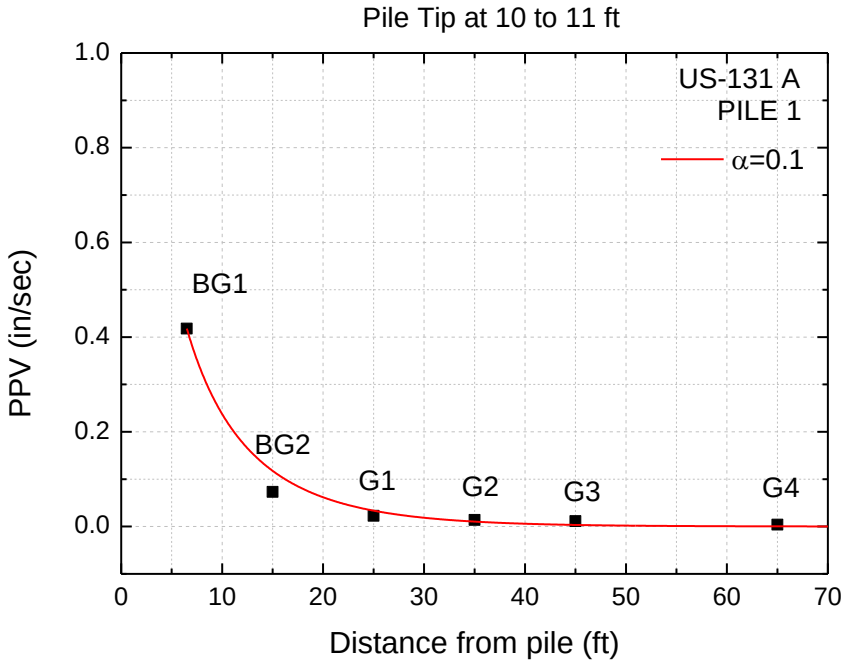

Figure 4-56 Attenuation curves for surface geophones, US-131 A site (Pile 1)

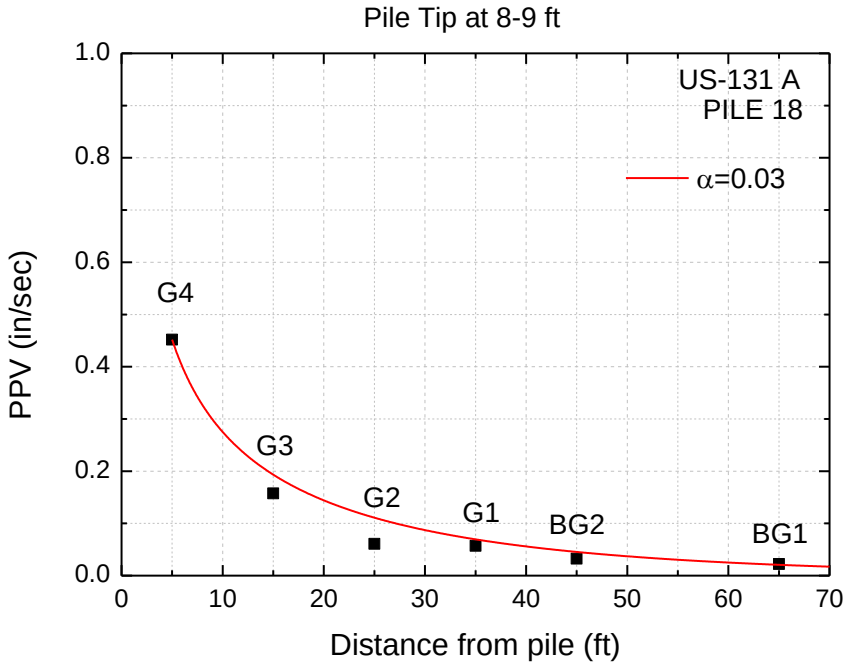

Figure 4-57 Attenuation curves for surface geophones, US-131 A site (Pile 18)

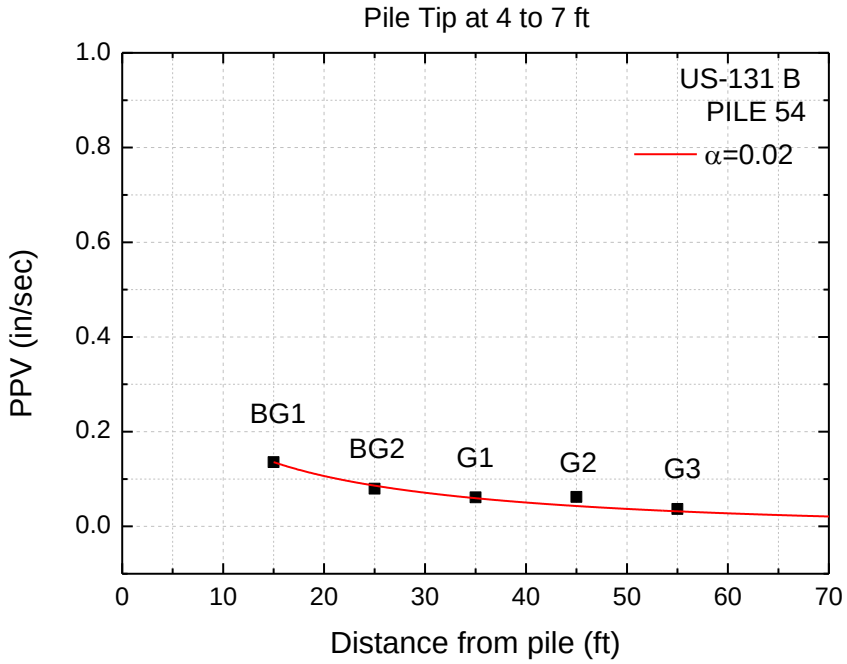

Figure 4-58 Attenuation curves for surface geophones, US-131 B site (Pile 54)

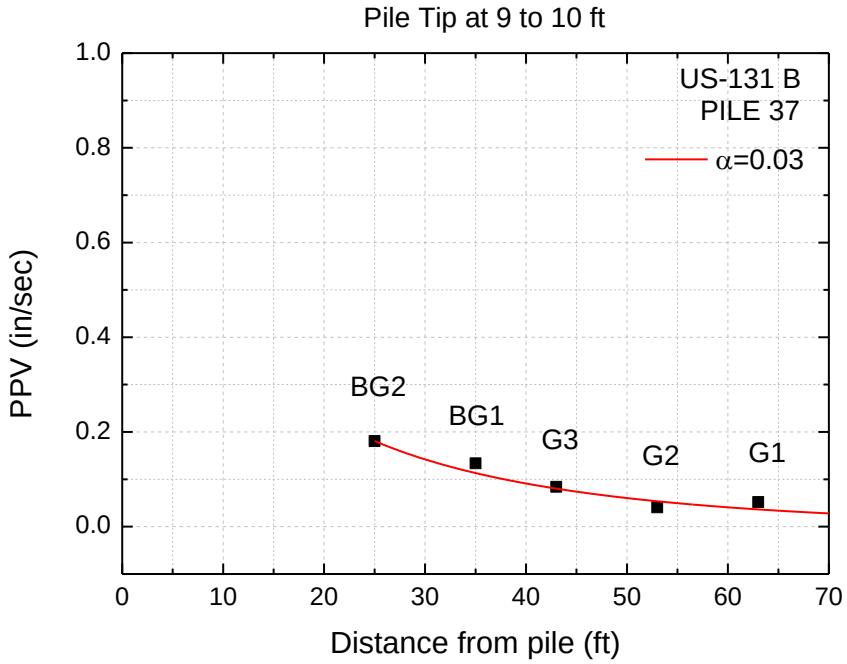

Figure 4-59 Attenuation curves for surface geophones, US-131 B site (Pile 37)

5 SETTLEMENT SOFTWARE TOOL

5.1 Summary of process for estimation of susceptibility of ground to shakedown settlement from pile driving

To evaluate the potential for a soil to undergo shakedown settlement from pile driving, the shearing strain amplitude in the region of the ground surrounding the pile must be estimated. There are two basic sources of energy emanating from the pile while it is being driven: pile shaft and pile tip. A mechanism of energy transfer from pile to soil must be employed for each of the basic energy sources. From the shaft, the energy transfer is limited by the maximum shearing strength of the soil beyond, in which there is relative motion between soil and pile. From the tip, the relative impedance between the pile and the soil controls the transfer of energy. After energy is coupled into the ground around the pile, it is attenuated traveling through the soil from both geometric and hysteretic phenomena. At any distance from the pile where shakedown potential is to be evaluated, particle motion (vibrations) from shaft and tip are summed constructively. Shearing strain is then calculated from summed particle velocity divided by appropriate shear wave velocity and compared with a widely accepted threshold strain.

The above calculations are based on a few basic parameters associated with any given pile driving operation:

- Type of pile and expected penetration
- Type and model of pile driver
- Ground stratification
- Ground properties (derived from SPT (N) and Unified Classification Symbols)

All of these elements can be formulated into a spreadsheet calculation for easy evaluation of likely ground settlement. Following are the steps of developing and applying a spreadsheet calculation.

5.2 Energy coupled into the ground from pile shaft

Massarsch and Fellenius (2008) presented an equation for predicting the maximum amplitude of soil motion (Peak Particle Velocity, PPV) that can be generated by shear between the shaft of the pile and the soil being penetrated (pile-soil interface):

$$\dot{z}_s = \tau/(\rho V_s^*) \qquad (5.1)$$

$\dot{z}_s$ = peak particle velocity in the soil at the pile-soil interface (ft/sec)
τ = shearing strength of soil (lb/ft^2)
ρ = mass density of the soil ($lb\text{-}sec^2/ft^4$)
V_s* = shear wave velocity of soil at the contact with the pile (ft/sec)

Equation (5.1) estimates the PPV that will be coupled into the soil and transmitted away from the pile shaft as a cylindrical shear wave. The value V_s* represents the shear wave velocity at large strain. Low strain V_s is calculated from a correlation equation between V_s and N:

$$V_s = 318N^{0.314} \quad \text{(Imai and Tonouchi, 1982)} \qquad (5.2)$$

V_s = shear wave velocity at very low strain (ft/sec)
N = SPT (blows/ft) (uncorrected)

Equation (5.2) was selected because it was the best fit with V_s measured using the Multichannel Analyses of Surface Waves (MASW) and N values at the sites. V_s* can now be calculated by applying a reduction factor to V_s:

$$V_s^* = RV_s \qquad (5.3)$$

R = dimensionless reduction factor (after Massarsch and Fellenius, 2008)

Selection of R was made after back calculation of V_s* from the monitored PPV of the closest to the pile embedded sensors (0.5 ft), indicating R=0.2 as the value to use.

The shearing strength (τ) can be estimated from the SPT blow count N. Friction angle (ϕ) is obtained through correlation between N and ϕ (Kulhawy and Mayne, 1990):

$$\phi \approx \tan^{-1}[N/(12.2+20.3\sigma_v'/Pa)]^{0.34} \qquad (5.4)$$

N = field standard penetration number (blows/ft.)
σ_v' = effective overburden stress (psf)
Pa = atmospheric pressure (2116 psf)
ϕ = friction angle (degrees)

Table 5-1 presents typical unit weights for various soils used to determine the effective overburden stress σ_v' in absence of exact values from laboratory tests. To indicate the consistency of granular soils which are of most interest, Table 5-2 is used to correlate the relative density (Dr) with N. Table 5-3 presents a correlation of undrained strength with N for cohesive soils.

Table 5-1 Typical unit weights for various soils (Coduto, 2001)

Soil Type	Classification	Dry unit weight, γ_d (pcf)	Saturated unit weight, γ_s (pcf)
GP, Poorly graded gravel	Sand	110-130	125-140
GW, Well graded gravel	Sand	110-140	125-150
GM, Silty gravel	Sand	100-130	125-140
GC, Clayey gravel	Sand	100-130	125-140
SP, Poorly graded sand	Sand	95-125	120-135
SW, Well graded sand	Sand	95-135	120-145
SM, Silty sand	Sand	80-135	110-140
SC, Clayey sand	Clay	85-130	110-135
ML, Low plasticity silt	Clay	75-110	80-130
MH, High plasticity silt	Clay	75-110	75-130
CL, Low plasticity clay	Clay	80-110	75-130
CH, High plasticity clay	Clay	80-110	70-125
PT, Peat	Clay	30	70

Table 5-2 Relative density of cohesionless soils versus N

N Value (Blows/ft)	Classification	Relative Density Dr (%)
0-4	Very loose	0-15
4-10	Loose	15-35
10-30	Medium Dense	35-65
30-50	Dense	65-85
>50	Very Dense	85-100

Source: Terzaghi and Peck (1967), Lambe and Whitman (1969)

Table 5-3 Approximate values of undrained shear strength versus N for cohesive soils

N Value (Blows/ft.)	Consistency	Su (psf)
<2	Very Soft	<250
2-4	Soft	250-500
4-8	Medium	500-1000
8-15	Stiff	1000-2000
15-30	Very Stiff	2000-4000
>30	Hard	>4000

Source: Terzaghi and Peck (1967)

5.3 Energy coupled into the soil from the tip of the pile

The energy coupled to the ground at the tip of the pile during driving is a function of the ratio of impedances of the pile and ground at the level of the tip. GRL WEAP and PDA analysis demonstrate that about 50% of the rated hammer energy reaches the top of the pile. This energy is called ENTHRU. Although energy is lost to shaft friction as the pile is driven, these losses have been neglected. It is conservatively assumed that all ENTHRU energy reaches the tip of the pile to maximize the predicted shear strain.

Particle velocity in the soil at the tip depends on the relative impendances of the pile and soil at the tip and the energy reaching the pile tip (Massarsch and Fellenius, 2008):

$$\dot{z}_t = 2R_R(Q_s/Q_P)(E_o)^{0.5}\cos\theta \qquad (5.5)$$

$\dot{z}_t$ = vertical component of particle velocity in the soil at pile tip (ft/sec)

R_R = dimensionless correction factor accounting for soil compaction in cohesionless soils and remolding in cohesive soils

R_R = 2 for loose to medium sand (dense sand need not be evaluated)

$0.2 < R_R < 0.5$ for normally consolidated to overconsolidated clay

Q_s = Impedance of soil at tip of pile = $A_c\rho_s V_{sp}$* (lb-sec/ft.)

Q_p = Impedance of pile at tip = $A_c\rho_p V_p$ (lb-sec/ft.)

A_c = contact area between pile and soil (ft^2)

V_{sp}* = Velocity of Biot wave of the second kind in soil (ft./sec)

V_p = Compression wave velocity in pile (ft./sec)

E_o = 0.5 times rated energy of hammer (ft-lb)

θ = angle between any ray of spherical wave and vertical (radians)

ρ_s = mass density of the soil ($lb\text{-}sec^2/ft^4$)

ρ_p = mass density of the pile ($lb\text{-}sec^2/ft^4$)

Wave velocity used in the soil impedance term (Q_s) in equation (5.5) is the Biot wave of the second kind, i.e. a wave with velocity slightly slower than the primary wave velocity in the soil (Richart et al, 1970). For this analysis the primary wave velocity (V_{sp}) can be used. This wave velocity in the soil will also be used to calculate strain caused by penetration of the pile at the tip at any point in the surrounding soil zone. The wave velocity V_{sp} can be calculated as follows:

$$V_{sp} = kV_s \qquad (5.6)$$

$$k = [2(1-\nu)/(1-2\nu)]^{0.5}$$

V_{sp} = primary wave velocity in the soil skeleton (ft/sec)
V_s = shear wave velocity in the soil based on equation (5.2) (ft/sec)
k = dimensionless ratio
ν = Poisson's ratio for soil (dimensionless)
use ν = 0.2 for granular soil yielding k = 1.63
and ν = 0.45 for cohesive soil yielding k = 3.32

$$V_{sp}^* = RV_{sp} \qquad (5.7)$$

V_{sp}^* = reduced primary wave velocity in the soil based on strain amplitude (ft/sec)
R = dimensionless reduction factor as in equation (5.3)

5.4 Attenuation of seismic waves

Multiple cycles of strain exceeding a threshold in a soil mass will cause volume change of the soil resulting in settlement of the soil. Using equations (5.1), (5.3), (5.5) and (5.7) the particle velocity in the soil next to the pile can be estimated. As the wave travels away from the pile, the amplitude of particle velocity decreases from both geometric and hysteretic damping.

The rate of attenuation of the shear wave travelling from the shaft of the pile (cylindrical) is different than the rate of attenuation of the primary wave travelling from the tip of the pile (spherical). A modified formula of the Bornitz equation (Richart et al, 1970) will be used to express the attenuation of both types of waves:

$$\dot{z}_2 = \dot{z}_1(r1/r2)^n \exp[-я\,(r2-r1)] \qquad (5.8)$$

$\dot{z}_2$ = particle velocity amplitude at point 2 (ft./sec)
$\dot{z}_1$ = particle velocity amplitude at point 1 (ft./sec) of known amplitude
r_1 = distance from source to point 1 = 0.1 in. = 0.0083ft

r_2 = distance from source to point 2 of unknown distance (ft.)
n = power exponent depending on wave type
    n = 0.5 for shear wave coming from the shaft (cylindrical)
    n = 1 for primary wave coming from the tip (spherical)
я = coefficient of attenuation for soil (1/ft.)

The attenuation coefficient я was calculated after fitting equation (5.8) to measured data from the sensors of the sites tested as discussed in section 4.4. According to the monitored data я was found to be approximately 0.1 for distances from the pile up to 10 ft. Beyond 10 ft. distances from the pile я is set as 0.02. The distance r_1=1 in. (≈ 0.1 ft.) represents the first point where the maximum amplitude of soil motion right next to pile shaft for cylindrical waves and below the pile tip for spherical waves is estimated. Then, using equation (5.8) the amplitude of particle velocity at any point in the soil mass can be determined when the amplitude of particle velocity at the pile shaft or tip is known.

5.5 Calculation of shearing strain at points in soil mass

Strain associated with the seismic waves can be calculated as particle velocity divided by wave velocity. For shear waves travelling from the shaft, shearing strain is calculated as:

$$\gamma_{shaft} = \dot{z}_s/V_s^* \quad (5.9)$$

γ = shearing strain
V_s^* from equation (5.3) where R is increased for each 5 feet of distance from the pile by 0.05 starting with R = 0.2 at the shaft.

For primary waves travelling from the tip, shearing strain is calculated as:

$$\gamma_{tip} = \dot{z}_t/V_{sp}^* \quad (5.10)$$

V_{sp}^* reduced from equation (5.3) in a manner similar to equation (5.9)

Summation of shaft and tip contributions of shear strain give the total shear strain which is the compared with the threshold strain (0.01%). With increased distances from pile, it is possible to determine the distance beyond which strain amplitude is less than the threshold.

5.6 Step by step process and example of use of spreadsheet

The previous calculations were implemented in a Microsoft Office Excel spreadsheet. An illustrative example is provided in the following section based on actual data collected at the M-139 site.

The following steps should be followed by the user in terms of the input data that are needed, in order to estimate the potential of nearby soil to settle from driving a pile.

1) Using the closest boring to the area that the pile will be driven, divide the soil profile into layers with similar soil properties. It is important to divide the layers by the classification based on the descriptions provided by the soil boring logs in order to distinguish between cohesive and non-cohesive soils. The ground surface elevation needs to be adjusted from the boring value if the area of the pile to be driven was excavated after the drilling. Calculate a representative N for every layer using the soil boring data for each layer (Figure 5-1).

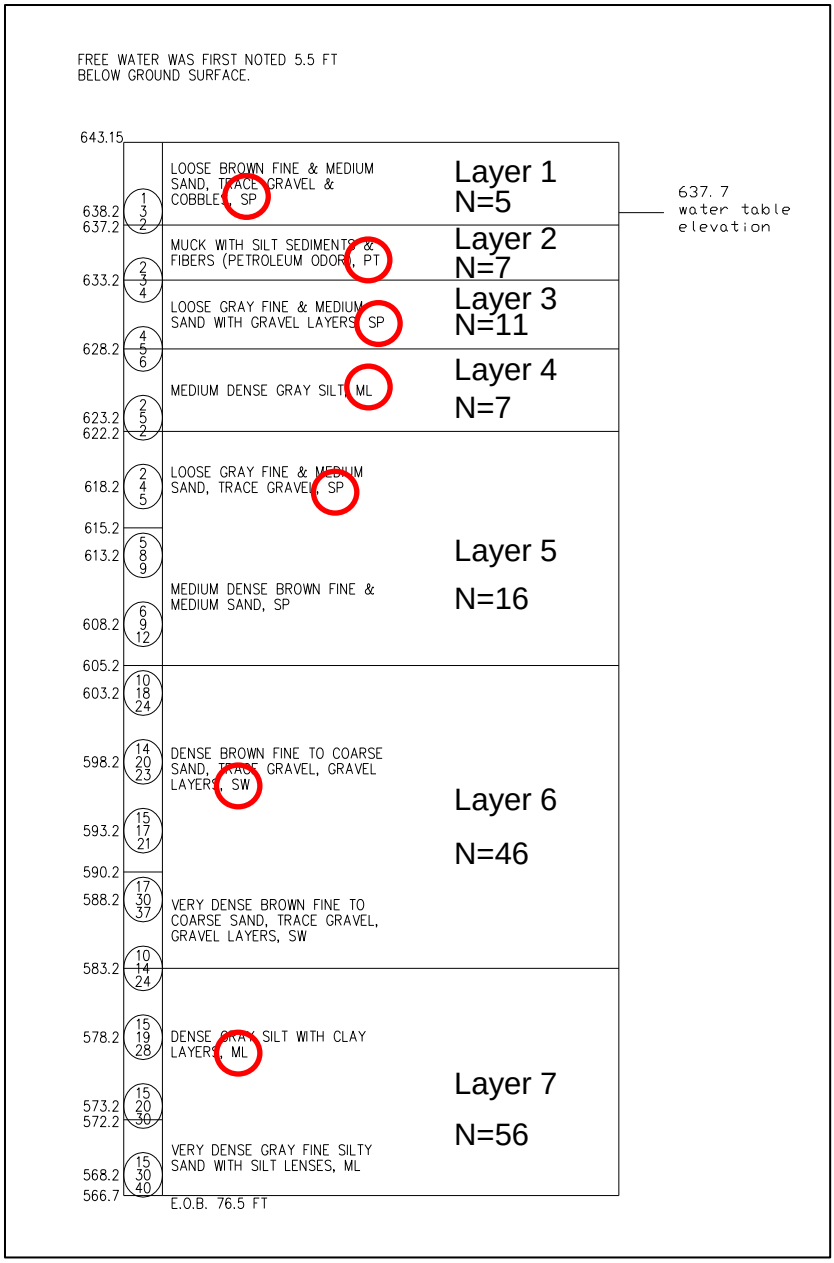

Figure 5-1 Division of soil profile into layers with same soil properties

In the tab “General Data” of the spreadsheet:

2) Input the adjusted ground surface elevation found in step 1 (Figure 5-2).

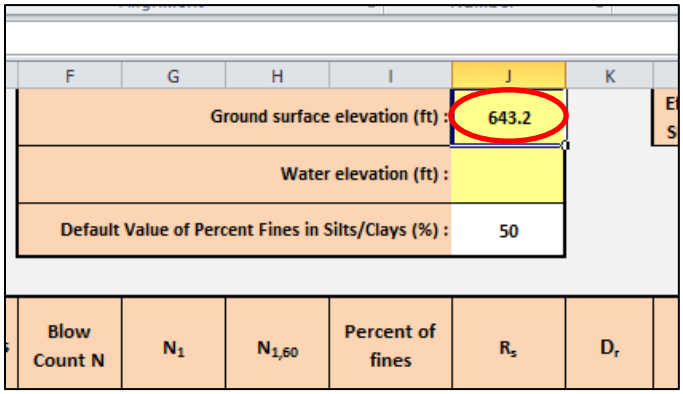

Figure 5-2 Input of ground surface elevation

3) Input the water table elevation (Figure 5-3).

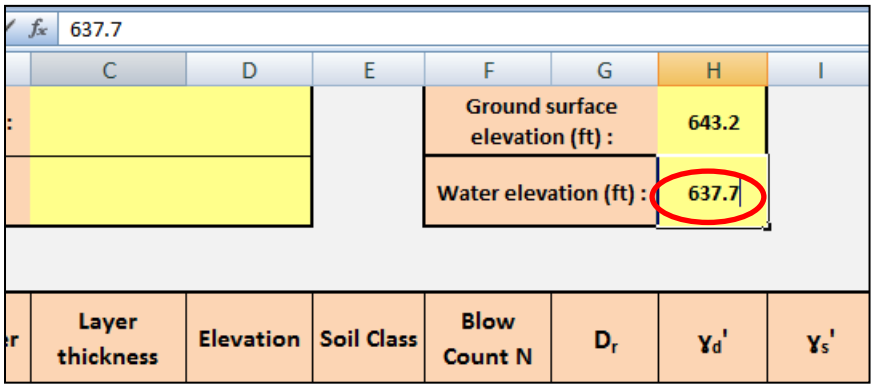

Figure 5-3 Input of water table elevation

4) Input the elevation at the bottom of each layer that you have divided the soil profile in step 1 (Figure 5-4).

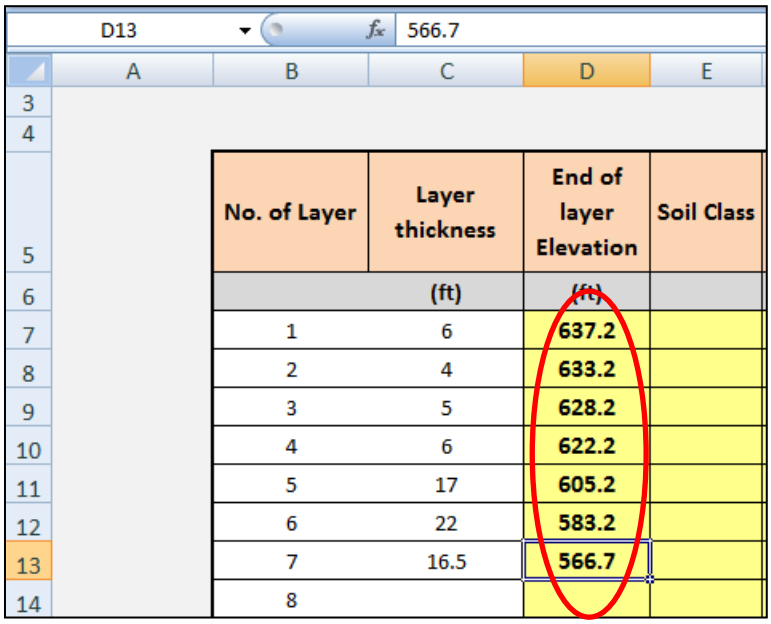

Figure 5-4 Input of elevation at end of each layer

5) Classify each soil layer by the Unified Soil Classification System based on the descriptions of the layers provided by the soil boring data (Figure 5-5)

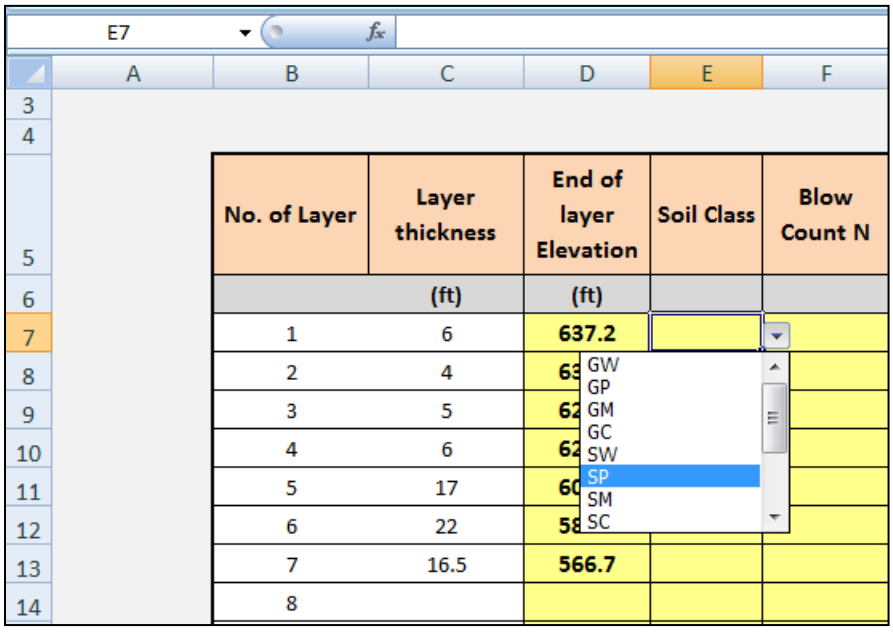

Figure 5-5 Soil layer characterization

6) Input the representative N for each layer calculated in step 1 (Figure 5-6). The corrected N_1 and $N_{1,60}$ will be automatically calculated in the next two columns.

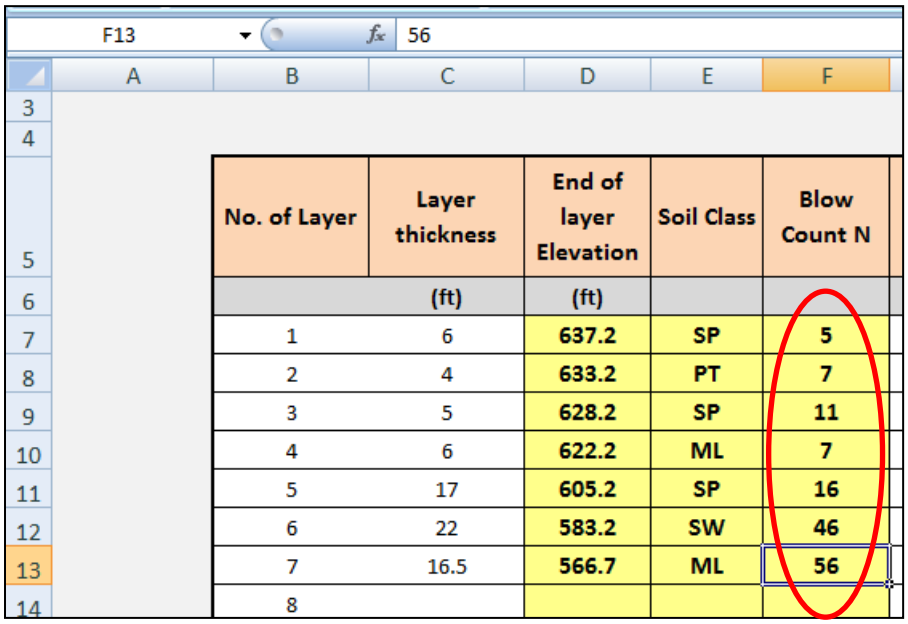

F13 | 56

	No. of Layer	Layer thickness	End of layer Elevation	Soil Class	Blow Count N
		(ft)	(ft)		
7	1	6	637.2	SP	5
8	2	4	633.2	PT	7
9	3	5	628.2	SP	11
10	4	6	622.2	ML	7
11	5	17	605.2	SP	16
12	6	22	583.2	SW	46
13	7	16.5	566.7	ML	56
14	8				

Figure 5-6 Input of average N for every soil layer

7) Select the size of the H-pile that will be driven (Figure 5-7).

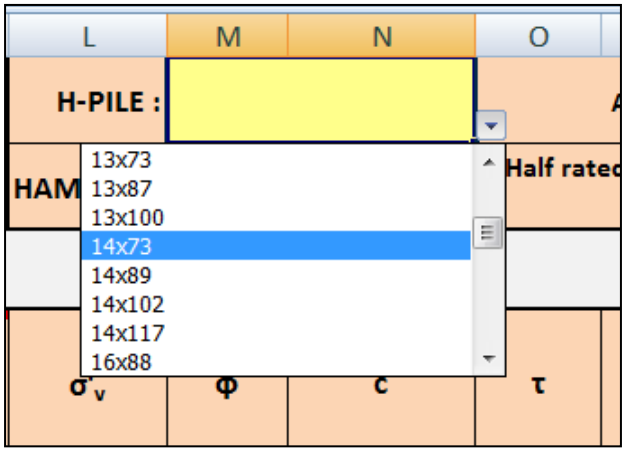

Figure 5-7 Selection of H-pile to be driven

8) Select the hammer that will be used to drive the pile (Figure 5-8).

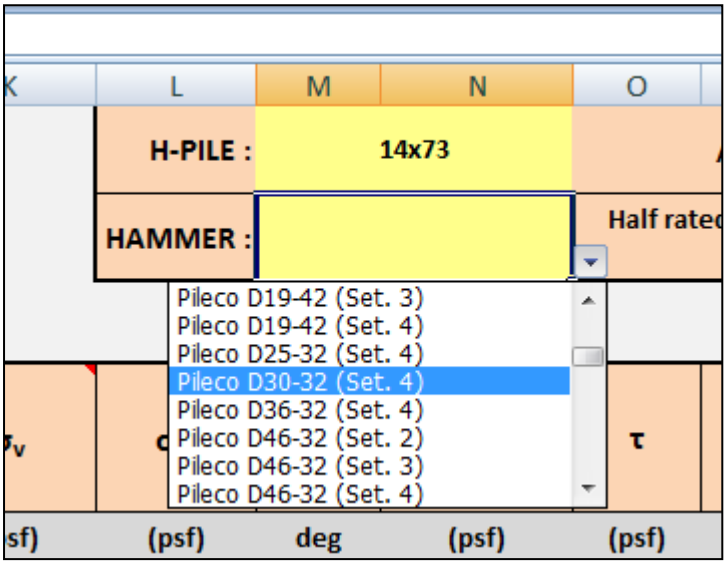

Figure 5-8 Selection of the hammer

Table 5-4 and Table 5-5 present available sizes of piles and the most common hammers used in MDOT projects respectively. Some hammers can be used with different fuel settings which affects the rated energy of the hammer. This issue is taken into account by including different pump settings in the list for the same hammer. If a hammer that is not on the list is encountered in a certain project, go to the "General Data" tab of the spreadsheet, column AP and AR, to input the name and rated energy (ft-lb) respectively (Figure 5-9). The list of hammers that you can choose from, will update automatically.

Table 5-4 Available sizes of H-piles used in MDOT projects

HP	A_c (in^2)
8x36	10.6
10x42	12.4
10x57	16.8
12x53	15.5
12x63	18.4
12x74	21.8
12x84	24.6
14x73	21.4
14x89	26.1
14x102	30.0
14x117	34.4
16x88	25.8
16x101	29.8
16x121	35.7
16x141	14.7
16x162	47.7
16x183	53.8
18x135	39.8
18x157	46.2
18x181	53.2
18x204	60.0

Table 5-5 Hammers used in MDOT projects

HAMMER	Max rated energy (ft-lb)
Delmag D12-42	33930
Delmag D16-32	39830
Delmag D19-42	48680
Delmag D25-32	66380
Delmag D30-32	75970
Delmag D36-32	90720
Delmag D46-32	122435
Pileco D12-42 (Set. 2)	19690
Pileco D12-42 (Set. 3)	24760
Pileco D12-42 (Set. 4)	29840
Pileco D19-42 (Set. 2)	28035
Pileco D19-42 (Set. 3)	35260
Pileco D19-42 (Set. 4)	42480
Pileco D25-32 (Set. 2)	38830
Pileco D25-32 (Set. 3)	52470
Pileco D25-32 (Set. 4)	58300
Pileco D30-32 (Set. 2)	51630
Pileco D30-32 (Set. 3)	62920
Pileco D30-32 (Set. 4)	69923
Pileco D36-32 (Set. 2)	55410
Pileco D36-32 (Set. 3)	69680
Pileco D36-32 (Set. 4)	83950
Pileco D46-32 (Set. 2)	70805
Pileco D46-32 (Set. 3)	89040
Pileco D46-32 (Set. 4)	107280
ICE I-19 (Set.2)	38175
ICE I-19 (Set.3)	42125
ICE I-19 (Set.4)	46170
ICE I-30 (Set. 2)	62925
ICE I-30 (Set. 3)	69435
ICE I-30 (Set. 4)	76070
APE D12-42 (Set. 2)	19647
APE D12-42 (Set. 3)	24707
APE D12-42 (Set. 4)	29768
APE D19-42 (Set. 2)	31107
APE D19-42 (Set. 3)	39119
APE D19-42 (Set. 4)	47132
APE D30-42 (Set.2)	55070
APE D30-42 (Set.3)	66977
APE D30-42 (Set.4)	74419

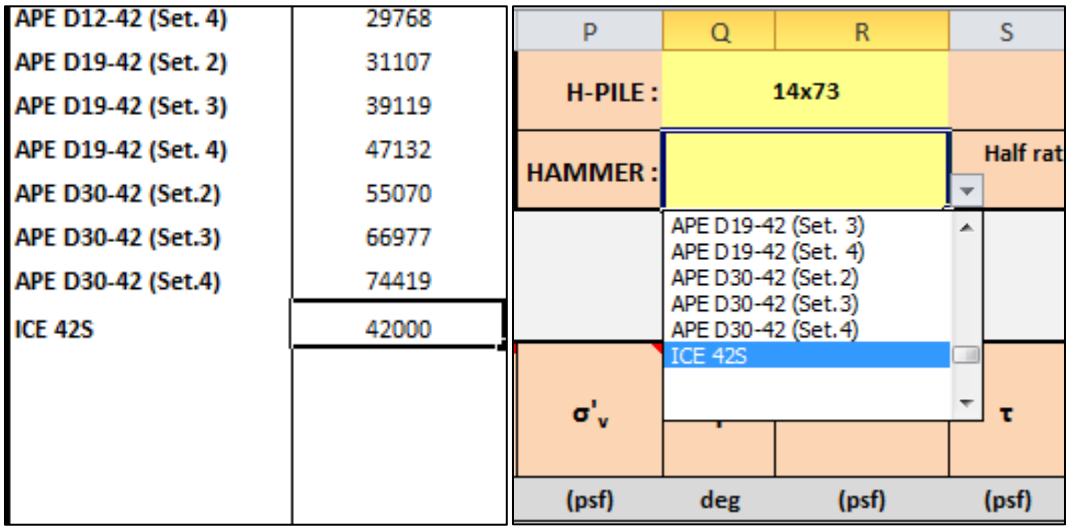

Figure 5-9 Input of hammer not included in the list

This concludes the needed input data. The calculations described in the previous sections will automatically take place in the tabs “General Data”, “Shaft” and “Tip”. The particle velocity calculated in the “General Data” tab is between the pile-soil interface. Moving to the “Shaft” tab, particle velocity and shearing strain are calculated for ten different distances from the pile (5-50 ft with 5 feet increments) at the center of every layer with same soil properties. Similar calculations are done in the “Tip” tab.

Figure 5-12 presents the factor by which the shear strain threshold should be divided to account for the fines content of each layer (after Borden and Shao, 1995). As a default value, 50% of fines content for clays and silts (passing #200 sieve) is used if no other information is available. If information is available for the fines content of some or all the layers in the soil profile, these values can be included in the spreadsheet as shown in Figure 5-13.

The total shear strain is computed by summing the shear strain contributions from both shaft and tip. This is presented in the tab “TOTAL” in tabular (Figure 5-10) and chart (Figure 5-11) forms. When the computed total shear strain exceeds the threshold (0.01%) for a specific granular layer, a red cell in the tabular form will alert the user. It can be seen in Figure 5-11 that the shear strain threshold is higher for cohesive soils but this does not imply that settlement will occur. The “TOTAL PLUGGED” tab follows the same calculations as in the “TOTAL” tab assuming that the pile tip is plugged.

No. of Layer	Layer Thickness	Depth	γ threshold	γ_{total} (%) r (ft)									
	(ft)	(ft)	%	5	10	15	20	25	30	35	40	45	50
1	6	6	0.01	0.01660	0.01120	0.00660	0.00438	0.00309	0.00227	0.00172	0.00132	0.00104	0.00082
2	4	10	0.267	0.08737	0.06922	0.04379	0.03001	0.02159	0.01604	0.01222	0.00948	0.00746	0.00595
3	5	15	0.01	0.02319	0.01597	0.00958	0.00641	0.00455	0.00335	0.00254	0.00196	0.00154	0.00122
4	6	21	0.267	0.07109	0.05614	0.03546	0.02429	0.01746	0.01298	0.00988	0.00766	0.00603	0.00481
5	17	38	0.01	0.03491	0.02844	0.01733	0.01156	0.00817	0.00599	0.00452	0.00349	0.00273	0.00217
6	22	60	0.01	0.03578	0.03018	0.01859	0.01243	0.00877	0.00643	0.00484	0.00373	0.00292	0.00231
7	16.5	76.5	0.267	0.14282	0.11360	0.07184	0.04921	0.03538	0.02629	0.02002	0.01553	0.01222	0.00974
8			#N/A										
9			#N/A										
10			#N/A										
11			#N/A										
12			#N/A										
13			#N/A										
14			#N/A										
15			#N/A										
16			#N/A										
17			#N/A										
18			#N/A										
19			#N/A										
20			#N/A										

Figure 5-10 Total shear strain for ten distances from pile at the center of every layer

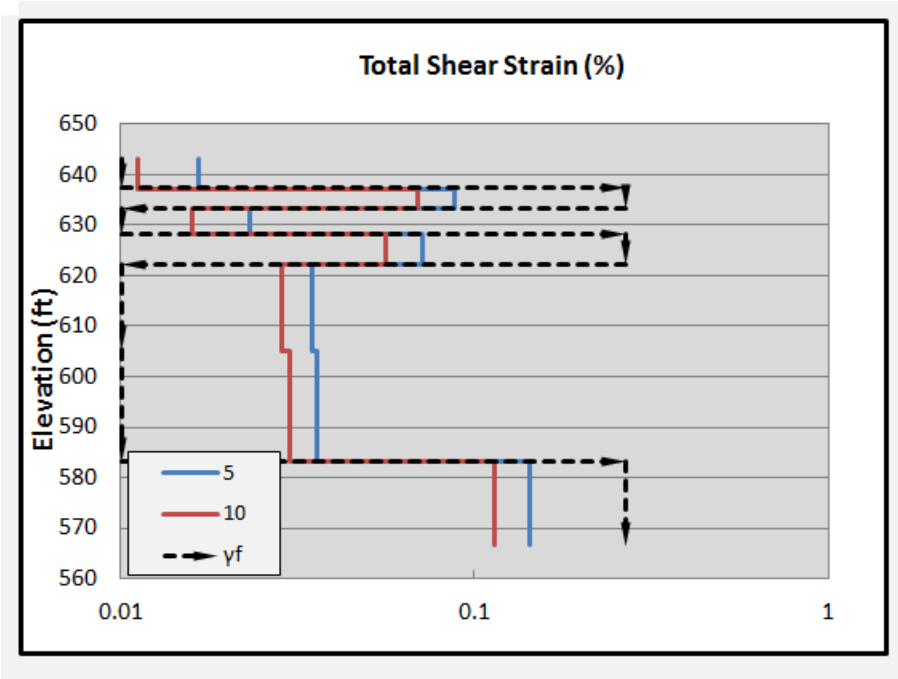

Figure 5-11 Total shear strain for two distances from pile

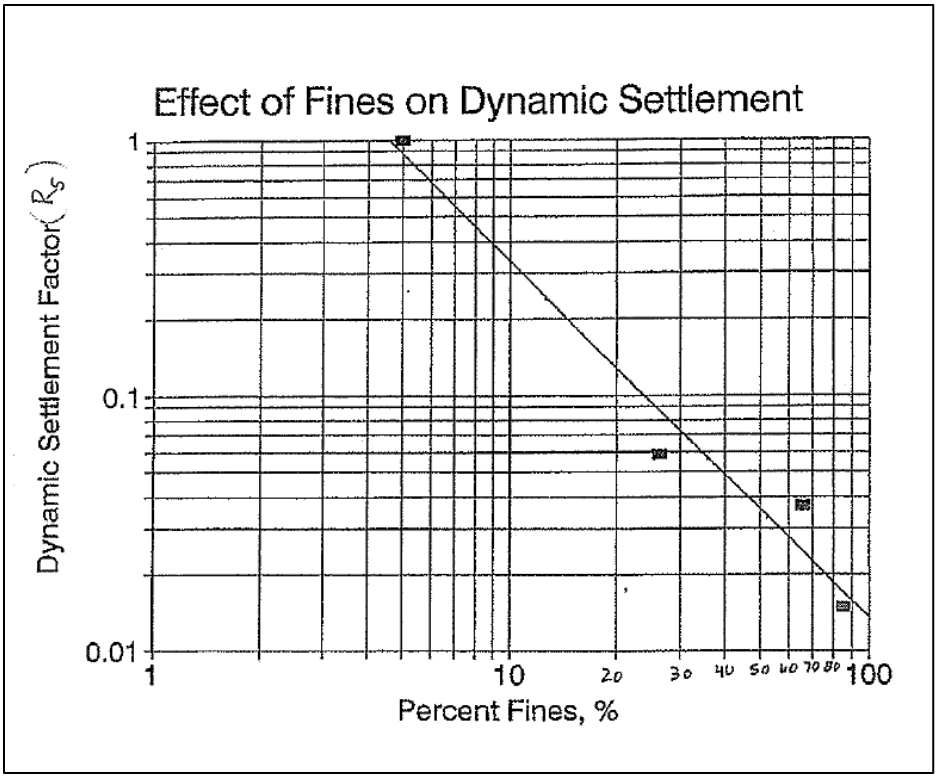

Figure 5-12 Effect of fines on dynamic settlement (after Borden and Shao, 1985)

Ground surface elevation (ft) :	643.2
Water elevation (ft) :	637.7
Default Value of Percent Fines in Silts/Clays (%) :	50

End of Layer Elevation	Soil Class	Blow Count N	N_1	$N_{1,60}$	Percent of fines	R_s
(ft)					(%)	
637.2	SP	5	7	9	12	0.2687225
633.2	PT	7	10	12		0.0374434
628.2	SP	11	15	19	25	1
622.2	ML	7	10	12		0.0374434
605.2	SP	16	18	22		1
583.2	SW	46	38	47		1
566.7	ML	56	39	49		0.0374434

Figure 5-13 Input of fines content

To check potential of settlement at distances that are different from the selected (i.e. 5-50 ft with 5 ft increments), input this distance at the “Shaft” tab like shown in Figure 5-14. This distance will automatically be also updated in the “Tip” and “Tip PLUGGED” tabs. Make sure to input the value of interest between the range that is preselected, i.e. to calculate total shear strain at 7.5 ft, change this value at the 10 ft table in “Shaft” tab.

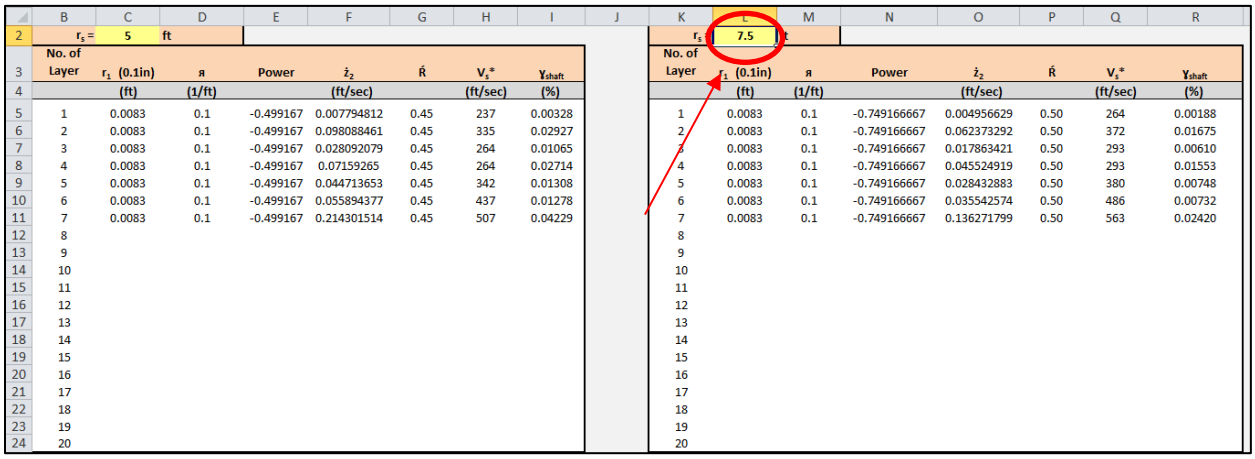

r_s =	5	ft

No. of Layer	r_1 (0.1in) (ft)	я (1/ft)	Power	$\dot{z}_2$ (ft/sec)	$\dot{R}$	V_s* (ft/sec)	γ_{shaft} (%)
1	0.0083	0.1	-0.499167	0.007794812	0.45	237	0.00328
2	0.0083	0.1	-0.499167	0.098088461	0.45	335	0.02927
3	0.0083	0.1	-0.499167	0.028092079	0.45	264	0.01065
4	0.0083	0.1	-0.499167	0.07159265	0.45	264	0.02714
5	0.0083	0.1	-0.499167	0.044713653	0.45	342	0.01308
6	0.0083	0.1	-0.499167	0.055894377	0.45	437	0.01278
7	0.0083	0.1	-0.499167	0.214301514	0.45	507	0.04229
8							
9							
10							
11							
12							
13							
14							
15							
16							
17							
18							
19							
20							

r_s =	7.5	ft

No. of Layer	r_1 (0.1in) (ft)	я (1/ft)	Power	$\dot{z}_2$ (ft/sec)	$\dot{R}$	V_s* (ft/sec)	γ_{shaft} (%)
1	0.0083	0.1	-0.749166667	0.004956629	0.50	264	0.00188
2	0.0083	0.1	-0.749166667	0.062373292	0.50	372	0.01675
3	0.0083	0.1	-0.749166667	0.017863421	0.50	293	0.00610
4	0.0083	0.1	-0.749166667	0.045524919	0.50	293	0.01553
5	0.0083	0.1	-0.749166667	0.028432883	0.50	380	0.00748
6	0.0083	0.1	-0.749166667	0.035542574	0.50	486	0.00732
7	0.0083	0.1	-0.749166667	0.136271799	0.50	563	0.02420
8							
9							
10							
11							
12							
13							
14							
15							
16							
17							
18							
19							
20							

Figure 5-14 Input of distance from pile if different from default values in spreadsheet in “Shaft” tab

6 COMPARISON OF MEASURED AND PREDICTED GROUND MOTION

6.1 Plugged/unplugged H-pile conditions

When the space between the flanges and web of an H-pile is packed hard with soil near the tip of the pile due to driving, the pile is called plugged for these analyses. If that space is not packed with soil, the condition is called unplugged. The unplugged condition was surmised from comparative calculations of ground vibration when the pile tip was in sand soils with blow counts (N) less than about 40 but may have been plugged when the tip was in clay soils and sands with blow counts higher than 40. There was no way to tell from the measured vibrations alone whether or not the pile was plugged or not but the calculation algorithm in section 5 allows a choice, plugged or unplugged, and calculated ground vibrations for both conditions were used to judge whether or not the pile in these tests was plugged. For all conditions where the soil profile indicated sand with N less than 40, the pile was considered unplugged for the measured versus predicted ground vibration comparisons in the next section.

6.2 Measured and predicted ground motion

Figure 6-1 to Figure 6-10 present comparisons between measured and predicted ground motion for the unplugged H-pile condition. This condition was found to correlate best between measured and predicted ground motion from pile driving when the pile tip was in loose to medium dense sand.

In general the correlation between measured and predicted ground motion was good for sensor elevations where the soil was loose to medium dense sand. Soil strata in Figures 6-1 through 6-10 have been shaded based on the soil classification. Tan and yellow shading indicates sand and gray shading indicates clay. The correlation was less good when the soil was med to dense sand and was not good when the soil at the elevation of the sensor was classified as clay. The latter condition is not surprising because the prediction model is based on the soil behaving as sand.

In Figure 6-1 the predicted vibration amplitude was about 12% lower than measured amplitude at the closest sensor (0.5 ft.) but predicted was same as or slightly over-predicted at other distances. For the shallow sensors at US-131A, the nearest (0.5 ft., Figure 6-2) sensor, the intermediate distance sensor (2.5 ft., Figure 6-3) and the furthest distance sensor (6.5 ft., Figure 6-4) predictions matched the measured. At the US-131A site the long distance predicted amplitude, over-predicted by about 100% in one direction (Figure 6-5) and over-predicted by

about 20% in the other (Figure 6-6). At US-131B predicted and measured motion were the same at 0.5 ft. (Figure 6-7), and over-predicted by about 20% at 2.1 ft. (Figure 6-8) and 6.5 ft. (Figure 6-9). The long distance prediction at US-131B significantly over-predicted at 90.65 ft. (Figure 6-10). Considering the many variables necessary for the prediction model and the heterogeneity of each soil profile tested, the agreement between predicted and measured ground motion is consider good.

6.3 Predicted limit distance to settlement threshold

Another important output of the settlement software tool is the distance beyond which vibrations strains do not exceed the settlement threshold. The prediction model uses principles from mechanics and ground vibration attenuation measured at the test sites, but actual settlements were not measured under controlled conditions such that comparisons could be made between measured settlement and settlement software tool. It should also be noted that the settlement software tool can be used to estimate the distance from the pile in any soil stratum at which strains exceed the generally accepted threshold for volume reduction, but cannot predict the magnitude of settlement. The magnitude of settlement is a function of number of cycles of large strain that the sand experiences and the relationship between number of cycles and amount of settlement has not been determined of the case of large numbers of cycles of vibration as from pile driving.

For the five sites tested Table 6-1 shows the distance beyond which settlement causing vibrations would not occur in sand soil based on the settlement software tool for conditions of plugged and unplugged pile tip. The soil strata for which these distances are valid are only those that can be classified as SP or SW. Strata with sands containing substantial fractions of passing #200 sieve will have longer safe distances.

Table 6-1 Shear Strain Threshold Exceedance Distances

Shear strain threshold exceedance in sand layers		
SITE	**Distance from pile (ft)**	
	Unplugged Tip	**Plugged Tip**
M-25	15	15
M-66	25	25
M-139	20	20
US-131 A	20	20
US-131 B	15	15

6.4 Influence of pile size and pile hammer energy

While the bridge replacement projects available for pile driving vibration measurements were limited and only two pile sizes and pile hammer types were used, the prediction software described in Section 5 could be used to judge the influence of pile and pile driving hammer sizes. Using the software, the M-139 site profile, and the M-139 pile driver; an increase in pile section from that actually used to two sizes larger, as listed in Table 5-4, did not make any difference in distance to settlement threshold exceedance. Also, for the M-139 site profile and actual pile section (H 14-73) but doubling the pile energy (not a specific pile driver), again the distance to settlement threshold exceedance did not increase. This second consequence further confirms the earlier conclusion that shaft transfer of energy into the surrounding soil is the most important component of energy transfer and the maximum ground vibration from the shaft is controlled by shearing strength of the soil not the pile or pile driver energy.

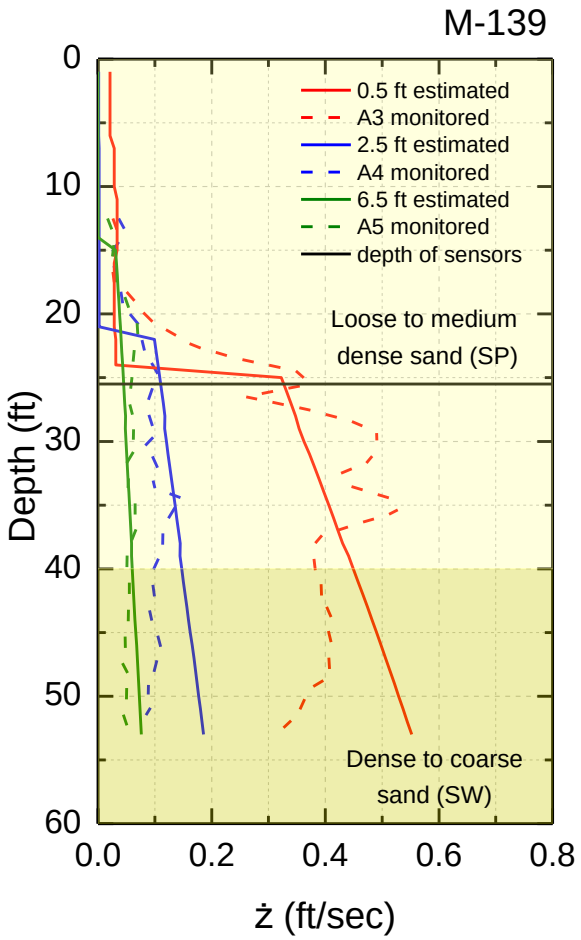

Figure 6-1 Measured and predicted ground motion at M-139 site

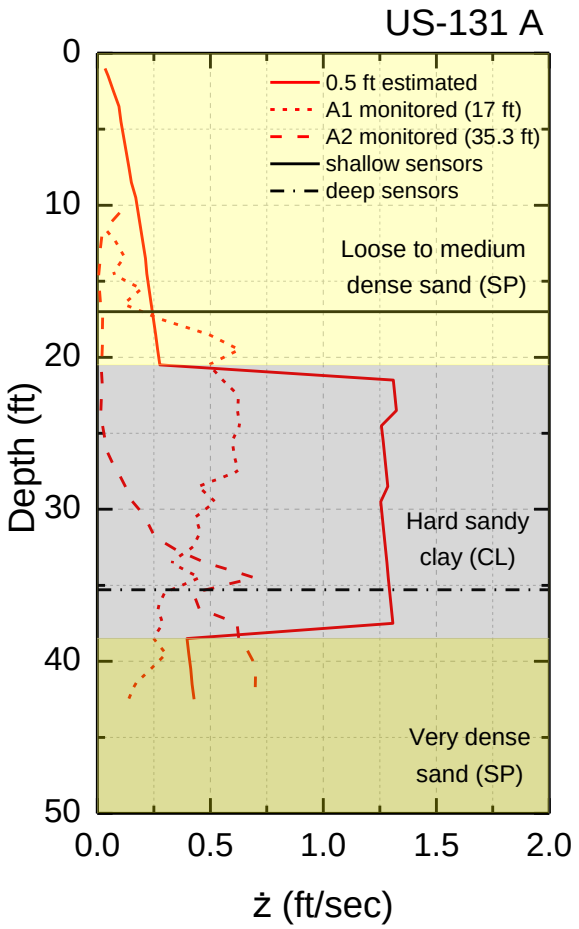

Figure 6-2 Measured and predicted ground motion at US-131 A site, 0.5 ft from pile 1

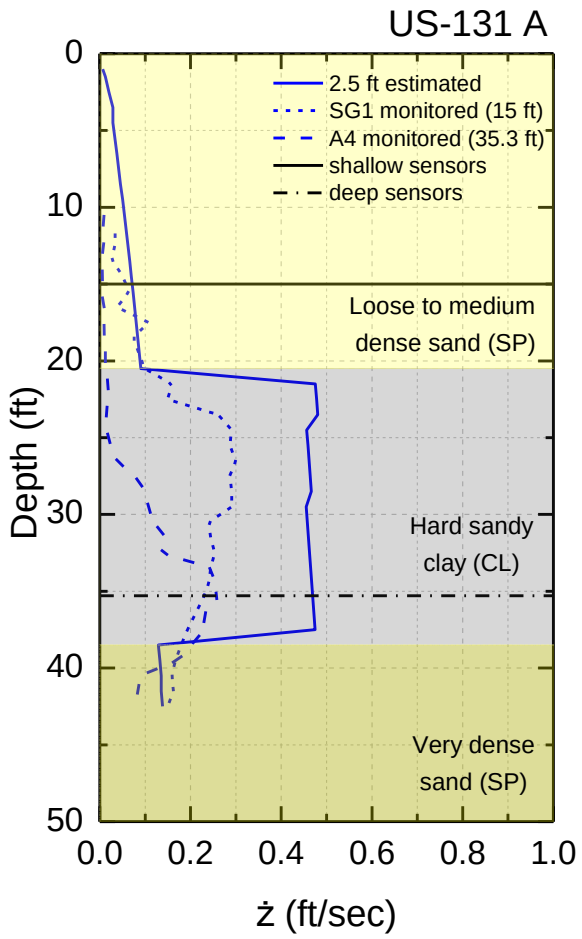

Figure 6-3 Measured and predicted ground motion at US-131 A site, 2.5 ft from pile 1

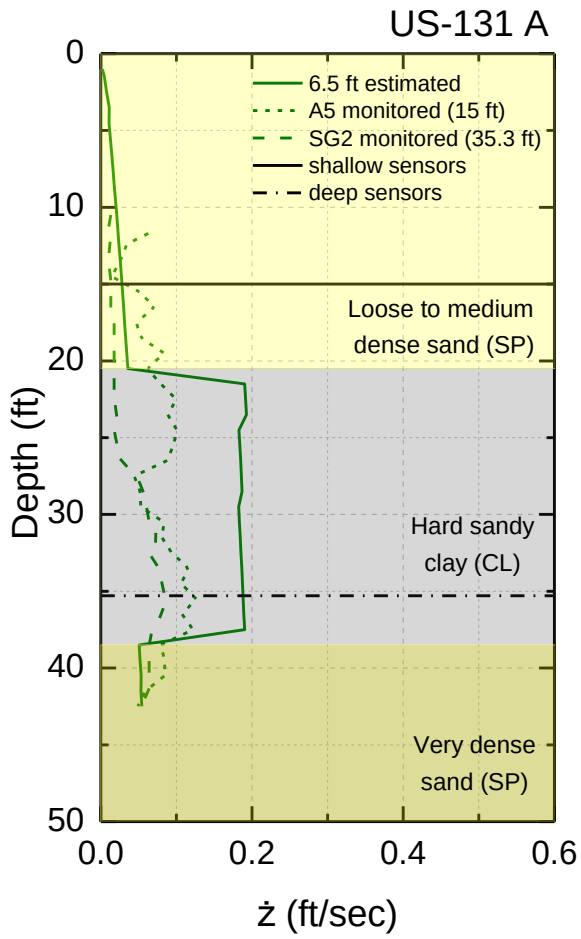

Figure 6-4 Measured and predicted ground motion at US-131 A site, 6.5 ft from pile 1

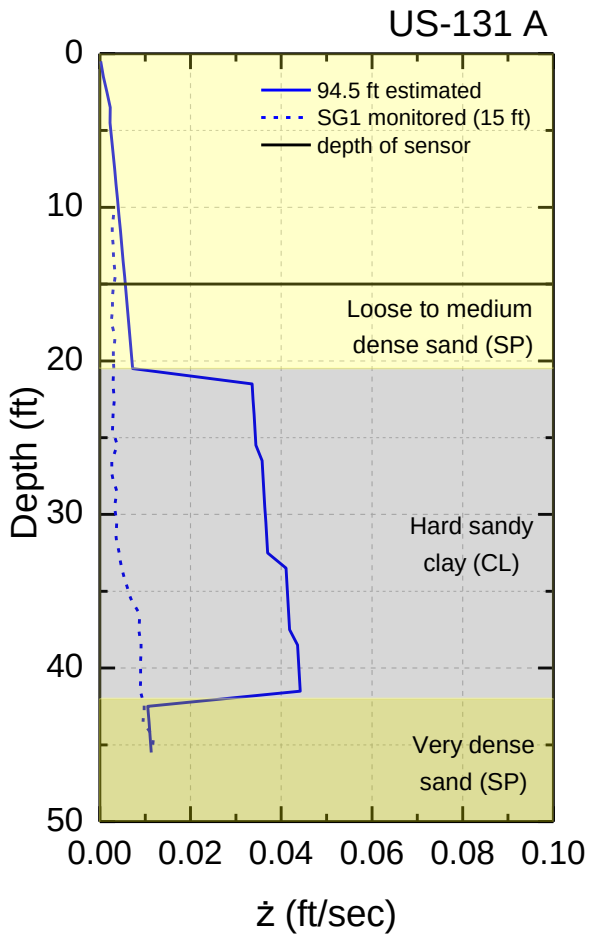

Figure 6-5 Measured and predicted ground motion at US-131 A site, 94.5 ft from pile 18

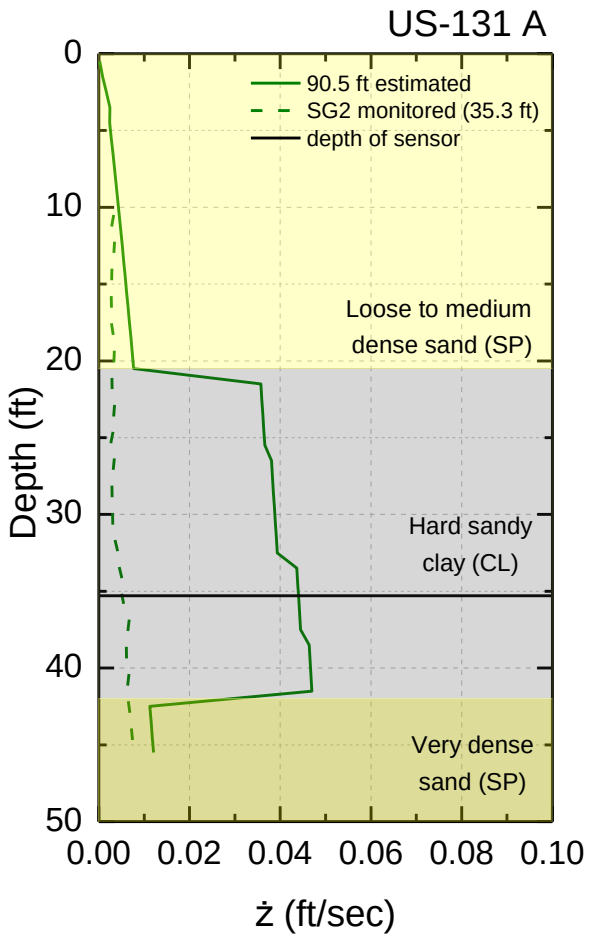

Figure 6-6 Measured and predicted ground motion at US-131 A site, 90.5 ft from pile 18

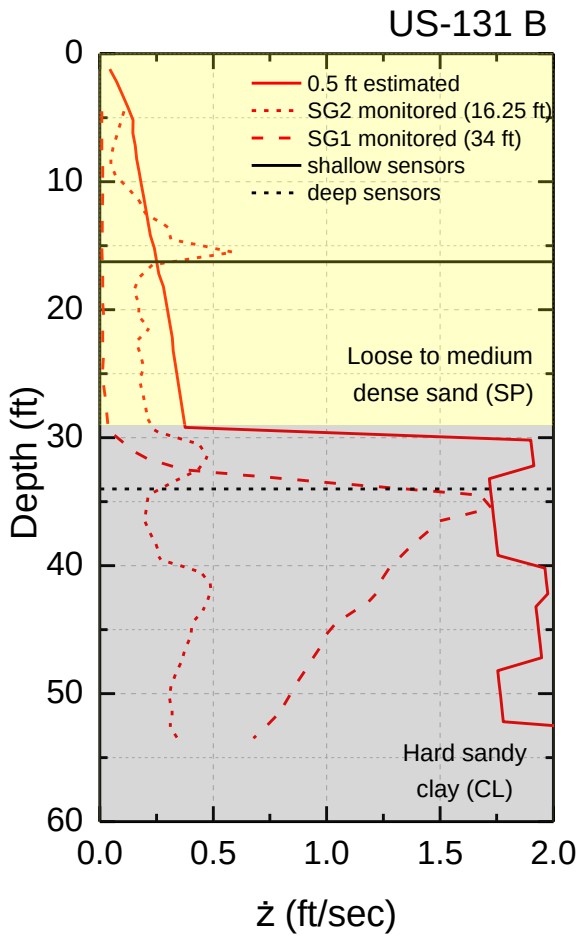

Figure 6-7 Measured and predicted ground motion at US-131 B site, 0.5 ft from pile 54

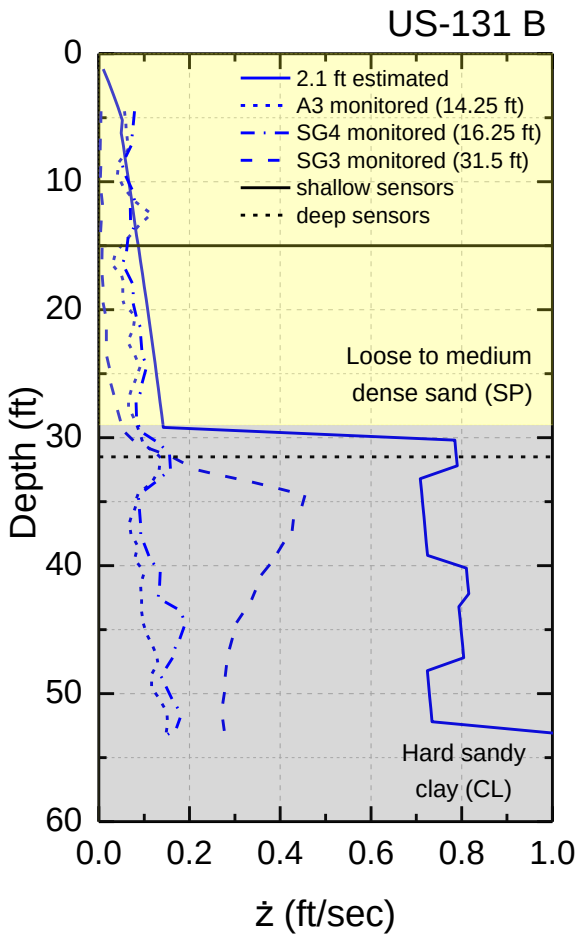

Figure 6-8 Measured and predicted ground motion at US-131 B site, 2.1 ft from pile 54

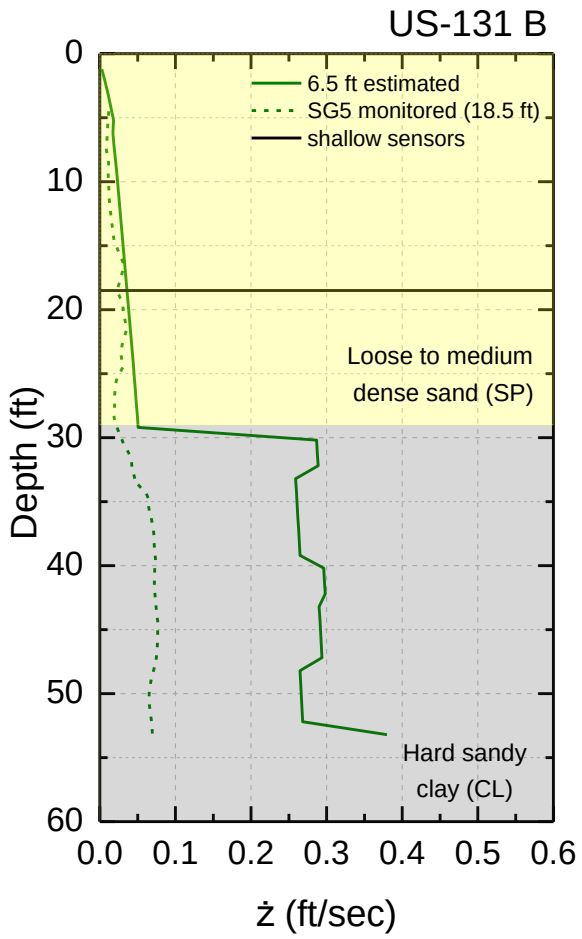

Figure 6-9 Measured and predicted ground motion at US-131 B site, 6.5 ft from pile 54

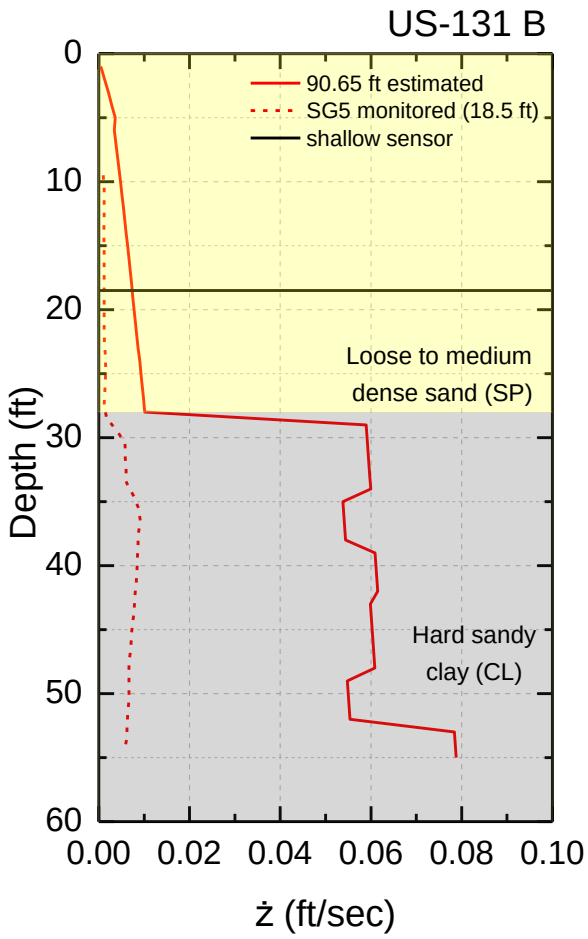

Figure 6-10 Measured and predicted ground motion at US-131 B site, 90.65 ft from pile 37

7 CONCLUSIONS AND RECOMMENDATIONS

7.1 Conclusions

The main research objectives of this research project were presented in section 1.3 and the following conclusions respond to those objectives.

7.1.1 Improvement and calibration of existing models for estimating shear wave attenuation and man-made ground vibration settlements

A literature search established the baseline from which an understanding of mechanisms of energy coupling from pile to ground results. In situ ground vibration measurements from pile driving during this research extended our understanding of these phenomena. The hypothetical model of energy transfer from pile to ground, represented by Figure 1-1 and Figure 1-2, is an incrementally improved model over what the literature presents and was refined from measurements during this research. Ground vibration measurements represented by peak vertical particle velocity (PPV or ż) confirmed the necessity to represent attenuation by two separate terms; geometric spreading and material damping. The Bornitz form of equation was determined to be the best way to most accurately represent attenuation. However, the conventional way of including material damping through the coefficient of attenuation, α, was determined to be too simple for driven piles as a source of energy, so a different symbol for coefficient of attenuation, я, has been chosen. Based on: (1) the limited pile type, (2) pile driver type and (3) site conditions encountered in this research, refined characterization of я could not be made but a simplified range was chosen: $0.1<я<0.15$ for distances from the pile up to 10 ft. For distances beyond 10 ft. $я=0.02$ was selected. Coefficient of attenuation, α, for typical ground material should not be used for attenuation of pile driving vibrations.

7.1.2 Characterization of typical vibration sources for MDOT projects

With regard to piles and pile drivers, the previous paragraph revealed the limited variety of structural pile sections and pile drivers that were studied. Table 5-4 and Table 5-5 list the hammers and pile sections typically used on MDOT sites. The only other specific ground vibration generating equipment employed on sites while this research was under way were vibrating pile drivers and large, front-end loaders. The loaders worked close to sites that were instrumented and produce only very low amplitudes of motion. Vibrating pile drivers were used only on sheet-piles (except at M-139) and most of that driving occurred before any field testing and vibration measurements were conducted by the research team.

7.1.3 Development of screening criteria for identifying potentially troublesome sites

Section 5 of this report describes the development of a spreadsheet calculation template for identifying potentially troublesome sites. This template requires input of only a basic soil stratigraphy, blow counts (N) for each strata, pile section and pile driver rated energy. Soil and attenuation properties are derived from correlations with blow count (N). The distance from the pile in each stratum through which vibration causing settlements can be propagated can be estimated from this spreadsheet. The potential for vibration caused settlement is judged based on the currently widely accepted threshold of shearing strain for granular soils, 0.01%. This threshold has not been studied or modified based on research reported here.

7.2 Recommendations

7.2.1 Vibrating pile driving operations

The research team arrived at every site after the contractor had started or completed installing sheet-pile cofferdams. Sheet-piles for the cofferdams were driven with vibrating pile drivers and caused unknown amounts of settlement in vulnerable soil strata. The mechanisms of energy/vibration transfer from vibratory driving of piles and sheet-piles are not known. Therefore, research into the mechanisms of energy transfer and settlement from vibratory pile driving is recommended.

7.2.2 Significance of directions of pile flange and open face on vibration propagation

Since H-piles are the common pile type for MDOT projects, it is necessary to establish the importance of the direction of the flange and open faces of the pile with respect to vibration propagation. While an attempt was made during this research to resolve this question, instrumentation failure prevented a definitive resolution of this question. It is recommended that additional research be performed to investigate the significance of the direction of the pile flange and open face.

7.2.3 Quantification of significance of percent fines on threshold of settlement

It is known that the amount of fines in a granular soil influences the threshold of shakedown settlement. Percent of fines is not always determined during the site exploration portion of a piling project. Whether or not a requirement for determining percent fines is sufficiently cost effective is not immediately evident. A parametric study of changes in distance of disturbance caused by impact pile driving should be made to determine whether or not a percent fines determination should be included in site characterization requirements.

7.2.4 Quantification of ground settlement at impact pile driving sites

Careful incremental settlement measurements need to be made in association with impact pile driving. Baseline ground elevations need to be established before any construction work is done and measurements repeated after each major step of construction. For example, before and after any operations like site excavation, after operation of any heavy equipment, after vibratory sheet-pile driving and after impact pile driving. It is only in this way that an estimate of the amount of settlement due to impact pile driving can be identified and separated from all other contributions to settlement.

8 RECOMMENDED IMPLEMENTATION PLAN

8.1 List of products expected from research

The products of this research include a report summarizing the research results from all the research tasks and presenting the recommended procedures and screening criteria to be used by MDOT for identifying potentially troublesome sites with respect to pile-driving induced ground settlement. Training materials will also be provided for the training session targeting MDOT engineers, but also consultants working with MDOT. A final "design aid" has been provided in Chapter 5.

8.2 Audience for research results

The main audience for the research results includes MDOT's bridge designers and geotechnical engineers and MDOT consultants. The extended audience can be other state DOTs and other government agencies involved in construction type projects that use vibration inducing equipment or techniques near existing structures.

8.3 Activities for successful implementation

Successful implementation of the recommended procedures and screening criteria to be used by MDOT for identifying potentially troublesome sites with respect to pile-driving induced ground settlement was initiated through a training session by the research team for MDOT personnel who will be involved in relevant projects.

Finally, the research team will work with MDOT to assist in the preparation of the necessary sections to be added to the Bridge Design Manual and/or bridge Design Guides.

8.4 Criteria for judging the progress and consequences of implementation

Prof. Woods, who is part of the research team, has extensive experience with QA/QC processes as a Professional Engineer, and he served as Quality Assurance and Control Officer of this research project. Prof. Athanasopoulos-Zekkos also has experience with independent project review as a member of the New Orleans levee failures investigation team in 2005 and as a consultant for several projects.

The judging of progress was achieved by close supervision of the graduate student researcher involved in this research project, Ms. Athena Grizi, the field investigation, and the GRL-WEAP analyses. Regular meetings of the U-M based research team were made during the

project to monitor progress and supervise the literature review and analyses. Additional meetings were also scheduled with the SME and SOMAT senior engineers who performed the GRL-WEAP analyses and reviewed the collected data and draft final report. An additional quality assurance and control of the research investigation will be implemented during submission of interim and final research publications in peer-reviewed scientific journals and conferences. This review process typically involves 2-3 independent reviews by researchers knowledgeable on the research topic.

8.5 Costs of implementation

The primary cost of implementation was the preparation of the final report and the preparation of the training session/s as needed for successful implementation of the final product of this research. This cost was included in the proposed budget.

9 REFERENCES

- Athanasopoulos, G.A. and Pelekis, P.C. (2000), "Ground Vibration from Sheetpile Driving in Urban Environment: Measurements, Analysis and Effects on Buildings and Occupants", Soil Dynamics and Earthquake Engineering, Vol. 19, No. 5, pp. 371-387, Elsevier.

- Attewell, P.B. and Farmer, I.W. (1973), "Attenuation of Ground Vibrations from Pile Driving", Ground Engineering, Vol. 3, No. 7, pp. 26-29.

- Barkan, D.D. (1960), "Dynamics of Bases and Foundations", McGraw-Hill Book Co., Inc., New York, N.Y., 1960.

- Borden, R.H., Shao, L. and Gupta, A. (1994) "Construction Related Vibrations, Report FHWA/NC/94-007, Center for Transportation Engineering Studies, North Carolina State University, Raleigh, N.C.

- Borden, R.H. and Shao, L. (1995) "Construction Related Vibrations: Field Verification of Vibration Induced Settlement Model," Report FHWA/NC/95-008, Center for Transportation Engineering Studies, North Carolina State University, Raleigh, N.C.

- Bornitz, G. (1931) Uber die Ausbreitung der von Groszkolbenmaschinen erzeugten Bodenschwingungen in die Tiefe, J. Springer (Berlin).

- Clough, G.W. and Chameau, J.L. (1980), "Measured Effects of Vibratory Sheetpile Driving", Journal of the Geotechnical Engineering Division, ASCE, Vol. 106, No. GT10, October 1980, pp. 1081-1099.

- Coduto, D.P. (2001), "Foundation Design: Principles and Practices", 2nd Ed., Prentice-Hall Inc.

- CTC & Associates LLC (2003), "Construction Vibration and Historic Buildings", Transportation Synthesis Report, Bureau of Environment Division of Transportation Infrastructure Development, July 2003.

- Dalmatov, B.I., Ershov, V.A. and Kovalevsky, E.D. (1968), "Some Cases of Foundation Settlement in Driving Sheeting and Piles," Proceedings International Symposium on Wave

Properties of Earth Materials, University of New Mexico, Albuquerque, New Mexico, pp. 607-613, 1968.

- Dowding, C.H. (1994), "Vibration Induced Settlement from Blast Densification and Pile Driving," Vertical and Horizontal Deformations of Foundations and Embankments, ASCE Geotechnical Special Publication No. 40, 1994, pp. 1672-1688.

- Drabkin, S., Lacy, H. and Kim, D.S. (1996), Parametric Assessment of Settlement on Sands Caused by Low Level Vibrations due to Operation of Construction Equipment, Pile Driving and Traffic", Journal of Geotechnical Engineering, Vol. 122, No. 11, November 1996, pp. 920-928.

- Drabkin, S. and Lacy, H. (1998), "Prediction of Settlements of Structures due to Pile Driving", Proc., Geotechnical Earthquake Engineering and Soil Dynamics III, Seattle, Washington, August 1998, pp. 1496-1505.

- Edwards, A.T. and Northwood, T.D. (1960), "Experimental Studies of the Effects of Blasting on Structures", The Engineer, Vol. 210, September 1960, pp. 538-546.

- Hardin, B.O. and Richart, Jr F.E. (1963), "Elastic Wave Velocities in Granular Soils", Journal of the Soil Mechanics and Foundation Division, ASCE, Vol. 89, No. SM1, February 1963, pp. 33-65.

- Hendriks, R. (2002), "Transportation Related Earthborne Vibrations", California Department of Transportation Division of Environmental Analysis, Office of Noise, Air Quality, and Hazardous Waste Management Sacramento, CA, Technical Advisory, Vibration TAV-02-01-R9601, February 2002.

- Imai, T. and Tonouchi, K. (1982), "Correlation of N Value with S-Wave Velocity and Shear Modulus", Proc. Of 2nd European Symposium on Penetration Testing, Amsterdam, pp. 67-72.

- Jackson, N.M. and Hammons, M.I (2007), "Use of Nondestructive Techniques to Estimate the Allowable Vibratory Compaction Level During Construction", Research Report FL/DOT/SMO/07-BDB-11, State Materials Office, March 2007.

- Jedele, L. (2005), "Energy-Attenuation Relationships from Vibrations Revisited", Soil Dynamics Symposium in Honor of Professor Richard D. Woods, ASCE, GSP 134, 2005.

- Jones and Stokes (2004), “Transportation-and Construction-Induced Vibration Guidance Manual”, California Department of Transportation Environmental Program Environmental Engineering, Noise, vibration, and Hazardous Waste Management Office, June 2004.

- Kulhawy, F.H. and Mayne, P.W. (1990), “Manual on Estimating Soil Properties for Foundation Design”, Electric Power Research Institute, Palo Alto, CA.

- Kim, D.S., Drabkin, S., Rokhavarger, A. and Laefer, D. (1994), “Prediction of Low Level Vibration Induced Settlement”, Vertical and Horizontal Deformations of Foundations and Embankments, ASCE Geotechnical Special Publication No. 40, 1994, pp. 806-817.

- Kim, D.S. and Drabkin, S. (1995), “Factors Affecting Vibration Induced Settlement”, Third International Conference on Recent Advances in Geotechnical Earthquake Engineering and Soil Dynamics”, St. Louis, Missouri, April 2-7, 1995, Vol. 3, pp. 1111-1115.

- Lacy, H.S. and Gould, J.P. (1985), “Settlement from Pile Driving in Sands”, Proceedings of a Symposium sponsored by the Geotechnical Engineering Division in conjunction with the ASCE Convention in Detroit, Michigan, October 1985, pp. 152-173.

- Lambe, T.W. and Whitman, R.V. (1969), “Soil Mechanics”, John Wiley and Sons, New York, 553 p.

- Leathers, F.D. (1994), “Deformations in Sand Layer during Pile Driving”, Vertical and Horizontal Deformations of Foundations and Embankments, ASCE Geotechnical Special Publication No. 40, 1994, pp. 257-268.

- Leznicki, J.K., Esrig, M.E. and Gaibrois, R.G. (1992), “Loss of Ground during CFA Pile Installation in Inner Urban Areas”, Journal of Geotechnical Engineering, ASCE, Vol. 118, No. 6, June 1992, pp. 947-950.

- Leznicki, J.K., Gaibrois, R.G. and Esrig, M.E. (1994), “Displacement of Landmark Building Resulting from Adjacent Construction Activities”, Vertical and Horizontal Deformations of Foundations and Embankments, ASCE Geotechnical Special Publication No. 40, 1994, pp. 222-232.

- Linehan, P.W., Longinow, A. and Dowding, C.H. (1992), “Pipe Response to Pile Driving and Adjacent Excavation”, Journal of Geotechnical and Geoenvironmental Engineering, ASCE, Vol. 118, GT2, February 1992, pp. 300- 316.

- Masoumi, H.R, Francois, S. and Degrande, G. (2007), “Numerical Prediction of Ground Vibrations Due to Pile Driving Using a Hybrid Formulation”, 4th International Conference on Earthquake Geotechnical Engineering, Thessaloniki, Greece, June 25-28, 2007, Paper No. 1707.

- Massarsch, K.R. and Broms, B.B. (1991), “Damage Criteria for Small Amplitude Ground Vibrations", Second International Conference on Recent Advances in Geotechnical Earthquake Engineering and Soil Dynamics, St. Louis, Missouri, March 11-15, 1991, Vol. 2, pp 1451-1459.

- Massarsch, K.R. (1992), “Static and Dynamic Soil Displacements caused by Pile Driving”, Keynote Lecture, Fourth International Conference on the Application of Stress-Wave Theory to Piles, The Hague, The Netherlands, September 21-24, 1992, pp. 15-24.

- Massarsch, K.R., Madshus, C. and Bodare, A. (1995), “Engineering Vibrations and Solutions”, Third International Conference on Recent Advances in Geotechnical Earthquake Engineering and Soil Dynamics”, St. Louis, Missouri, April 2-7, 1995, Vol. 3, pp 1349-1354.

- Massarsch, K.R., (2002), “Effects of Vibratory Compaction”, TransVib 2002 – International Conference on Vibratory Pile Driving and Deep Soil Compaction, Louvain-la-Neuve, Keynote Lecture, pp. 33-42.

- Massarsch, K.R., (2000). ”Settlements and Damage caused by Construction-Induced Vibrations”. Proceedings, Intern. Workshop Wave 2000, Bochum, Germany, December 13-15, 2000, pp. 299-315.

- Massarsch, K.M. and Fellenius, B.H. (2008), “Ground Vibrations Induced by Impact Pile Driving”, Sixth International Conference on Case Histories in Geotechnical Engineering, August 12-16, Arlington VA, Virginia, 2008, 38 p.

- Picornell, M. and Monte, E. (1985), “Pile Driving Induced Settlements of a Pier Foundation”, Proceedings of a Symposium sponsored by the Geotechnical Engineering Division in conjunction with the ASCE Convention in Detroit, Michigan, October 1985, pp. 174-186.

- Richart, F.E., Woods, R.D. and Hall, J.R. (1970), “Vibrations of Soils and Foundations”, Prentice-Hall, Inc., Englewood Cliffs, New Jersey, 414 p.

- Seed, H.B. and Silver, M.L. (1972), “Settlement of Dry Sands during Earthquakes”, Journal of Soil Mechanics and Foundations, ASCE, Vol. 98, No. SM4, April 1972, pp. 381-397.

- Selby, A.R. (2002), “Computation of ground waves due to vibro-driving of piles”, Numerical Models in Geomechanics-NUMOG VIII, Pande & Pietruszczak, 2002.

- Silver, M.L. and Seed, H.B. (1971), “Deformation Characteristics of Sands under Cyclic Loading”, Journal of Soil Mechanics and Foundations, ASCE, Vol. 97, No. SM8, August 1971, pp. 1081-1098.

- Siskind, D.E. and Stagg, M. (2000), The Co-Report. Blast Vibration Damage Assessment Study and Report, Miami-Dade County, C3TS Project No.: 1322-01.

- Szechy, K. and Varga, L. (1978), “Foundation Engineering”, Akademiai Klado, Budapest, 1978.

- Terzaghi, K. and Peck, R.D. (1967), “Soil Mechanics in Engineering practice”, 2nd Ed., John Wiley and Sons, 729 p.

- Wiss, J.F. (1981), “Construction Vibrations: State-of-the-Art”, Journal of the Geotechnical Engineering Division, ASCE, Vol. 107, No. GT2, February 1981, pp. 167-181.

- Woods, R.D. and Jedele, L.P. (1985), “Energy-Attenuation Relationships from Construction Vibrations”, Proceedings of a Symposium sponsored by the Geotechnical Engineering Division in conjunction with the ASCE Convention in Detroit, Michigan, October 1985, pp. 229-246.

- Woods, R.D. (1997), “Dynamic Effects of Pile Installations on Adjacent Structures”, Synthesis of Highway practice 253, National Cooperative highway research program, Washington, D.C., 1997.

- Yang, X.J. (1995), “Evaluation of Man-Made Ground Vibrations”, Third International Conference on Recent Advances in Geotechnical Earthquake Engineering and Soil Dynamics”, St. Louis, Missouri, April 2-7, 1995, Vol. 3, pp. 1345-1348.